1966

Internal friction of sodium chloride

Gerald Keith Fehr
Iowa State University

66–6979

FEHR, Gerald Keith, 1937–

INTERNAL FRICTION OF SODIUM CHLORIDE.

Iowa State University of Science and Technology
Ph.D., 1966
Engineering, chemical

University Microfilms, Inc., Ann Arbor, Michigan

INTERNAL FRICTION OF SODIUM CHLORIDE

by

Gerald Keith Fehr

A Dissertation Submitted to the

Graduate Faculty in Partial Fulfillment of

The Requirements for the Degree of

DOCTOR OF PHILOSOPHY

Major Subject: Ceramic Engineering

Approved:

Signature was redacted for privacy.

In Charge of Major Work

Signature was redacted for privacy.

Head of Major Department

Signature was redacted for privacy.

Dean of Graduate College

Iowa State University
Of Science and Technology
Ames, Iowa

1966

TABLE OF CONTENTS

		Page
I.	INTRODUCTION	1
II.	REVIEW OF LITERATURE	2
	A. Definition of Internal Friction	2
	B. Techniques of Internal Friction Measurement	4
	C. Dislocation Damping Mechanism	7
	1. Low temperature dislocation relaxation (Bordoni region)	7
	2. High temperature dislocation damping	7
	3. Dislocation resonance	8
	4. Transient cold-work internal friction	8
	5. Deformation hysteresis	8
	6. Dislocation hysteresis	9
	D. Internal Friction Research on Metals and Ceramics	21
	E. Internal Friction Research on Alkali Halides	23
III.	METHOD OF PROCEDURE	35
IV.	FINDINGS	50
	A. Room Temperature Findings	50
	B. Raised Temperature Findings	69
V.	DISCUSSION	82
	A. General Theory	82
	B. Room Temperature	83
	C. Raised Temperature	87
VI.	CONCLUSIONS	93
VII.	LITERATURE CITED	95
VIII.	ACKNOWLEDGMENTS	102
IX.	APPENDIX	103

I. INTRODUCTION

The phenomenon by which a vibrating solid, completely isolated from its surroundings, converts its mechanical energy of vibration into other forms causing vibration damping is called internal friction or damping capacity. The specific purpose of this dissertation was to report the effect of grain boundaries and temperature on the amplitude dependent internal friction of sodium chloride. This work was part of a larger program to gain information on the causes of ceramic brittleness.

Although sodium chloride is not a useful structural material, it has the same crystal structure as magnesium oxide and the atomistic processes of plastic deformation (dislocation motion) have been shown to be similar in the two materials. Since the single crystals of sodium chloride and magnesium oxide show appreciable ductility, this research will produce information that will increase the understanding of ductile deformation of polycrystalline cubic ionic solids.

II. REVIEW OF LITERATURE

The research work reported in this dissertation is a continuation of the author's Master of Science thesis (1) which includes additional information on internal friction.

A. Definition of Internal Friction

Internal friction has been defined by Dieter (2) as "the ability of a vibrating solid which is completely isolated from its surroundings to convert its mechanical energy of vibration into heat." If materials behaved as perfect elastic materials at stresses below the nominal elastic limit, there would not be any internal friction. However, the fact that damping effects can be observed at stress levels far below the macroscopic elastic limit indicates that some materials have a very low true elastic limit.

Internal friction effects correspond to a phase lag between the applied stress and the resulting strain. At a high stress level the phase lag may be due simply to plastic deformation. At low stress levels it may be due to thermal, magnetic, or atomic rearrangements. For energy to be dissipated by internal friction mechanisms, the strain must lag the applied stress. The phase angle α or lag angle was used as a measure of internal friction by Dieter (2):

$$\alpha = \frac{\varepsilon_2''}{\varepsilon_1'} \qquad (1)$$

where ε_2'' = nonelastic strain component 90° out of phase with the stress and ε_1' = elastic strain in phase with the stress.

For a condition of forced vibration in which the specimen is driven at a constant amplitude, a measure of the internal friction is the fractional decrease in vibration energy per cycle. The vibrational energy is proportional to the square of the amplitude (2), so that the logarithmic decrement δ can be expressed by

$$\delta = \frac{\Delta W}{2W} \tag{2}$$

where ΔW is the energy lost per cycle and W is the vibrational energy at the start of the cycle.

Internal friction is frequently measured by an oscillator which is set into motion with a certain amplitude A_0 and then allowed to decay freely. The amplitude A_t at any time t can be expressed by

$$A_t = A_0 \exp(-\beta t) \tag{3}$$

where β is the attenuation coefficient. The logarithmic decrement is the logarithm of the ratio of successive amplitudes.

$$\delta = \ln \frac{A_n}{A_{n+1}} \tag{4}$$

If the internal friction is independent of amplitude, a plot of the logarithm of A versus the number of cycles of vibration will be linear and the slope of the line is the decrement. If the damping is amplitude-dependent, the decrement is given by the slope of the curve at that amplitude. The logarithmic decrement is related to the lag angle by

$$\delta = \pi\alpha. \tag{5}$$

By measuring the vibrational rate of decay information can be gained on the internal structure and atom movements of solids.

Internal friction studies have provided information on diffusion, ordering and solubilities of interstitial elements, and about dislocations in crystals. Advantages of internal friction measurements derive from the sensitivity of the method, the selectivity of the measurement, the fact that the results can be made quantitative, and the fact that the measurements are nondestructive. A disadvantage is that a detailed model of the reaction is required to interpret the results.

B. Techniques of Internal Friction Measurement

Internal friction can be measured by a number of techniques. Kingery (3) discusses both low frequency devices and high frequency devices. Only techniques used to study dislocations in crystals will be discussed here. Two high frequency methods commonly used are the Forster (4) method and the piezoelectric composite oscillator method. Mason (5) discusses piezoelectric crystals and their various applications.

Internal friction measurements by the composite oscillator technique evolved from the piezoelectric resonator research. The use of the composite piezoelectric resonator is based on the theorem, first developed by Butterworth (6) and later independently by Cady (7) and Van Dyke (8), that a linear mechanical vibrator driven by a condenser coupled electro motive force behaves electrically like a simple combination of circuit elements. Later, Quimby (9) made an analysis of the vibrations of solid bars driven by a piezoelectric crystal. Balamuth (10) first employed drivers and specimens of matching fundamental frequency in 1934. Subsequent investigators applied the two-component resonator primarily to the measurement of the elastic constants of ionic crystals (11), organic

materials (12), and polycrystalline metals (13). Read (14) was first to measure the internal friction of metal single crystals with a composite resonator.

The three-component resonator as described by Marx (15) for use in the kilocycle range was driven by a -18.5 X-cut quartz bar of rectangular cross section which was excited into longitudinal vibration by an alternating electrical signal applied to full length adherent electrodes. A specimen closely matching the driver in fundamental frequency was cemented to one end. A second quartz bar, also of matched frequency, was cemented to the other end of the driver. The lateral faces of the second quartz bar were provided with suitable electrodes to make it serve as a piezoelectric gauge. The maximum vibrational strain amplitude in the specimen (Figure 1) may be computed directly from the gauge signal, while the ratio of the driving emf to the gauge signal at resonance is proportional to the logarithmic decrement. The strain amplitude may be varied from below 10^{-8} to above 10^{-5}, depending upon the specimen damping.

Measurements by the composite oscillator technique as a function of temperature and strain amplitude are easy as compared to measurements as a function of deformation, frequency, and orientation.

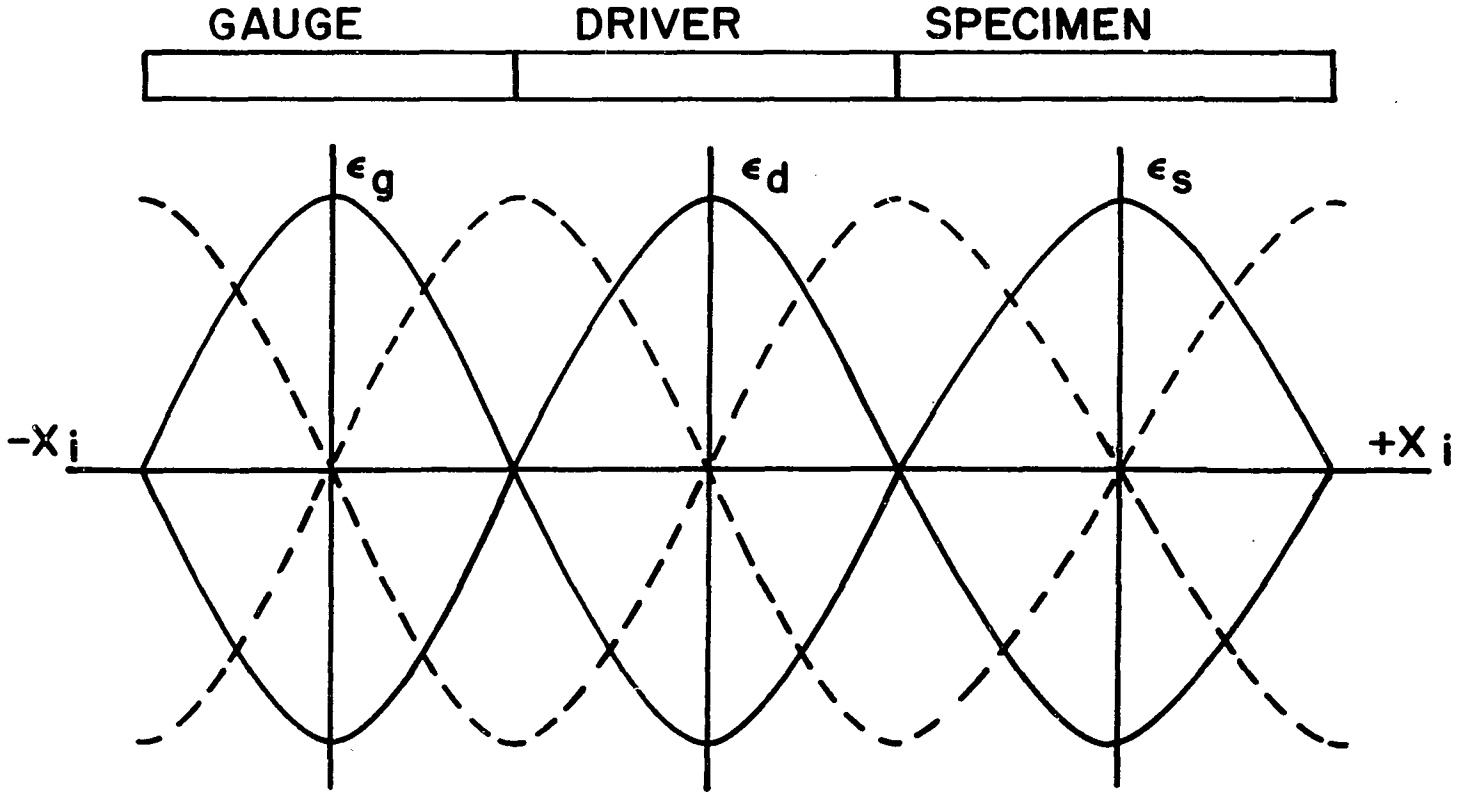

Figure 1. Vibrational displacement limits (----) and vibrational strain limits (——) as located on composite oscillator.(15)

C. Dislocation Damping Mechanism

There are numerous causes of internal friction (2), many of which are not related to dislocations. These were discussed in detail by various authors (16 through 22). Ductility has been related to dislocation motion (3), hence dislocation damping will be discussed here. Dislocations are an important source of internal friction in solids. Dislocation damping is characterized by a strong dependence on previous plastic deformation. Van Bueren (17) divides dislocation damping into six types of internal friction caused by six different dislocation mechanisms. It is possible to separate these six mechanisms experimentally only because they occur in different regions of frequency or temperature. The divisions, although not really distinct, have been established for discussion purposes and as such will be used here.

1. Low temperature dislocation relaxation (Bordoni region)

Bordoni (23) discovered the existance of a fairly broad internal friction peak of the relaxation type in single crystals of copper at 90°K with a measurement frequency of 49 kilocycles per second. Similar peaks have been found in different metals. Theories on the cause of the Bordoni effect have been advanced by Mason (24) and Seeger (25).

2. High temperature dislocation damping

At temperatures above 400°C a marked increase of the medium and low frequency damping in various metals (copper, aluminum) was noted (17). This increase was especially noticed when the internal friction was observed at very small strain amplitudes where the internal friction

increases exponentially with the temperature. The inverse-frequency variation and the exponential temperature dependence can be understood as the natural result of the action of one or two thermally activated relaxation processes with long relaxation times.

3. Dislocation resonance

Theoretically, near the high frequency end of the range investigated in internal friction experiments (3 to 300 megacycles per second) a third kind of dislocation damping can occur. This damping can be associated with the resonance motion of dislocations within the equilibrium potential valleys between atom rows. The dislocation resonance should not have any effect on experimental work accomplished in the kilocycle range.

4. Transient cold-work internal friction

Van Bueren (17) defines transient cold-work internal friction as the increase of the low- and medium-frequency internal friction that occurs immediately after deformation of a metal at not too high a temperature. The damping shows appreciable recovery in a very short time interval, even when the metal is kept at a temperature far below that of mechanical recovery or recrystallization. In NaCl this damping was studied as a function of irradiation with X rays by Gordon and Nowick (26). An exponential recovery rate was observed.

5. Deformation hysteresis

Deformation hysteresis internal friction, which bears resemblance to transient cold-work internal friction, occurs at low frequencies and

large strain amplitudes in slightly cold-worked metals. Storing the metal at room temperature resulted in a rapid lowering of the internal friction. The deformation hysteresis differs from the transient internal friction in that the deformation hysteresis has a strong amplitude dependence.

6. Dislocation hysteresis

Dislocation hysteresis internal friction is the frequency-independent, strain amplitude dependent type of loss. It occurs most conspiciously in the kilocycle frequency range at not too small strain amplitudes. This is by far the most important kind of internal friction originating from the presence of dislocations. Dislocation hysteresis internal friction is sensitive to previous cold work. The strain amplitude dependence points to a non-linear process underlying this type of damping. It is not surprising that an explanation of strain amplitude dependence has been sought in terms of irreversible dislocation motion.

Granato and Lücke's (27, 28) model has been used to explain dislocation hysteresis internal friction. They assumed in their model that a pure single crystal contains, before deformation, a network of dislocations. The length of loop determined by the intersection of the network loops is further pinned by the impurity particles present through the Cottrell (29) mechanism. There are therefore, two characteristic lengths in the model: the length L_n determined by the networks and the length L_c determined by the impurities. The mathematical treatment takes into account that a distribution of lengths occur.

If an external stress is applied, the total strain is composed of

elastic strain and dislocation strain. At high frequencies the stress-dislocation strain law is a function of the frequency. It is independent of frequency for lower frequencies, including the kilo-cycle range. Qualitatively, the action of a dislocation length under the influence of an increasing external stress can be seen in Figure 2 (27). For zero applied stress the network length is further pinned by the impurity particles (A). For a very small stress (B), the dislocation loops pinned by the impurities bow and continue to bow until the breakaway stress is reached. At the breakaway stress (C-D), a large increase in the dislocation strain occurs for no increase in the stress. For further increases in the stress the loop length L_n bows (D-E) until the stress required to activate the Frank-Read source or some other dislocation multiplication process is reached. The network pinning is assumed to be so strong that no breakaway of network lengths occur. Further increases in the applied stress lead to creation and expansion of new closed dislocation loops (F-G). The dislocation strain due to this step is known to be irreversible and accounts for plastic strain. It is apparent that there are two different types of energy losses.

The first loss is obtained since the measurement is a dynamic one. There is a phase lag for the oscillating stress because the motion forced by the external stress is opposed by some damping mechanism. This dynamic loss is frequency dependent and is the largest near the resonant frequency determined by the loop length L_n. The loss disappears at frequencies substantially above or below the L_n resonant frequency.

The second type of loss results during the unloading part of the stress cycle (D-A). The long loops L_n collapse elastically along a path

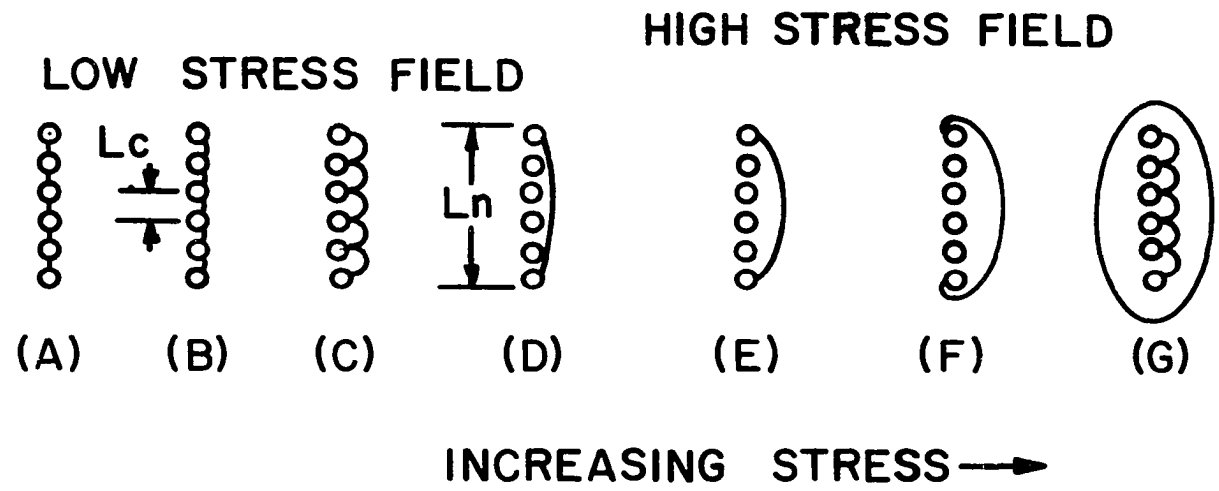

Figure 2. The successive drawings indicate schematically the bowing of a pinned dislocation line by an increasing applied stress (27)

determined by the loop length L_n, thus giving a hysteresis effect. The hysteresis energy loss is proportional to the area enclosed by the stress-dislocation strain loop. For small enough stresses the loss does not occur. Since in the kilocycle range, the stress-dislocation strain law is independent of frequency, the hysteresis loss is frequency independent (27).

The two losses, strain amplitude dependent loss Δ_H and the frequency dependent loss Δ_I are given by Granato and Lücke (27) as

$$\Delta_H = \frac{\Omega \Delta_0 \Lambda L_n^3}{\pi L_c} \frac{K\varepsilon' A}{L_c} \frac{1}{\varepsilon_0} \exp\left(-\frac{K\varepsilon' a}{L_c} \frac{1}{(\varepsilon)_0}\right) \qquad (6)$$

and $$\Delta_I = \frac{\Omega \Delta_0 \Lambda L_e^4 BW}{\pi^2 C} \qquad (7)$$

where

L_e = effective loop length = 3.3 L_c

Δ_0 = constant of order of 1

Λ = total length of movable dislocation line per unit volume (dislocation density)

a = lattice parameter

ε_0 = strain amplitude

W = circular frequency

K = unknown parameter which is a function of orientation and anisotropy

Ω = orientation factor

A = effective mass per unit length

ε' = difference in atomic radii/atom radius of the solvent atom

B = damping force per unit length

C = impurity concentration.

Some serious criticisms of Granato and Lücke's model have been made (27, 28). There is doubt that the dissipative mechanism can be described by assuming a dissipative term proportioned to the velocity. The largest possible displacements allowed the dislocation line are of the order of only a few lattice spacings; hence, the interaction energy between an impurity and a segment of dislocation line varies only a little during the breakaway process, making the concept of breakaway questionable. The Granato-Lücke analysis ignores the fact that thermal activation aids the applied stress in the unpinning process; hence their theory is applicable strictly only at 0°K. However, the Granato-Lücke theory has had more success explaining the experimental results than any other theory, so modifications of the Granato-Lücke theory have been published (30, 31, 32).

Swartz and Weertman (30) present a theory based on the Granato-Lücke theory but with two modifications. The first modification is that the pinning force F of the impurity atom which arises from elastic interactions depends on the orientation of the dislocation line. It is assumed that impurities interact only with the edge component of any dislocation. Evaluating Cottrell's (29) equation

$$F \simeq 4\mu b\epsilon r^3\, \partial(\sin\theta/R)\partial X = 4\mu b\epsilon r^3 \sin\frac{2\theta}{R^2} \qquad (8)$$

they (30) found

$$F = \frac{\mu\varepsilon b^2}{4} \qquad (9)$$

for a pure edge dislocation. In Equation 8 and 9 μ is the shear modulus b the length of the Burgers vector, ε the fractional difference in radius between the impurity and the host atom, r the radius of the host atom, R and θ are the polar coordinates of the impurity atom relative to the dislocation line and the slip plane (evaluated at $\theta = 5\pi/4$ and $R = \sqrt{2}a$), and $x = R \cos \theta$.

The second modification of the model in Figure 2 is shown in Figure 3. Swartz and Weertman (30) assume that once a dislocation has broken away from its pinning points its motion is not necessarily limited by its line tension, (C), Figure 2. The distance the dislocation moves may be determined by the stress field of neighboring impurity atoms as given by the Mott-Nabarro theory (33). In Figure 3, (a) and (b) are the same as in Figure 2. When breakaway occurs at a low stress, the dislocation bows to the limit of its line tension as shown in (c) Figure 3. At higher stresses the dislocation motion is limited to approximately $\lambda/2$, (d), Figure 3, where λ is the average distance between the randomly distributed impurity atoms. The average distance, $\bar{x}$, a dislocation will move during breakaway will be one of the two following values:

(a) Line tension controlled, (c) in Figure 3

$$\bar{x} = \frac{1}{6} (\sigma L_n^2/\mu b) \qquad (10)$$

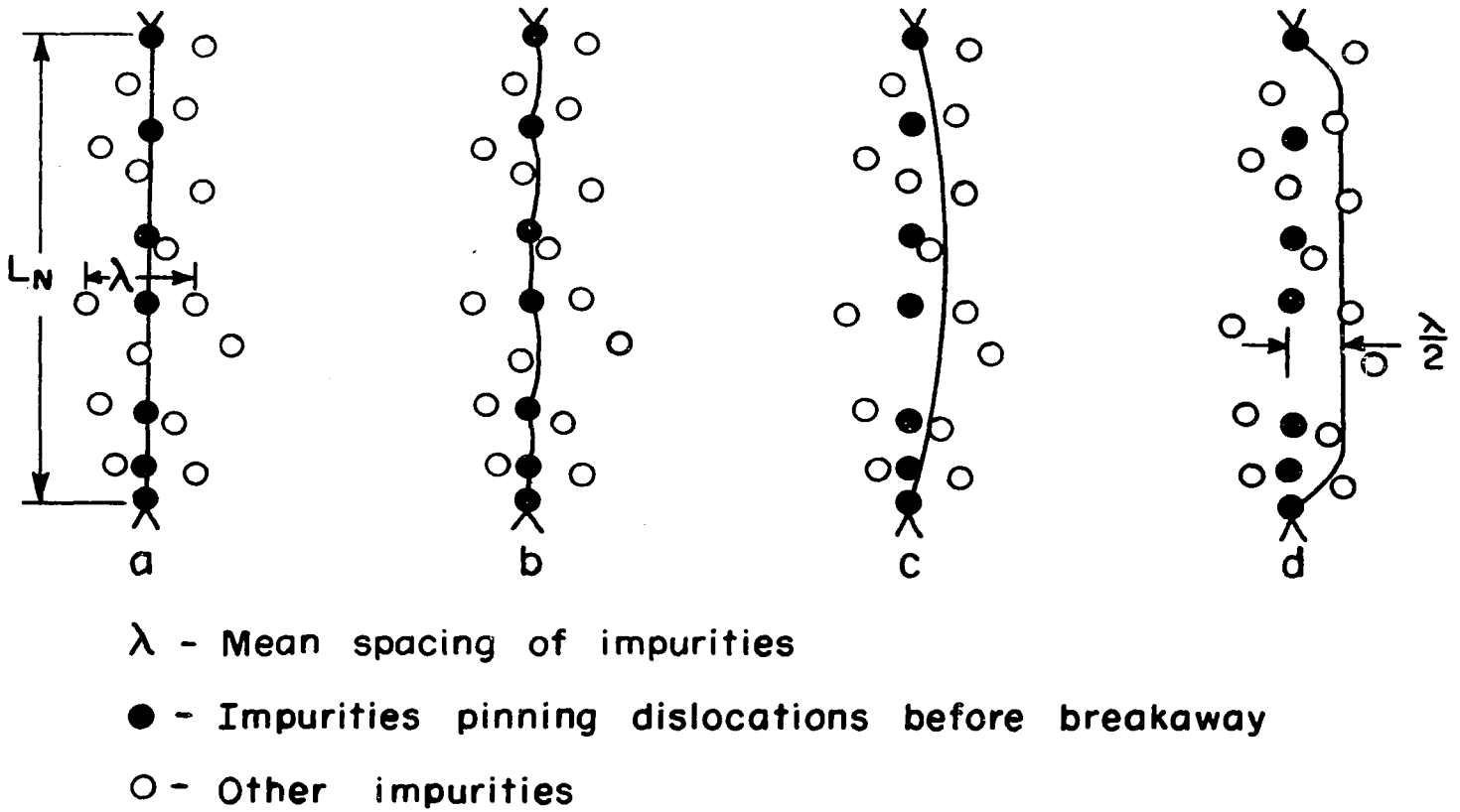

Figure 3. The Granato-Lücke model modified by the restraining effect of impurities near the dislocation (30)

where σ is the applied stress and L_n is the distance between radial pinning points of the dislocation network.

(b) Impurity spacing controlled, (d) in Figure 3

$$x \approx \lambda/2 = b/2C^{1/3} \tag{11}$$

where C is the atom fractions of impurity. $\bar{x}$ will be determined by whichever equation (Equation 10 or 11) gives the smaller value.

Figure 4 illustrates the hysteresis in the dislocation strain resulting from breakaway. In Figure 4 (a) shows the hysteresis loop for line tension limited motion while (b) shows the hysteresis loop for impurity limited motion. It is clear from Figure 4 that the dislocation strain resulting from breakaway increases linearly with the breakaway stress as Equation 10 specifies. When the dislocation motion after breakaway is limited by the neighboring impurities the resulting stress field varies much more rapidly than linearly with the dislocation strain, (b) in Figure 4.

The area enclosed in a hysteresis loop represents the energy lost during the stress cycle. The area of the loop of (a) in Figure 4 is half the product of the stress σ at the moment of breakaway and the dislocation strain resulting from breakaway. The area of the loop in (b) is greater by a factor between 1 and 2. Hence we may write

$$\text{Energy lost per cycle} = \beta\sigma b L_n \bar{x} \tag{12}$$

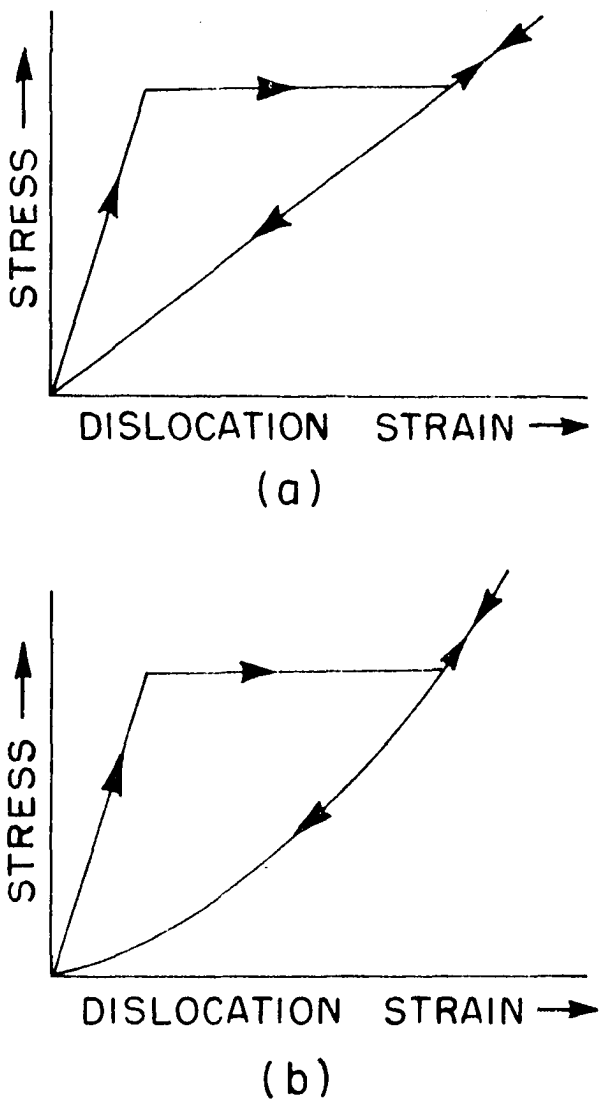

Figure 4. Hysteresis in the stress-dislocation strain diagram for (a) tension limited motion, and (b) impurity-limited motion (30)

where β is a parameter equal to one for tension-limited motion and between one and two for impurity limited motion. To compute the decrement resulting from dislocation hysteresis, the energy loss of Equation 12 must first be summed for all dislocations which break away. The logarithmic decrement is the total energy loss per cycle divided by twice the vibrational energy in a unit volume. Swartz and Weertman (30) published two equations for the decrement Δ due to the hysteretic dislocation motion. For low stresses and line tension controlled displacement

$$\Delta = \frac{N L_n^3 b}{9\pi F_o} \sigma_o \qquad (13)$$

where $F_o = \frac{\mu\varepsilon b^2}{4}$. For impurity controlled dislocation displacement

$$\Delta = \frac{2\beta\mu N b L_n F_o}{\pi\sigma_o^2 C^{1/3} L^2} \int_0^{\pi/2} \int_0^{\sigma_o} \frac{\sin\alpha}{\sigma} \exp\left(-\frac{2F_o \sin\alpha}{\sigma b L}\right) d\sigma d\alpha \qquad (14)$$

which at low stresses ($\sigma_o bL << 2F_o$) approximates

$$\frac{\beta\mu N b^3 L_n}{4\pi C^{1/3} F_o} = \frac{\beta N b L_n}{\pi C^{1/3} \varepsilon} \qquad (15)$$

The symbols in Equations 13, 14, and 15 have the same meaning as in Equations 9 through 12 with the following additions.

$L = \frac{b}{C}$ the average distance between impurity and a dislocation line

N total length of dislocation line

σ_o amplitude of stress oscillation

α the angle between the Burgers vector and tangent to the dislocation line ($\sin\alpha = 1$ for edge dislocation; $\sin\alpha = 0$ for screw dislocation).

It is proper to use the equation which predicts the lowest damping since this involves the smaller breakaway distance. At very low stresses the breakaway distance is line-tension controlled and the decrement resulting from the hysteretic motion is proportional to stress. At somewhat higher stresses, the breakaway distance is limited by the stress field of impurity atoms, in which case the decrement becomes independent of stress. At stresses sufficiently high to break away the edge dislocation, Equation 14 predicts decrements varying exponentially with reciprocal stress such as predicted by Granato and Lücke (27, 28). Rogers (31) allows the minor pins a random distribution on the dislocation line. The major pins in the system need not be only network pins but can be any type of pin which is not broken by the maximum forces applied. The minor pins may be impurities or other defects which do allow breakaway. The major limitation is the high number of minor pins required, i.e., L_n/L_c must not be small. The main addition by Rogers is the idea of amplitude dependence in the frequency dependent region.

Teutonico, Granato and Lücke (32) consider the aspect of thermal breakaway of the pinned dislocation line with application to damping. With the addition of thermal energy, less stress is required to cause dislocation breakaway. However, even with the aid of thermal energy a stress threshold will exist. The authors (32) present expressions for damping in the case of a single pinning point and in the case of a continuous pinning agent. Despite their success, application of the theory to experimental data is very difficult. The resulting formulas are too

complicated. The integrals cannot be evaluated and it is not possible to recognize and analyze simply the effect of changes of the different parameters as is necessary for comparison with experiments. Also, the models utilized are not very realistic, dislocations are anchored by many discrete pinning points, where as in the paper only the two extremes, single point pinning and continuous pinning, are considered. They (32) assume that thermal breakaway from a single pinning point and the corresponding activation energy control the breakaway of the whole network length, since breakaway from the first pinning point may eventually lead to a breakaway from all the other pinning points in the network length.

Granato et al. (34) compute the entropy factor and effective jump frequency for the thermally activated unpinning of dislocations by use of the statistical mechanics treatment of absolute rate theory. The entropy factor was very large for long loop lengths and increased with pinning strength. As the pinning strength reached infinity (no breakaway) the entropy factor did also. For a typical case of a binding energy of 1/10 electron volt, the frequency factor for a dislocation pinned at its center is the order of 5×10^{10} cycles per second, independent of the loop length or of the attack frequency. This would mean that at reasonable temperatures (room temperature and above) the thermal unpinning should be greater than breakaway unpinning.

In summary, there are a number of ways in which dislocations can contribute to internal friction. A dislocation segment oscillating between two pinning points (vibrating string model) gives one type of damping (low amplitude resonance). Dislocations which break away from pinning

points under stress lead to another type (amplitude dependent damping). Dislocations which move by overcoming Peierls barriers are supposed to give rise to the low-temperature Bordoni peaks. There is not yet a suitable model for the highly deformed state. However, the single dislocation segment model which neglects interactions between dislocations works surprisingly well for moderate deformation.

D. Internal Friction Research on Metals and Ceramics

Most of the past internal friction research was accomplished on metals (35 through 52) or if done on ionic bonded materials was done in the so called amplitude-independent frequency dependent region (53-57). However, these reports do lead to general results. Some of the more important conclusions will be discussed. Thompson and Holmes (42) give evidence to prove that the number of dislocation segments available for bowing, the effective dislocation density, is temperature dependent with an activation energy. Hutchison and others (40, 41 and 49) conclude that as the temperature is raised major pinning points can become minor pinning points by thermal activation. Many of the original minor pinning points are weakened or eliminated. Thermal energy required to eliminate minor pinning points is greater than that required for the conversion of major to minor pins. As the temperature of the test specimen is lowered the reverse process would be true. Fiore and Bauer (43) find results which agree with the above process. They produced Equation 16 and 17 which predicted such results.

$$L_c = \frac{2r_o}{C_o} \exp(-\frac{U_B}{kT}) \tag{16}$$

$$\Delta H = \frac{\Lambda L_n^3 \Lambda_1}{L_c \varepsilon_o^{1/2}} \exp(-\frac{A_2}{L_c \varepsilon_o}) \tag{17}$$

where

L_n = distance between major pinning points

L_c = average distance between breakable pinning points

r_o = radius of solvent atom

C_o = probability that any atom in the solid solution is a solute atom

U_B = binding energy between dislocations and solute atom

k = Boltzmann's constant

T = absolute temperature

A = total length of edge-type dislocation free to vibrate in a cubic centimeter of solid

ϵ_o = maximum strain amplitude of the solid in its longitudinal mode of vibration

A_1, A_2 = Granato and Lücke's (27, 28) constants involving geometric and orientation parameters and the pinning force between solute atoms and dislocations.

Equations 16 and 17 predict that as the temperature increases and L_c decreases, Δ_H should increase. Their (43) results follow the prediction of Roger's (31) modifications of the Granato-Lücke (27, 28) analysis. They (43) also find that as the temperature increases, the strain amplitude marking the onset of amplitude dependence decreases.

Niblett and Wilks (58) published a report on dislocation damping which was essentually a literature review of the work done up to 1956. They do not delve too deeply into any part of the subject, but only mention the more important ideas. Most of the models used to study ionic bonded materials are based upon previous work done on metals.

E. Internal Friction Research on Alkali Halides

Some of the first internal friction work on rock salt crystals was done by Frankl (59). He found that the internal friction of rock salt crystals was markedly decreased by X-irradiation. This was interpreted as the pinning of dislocations by cation vacancies liberated from vacancy pairs on the trapping of photo-electrons. Very small applied stresses were capable of breaking the pinning points and thus increasing the internal friction. The main objection to this work was the treatment of the crystals before testing. Frankl (59) reduced the crystals to correct size by cutting with a fine jewelers saw and then dry grinding on abrasive paper. Annealing would not remove the many dislocations added by this treatment.

In 1956 Gordon and Nowick (26) reported on the pinning of dislocations by X-irradiation of alkali halide crystals. They demonstrated that modulus change on irradiation corresponds exactly to the elimination of the modulus decrease due to oscillating dislocation loops through the creation of pinning points along the dislocations. They assumed that vacancies, released within the volume of the crystal through the action of radiation, migrate to dislocations and contribute to the formation of pinning points.

Johnston and Gilman (60) measured the velocities of individual dislocations in LiF, covering a range in magnitudes from 10^{-9} cm/sec to 10^{5} cm/sec. The low velocities were extremely sensitive to applied stress. They also found a minimum stress for dislocation motion, below which dislocations could not move. The edge components of the dislocation loops moved considerably faster than the screw components. The upper

limit for dislocation velocity appeared to be the velocity of sound in the crystal. The effects of temperature, impurities, and radiation damage on the dislocation velocity were described. The velocity in different crystals varied with the hardness. The yield stress of LiF was found to be determined by the stress required to move a dislocation in an otherwise dislocation free region of the crystal. The yield stress was not influenced by the state of pinning, or the geometrical arrangement of the dislocations in an as grown crystal, as such dislocations did not take part in the deformation. The dislocation density increased and the distribution of dislocations during deformation were described. The glide dislocations multiplied, by an undetermined mechanism, as they moved through the crystal. The rate of multiplication was a function of the applied stress and the dislocation velocity. Etch pit counts showed that the average dislocation density in the crystal increased linearly with the plastic strain for the range covered.

Whitworth (61) studied the effects of vibration on the internal friction of sodium chloride. He found that the internal friction of sodium chloride specimens annealed at 650°C and cooled slowly was approximately 10^{-5} at low amplitude, and rose to about 10^{-4} at strains of 4×10^{-5}. He concluded that the damping of a truly undeformed "pure" crystal would be amplitude independent at low strain amplitudes. He also found that plastic deformation of such pure annealed crystals increased its internal friction. According to Whitworth the internal friction of sodium chloride measured in experiments of this type was due to the motion of those dislocations which were introduced into the specimen after it had been annealed. Whitworth (61) used the Granato-Lücke (27, 28) theory to explain

the amplitude dependent results which he obtained.

Johnston and Gilman (62) presented experimental observations of dislocation multiplication, of the defect structure left behind by a moving dislocation, and of the cross-glide of individual dislocations in LiF crystals. New dislocation loops form at many different sites in the wake of a moving dislocation. These loops have the same Burgers vector as the parent dislocation but do not, in general, lie on the same atomic plane. The rate of formation of new loops depends upon the magnitude of the applied stress. Such creation of new loops leads eventually to the formation of wide glide bands. Dislocations form in dislocation-free regions of LiF crystals only if small precipitates or other stress raisers are present. It was shown that dislocations do not form in completely defect-free regions of LiF at stresses as high as G/85 where G is the shear modulus.

Bauer and Gordon (63) measured the internal friction as a function of strain amplitude on deformed sodium chloride single crystals. These were followed by elastic modulus measurements made during X-irradiation of the same crystal. They found that the dislocation density increased rapidly with small amounts of deformation, indicating that fresh dislocations are created as plastic deformation proceeds, and that grown in dislocations probably play a minor part on the plastic flow of rock salt.

Davidge and Whitworth (64) published evidence for the production of debris by moving dislocation in sodium chloride. Several kinds of etch pits were formed when the NaCl was etched with a mixture of acetic acid and methyl alcohol. Shallow pointed pits, when compared to normal

dislocation etch pits, on the slip bands were considered to be evidence of debris left behind by moving dislocations. The debris was considered to be such things as close dipoles, columns of defects and very small dislocation loops. Whitworth (65) later published a sequal to his earlier work (61 and 64) on the changes of elastic modulus associated with internal friction in sodium chloride.

Taylor (66) found low-temperature internal friction peaks in single crystals of NaCl and LiF. A temperature range of 20°K to 220°K at a strain amplitude of 1×10^{-6} was covered at two different frequencies. Small amounts of plastic deformation gave rise to a well defined internal friction peak. No amplitude dependent data was given.

Bauer and Gordon (67) in a follow up to their previous work (63) published a mechanism for dislocation pinning in the alkali halides. They set up the following requirements for their pinning model:

a. Defects must be created at, or in the immediate vicinity of, free dislocation segments.

b. These defects must act as strong pinning points.

c. The pinning defect must possess a characteristic optical absorption band and be simple enough to be "dissolved" when it is ionized or excited.

d. The defect must occur generally in the alkali halides (with the possible exception of LiF).

e. The model must also be capable of explaining how dislocation pinning can be reversed at low temperatures but converted to a permanent-type of pinning if the crystal is warmed to room temperature.

f. The model must also explain how low energy illumination is capable of unpinning dislocations at low temperatures while high energy illumination can cause additional dislocation pinning at all temperatures.

The terminating row of ions in the extra half-plane of an edge dislocation in the NaCl type lattice can be schematically represented by a row of alternating alkali and halogen ions as $A^+ H^- A^+ H^- A^+$. Suppose that during X-irradiation, a halogen ion located near the dislocation and below its slip plane loses an electron (by capture of a hole). Suppose further that the halogen atom so formed moves one or two atom distances to form a jog on the dislocation and a halogen ion vacancy. The vacancy and the halogen atom each could then capture an electron, forming an F center and a halogen ion attached to the extra half plane of the dislocation. Bauer and Gordon (67) hypothisize that the defect complex formed in this way is the dislocation pinning point produced by X-irradiation at low temperatures which reduced the internal friction. To reverse the sequence and thereby unpin the dislocation the F center need only be ionized, provided it has not diffused away from the dislocation as can happen if the temperature is raised.

To form the F center, a halogen ion would have to be available for the jump to the dislocation plane. The ionic positions near the core of an edge dislocation in NaCl have been calculated by Huntington et al. (68) and are reproduced in Figure 5. At least 8 negative ions are in favorable positions to make a jump into the dislocation core (labeled 1 in Figure 5). Two of the positions (labeled b in Figure 5) are in the plane of the drawing. The other six are the negative ion positions

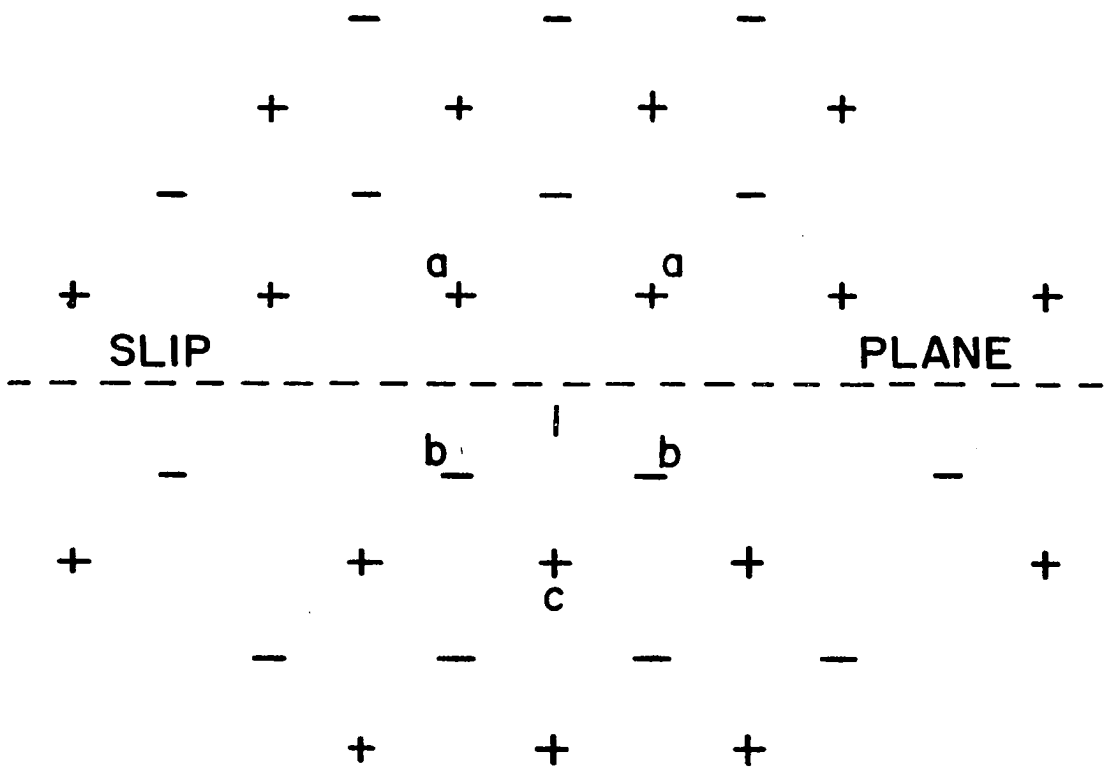

Figure 5. Distributions of ions around the core of an edge dislocation in NaCl by Huntington et al. (68)

directly above or below the positive ions (labeled a and c in Figure 5). In order to act as a pinning point the defect must impede the motion of a dislocation along the slip plane. For slip to occur the halogen ion (position 1 in Figure 5) must move very close to another negative ion. The electrostatic repulsion, coupled with elastic influence, could immobilize the dislocation at this point, pinning the dislocation. Bauer and Gordon (67) offer no proof except that this mechanism could account for the experimental observations.

Low temperature internal friction of LiF single crystals was studied by Gibbons and Chirba (69). Amplitude dependence was not measured. After deformation of approximately 1 per cent in compression, the attenuation of lithium fluoride contained a large peak in the neighborhood of 65°K for a frequency of 80 kilocycles per second. The frequency variation of the attenuation peak position gave an activation energy of approximately 0.2 electron volts per atom. The attenuation in an underformed crystal did not show such an attenuation maximum. The position and activation energy depended upon the purity of the crystal. The maximum peak attenuation decreased with annealing at room temperature, and a 5 minute X-irradiation from a 50 kilovolt, 10 milliamp tungsten target completely removed the attenuation maximum. Possible mechanisms for this behavior were discussed.

Taylor (70) studied the effect of room temperature plastic deformation upon the internal friction of monocrystalline bars of LiF over the temperature range 20 to 273°K at 6 and 40 kilocycles per second at about 1×10^{-7} strain amplitude. Slight deformation increased the overall internal friction and gave rise to a well defined peak at about 72°K at

40 kc/sec. Further deformation up to 5 per cent increased the height of this peak and caused the appearance of a second peak at approximately 169°K. Ageing lowered the height of the 160°K peak more rapidly than that of the lower temperature peak, while annealing at 650°C removed both peaks. From the variations of the peak temperature with frequency, activation energies of approximately 0.15 electron volts and 0.4 electron volts were calculated for the 72°K peak and the 160°K peak respectively. The peak temperature was dependent upon the concentration of impurities, which implied that the activation energy varied with impurity concentration.

Baker (71) measured the amplitude dependent dislocation damping in LiF in 1962. He found that the average dislocation velocities comparable to those present during plastic deformation occurred under periodic stresses more than an order of magnitude below the macroscopic yield stress. This implies that the impediments to dislocation motion effective in plastic deformation were localized at widely separated points along the dislocation. Thus a Peierls-type force would not explain the yield stress. Baker's (71) data fit well with the Granato-Lücke theory. It was concluded that the major pinning points (those responsible for the yield stress) were such things as precipitates.

Okada and Suita (72) subjected sodium chloride crystals to gamma irradiation from zero to about 10^7 röentgen in total doses at room temperature. They were examined during deformation by observation of the yield point on stress strain relationships and by observation of the ultrasonic attenuation changes as a function of load, and by observation of the birefringence band. The yield stress of irradiated sodium chloride

crystals, in general, increased with a gamma dose. For irradiated crystals the attenuation decreased by a small amount, just above the yield stress notwithstanding the onset of plastic deformation, and increased with increasing load. Birefringence due to dislocations in glide bands of sodium chloride crystals clearly showed the initiation of the plastic flow in an unirradiated crystal as well as irradiated.

Crystals of NaCl and LiF with an initial dislocation density of 10^4 per cm^2 were subjected to the actions of a longitudinal stationary wave by Shvidkovsky et al. (73). As the amplitude increased, new dislocations were generated and there appeared first single and then broad diffuse slip bands. Simultaneous measurements of internal friction at a strain amplitude of 10^{-7} established that the internal friction increased as the new dislocations arose, reached its maximum when single slip bands developed, and then decreased as broad slip bands appeared.

Stepanova (74) established a procedure whereby he could etch and photograph the surface of NaCl crystals during deformation. Dislocations occurred in the <110> planes at low stresses. New dislocations were formed in other planes as the stress increased, but the original dislocations were not displaced. At lower stresses the dislocations occurred only in edge planes, but at higher stresses the dislocations appeared in screw planes.

Belozerova et al. (75) studied experimentally the influence of vibrational action on the behavior of dislocations in lithium fluoride and sodium chloride crystals. It was shown that an increase in the amplitude of vibration was accompanied by a nucleation of fresh dislocations, forming single slip bands and subsequently disperse slip bands.

Dependence of dislocation density on vibration time for lithium fluoride crystals was shown. It was concluded that dislocation multiplication in ionic crystals occurred by a means of cross glide mechanism. The yield point of sodium chloride was given as 200 gm/mm^2.

Nadgornyi and Stepanov (76) presented the results of a study of sodium chloride crystals having different impurity contents from the point of view of the characteristics of selective etching, dislocation structure of artificial slips and dislocation glide. The process of slip formation was one of two stages, a stage in which "slip nuclei" were formed and a stage of "slip nuclei" growth, in which the nuclei were propagated in the body of the crystal under the action of low external stresses. Slip nuclei were formed by the application of large local stresses on the surface of the crystal.

Whitworth (77) reported theoretical views on the atomic mechanism for the transport of electrical charge by dislocation in NaCl type crystals. Dislocations on $\{110\}$ planes may be electrically charged due to jogs or vacancies on their cores. Motion of jogs with dislocations could lead to transport of charge in the direction of the Burgers vector. Motion of vacancies, could in principle, produce a flow of charges in any direction on the slip plane, but whether such processes occur and whether thermal activation is necessary depend on the energies of the possible configurations of a vacancy at the core. Experimental work to study in which directions charge is in fact carried and how this depends on temperature is needed. It should then be possible to learn more about the nature of the cores of dislocations.

Anion diffusion in NaCl crystals was studied by the isotopic exchange

technique (78). Diffusion was found to occur both by single vacancies and by vacancy pairs. Diffusion coefficients and activation energies for pure and doped crystals were given.

Stokes (79) has reviewed the mechanical properties of polycrystalline sodium chloride. The tensile behavior of fully dense polycrystalline sodium chloride was correlated with deformation at different temperatures. The transition from brittle to ductile behavior was found to be approximately 175°C for polycrystalline NaCl and was about 100°C lower for single crystal NaCl. Below 150°C there was little plasticity in the polycrystalline NaCl. Slip bands were straight and the strain discontinuity could not be accommodated at the grain boundaries. Above 150°C the onset of wavy slip permitted adjacent grains to conform and there was a marked increase in plasticity. Above 200°C deformation was accompanied by grain boundary sliding, polygonization and recrystallization and the specimens elongate for a truly ductile fracture. These observations were compared with recent observation on polycrystalline magnesium oxide.

Using dielectric measurements Dryden et al. (80) have provided information about the manner in which certain divalent cations are incorporated in the NaCl, KCl, and LiF lattices. It is well known that the hardness of alkali halides increases considerably when low concentrations of divalent cations are incorporated in the crystal lattice. The measurements reported were on NaCl; Ca^{++}, NaCl; Mn^{++}, KCl; Sr^{++}, KCl; Ba^{++} and LiF; Mg^{++}. The principal results were: (1) the increase in critical shear stress were proportional to $c^{2/3}$, where c was the concentration of divalent ion-vacancy pairs, (2) there was no increase in

hardness as these divalent ion-vacancy pairs aggregate into groups of three (trimers), (3) in NaCl:Ca^{++} there was no increase in hardness as those trimers grew into larger aggregates, and (4) in NaCl:Ca^{++} the hardness increases as a second region of dielectric absorption appears. It was concluded that although the structure of the trimer was the same in all the crystals, the trimer could grow in two ways, one of which produced an increased resistance to the movement of dislocations. It was suggested that the aggregates which contribute to the increase in hardness in NaCl:Ca^{++} are different in structure and do not grow from the trimers.

It is clear that internal friction studies have provided information concerning defect interactions of importance in understanding the mechanical behavior of crystals. The atomic configuration making up a pinning point in NaCl was identified. Deformation in the common alkali halides is determined by the motion of pinning points. The dislocation is free to move between such points. Dislocation multiplication occurred by means of a cross glide mechanism.

III. METHOD OF PROCEDURE

The internal friction of NaCl was measured by the composite oscillator technique. This method was chosen for several reasons. It yields virtually instantaneous values for both the decrement and the strain amplitude. Relatively precise values of strain amplitude can be computed in 10^{-8} to 10^{-4} region. The decrement can be measured when the resonator is vibrating exactly at its maximum strain amplitude, which is essential for the valid measurement of any amplitude dependent decrement.

The variables introduced were grain boundaries, strain amplitude, temperature (23° - 300°C), and dislocations. Measurements taken were the logarithmic decrement and the dislocation density. All factors were correlated.

Two -18.5 degree X-cut quartz crystals were obtained from the Northern Engineering Corporation. Each crystal was 0.158 inch square and approximately 1 inch long. The exact length was cut so the longitudinal fundamental mode of vibration was approximately 100,000 cycles per second. The frequency of the two crystals, verified with a Model 522B Hewlett Packard electronic counter, was matched to within 0.02 per cent. To prevent electrical coupling the crystals were silvered and placed together as shown in Figure 6. The dummy fused quartz rod was 0.158 inch in diameter and approximately 4.55 inches in length. The length was cut to match 4 times the fundamental vibration mode of the quartz crystals. The use of the fused quartz rod allowed the salt to be tested at raised temperatures while the piezoelectric crystals remained at room temperature. The piezoelectric crystals and the fused quartz rod were permanently

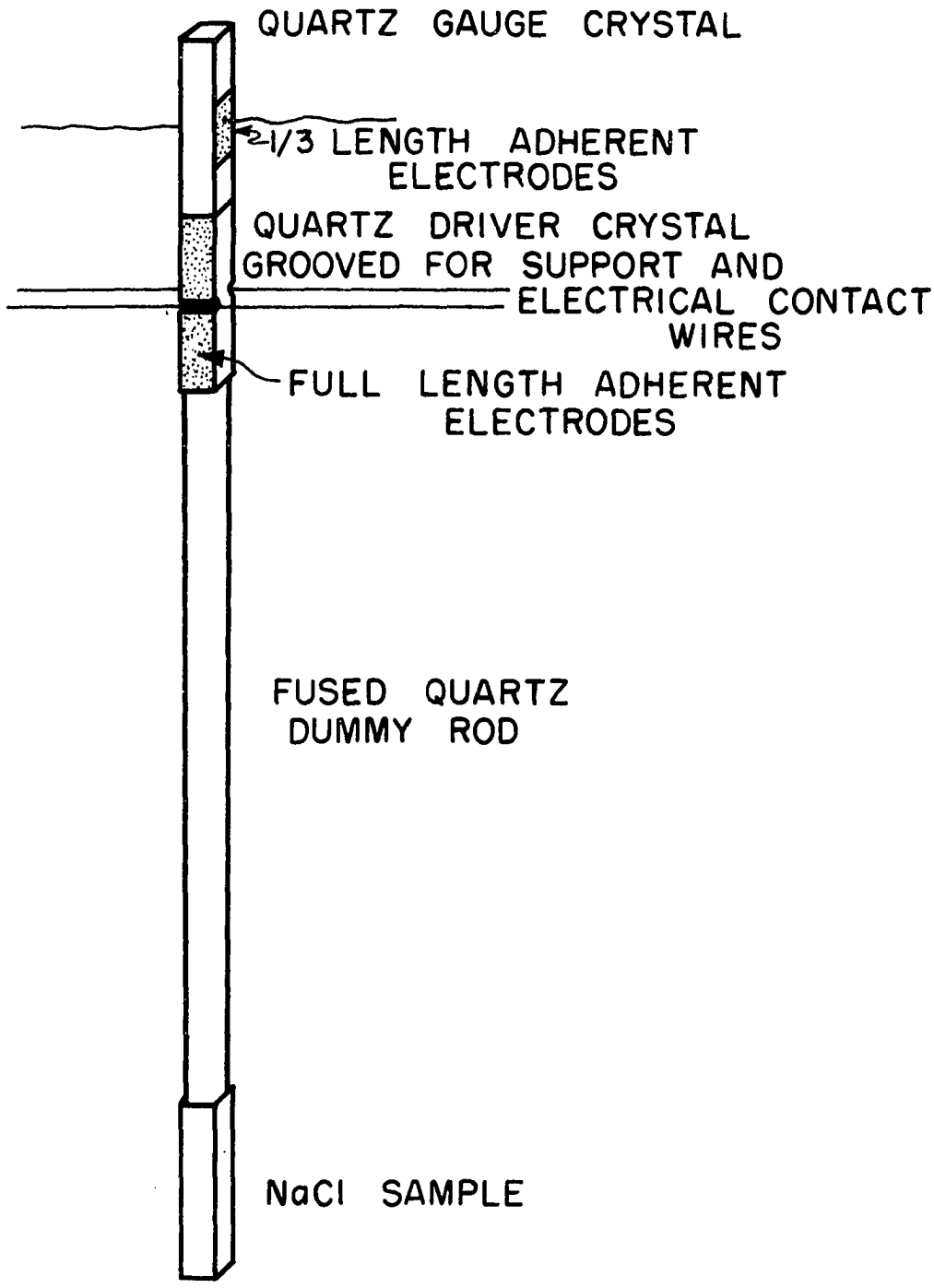

Figure 6. Composite oscillator

glued with Armstrong A-12 cement. The NaCl specimen was glued to the dummy rod with Sauereisen No. 1 cement.

Spectroscopic quality NaCl was obtained from Harshaw Chemical Company and Isomet Chemical Corporation in single crystal bulk sections approximately 2 inches square by 1 inch thick. Impurity concentrations were as shown in Table 1.

Table 1. Impurity concentrations

Impurities	Isomet NaCl	Harshaw Stockbarger NaCl	Harshaw Kyropoulos NaCl
Al	5-10 ppm	50	4-5 ppm
Ca	50	10	4-5
Cu	< 1	50	< 1
Fe	< 1	--	1-2
Mg	< 1	--	2
Si	2	10	1-2

Polycrystalline NaCl was formed by straining a single crystal, either by extruding the single crystals (2:1 reduction in diameter) or by compressing the single crystal, and then recrystallizing the NaCl at 650°C for a period of 24 hours. A string saw (81) was used to cut the bulk crystals, either single or polycrystalline, to approximate test size. A small amount of water polishing was then required to produce a test specimen with a resonant frequency matching that of the composite oscillator. The test specimens were then annealed at 600°C for 24 hours.

The electrical circuit of the system is shown in Figures 7 and 8. An a.c. electrical signal applied to the driver crystal caused the oscillator to vibrate. The gauge crystal developed an alternating voltage between its electrodes which was used as a measure of the standing longitudinal vibration amplitude. This signal was measured with a high impedance circuit which contained the output voltage gauge, the oscilloscope, and the cathode follower. The cathode follower measured part of the gauge signal to control the input signal, allowing the composite oscillator to seek its own resonant frequency.

The dislocation density of the crystals was measured after vibration at each increasing amplitude. The crystals were allowed to vibrate at each amplitude for approximately one minute. The crystals were etched for 15 seconds with a concentrated $FeCl_3$-glacial acetic acid solution. Photographs (Figures 9a and 9b) were taken of the etched surfaces at required magnifications. The magnifications were verified with a stage micrometer. The number of etch pits per square centimeter were counted.

The logarithmic decrement was determined at various strain amplitudes and temperatures (23°C to 300°C) by measuring the free vibration rate of decay of the composite oscillator. The driving voltage was disconnected and the resulting damped vibrations were displayed on an oscilloscope. The oscilloscope trace was photographed (Figure 10) and measurements made on the photograph. The NaCl test specimen was not removed from the oscillator at any time during a test. Figure 11 shows the composite oscillator in the support apparatus. All testing was accomplished in a 0.1 to 0.5 micron vacuum. A photograph of the assembled test equipment is shown in Figure 12.

Figure 7. Block diagram of electrical circuits

Green and yellow - gauge circuit
Red - driver circuit
Black - electrical ground

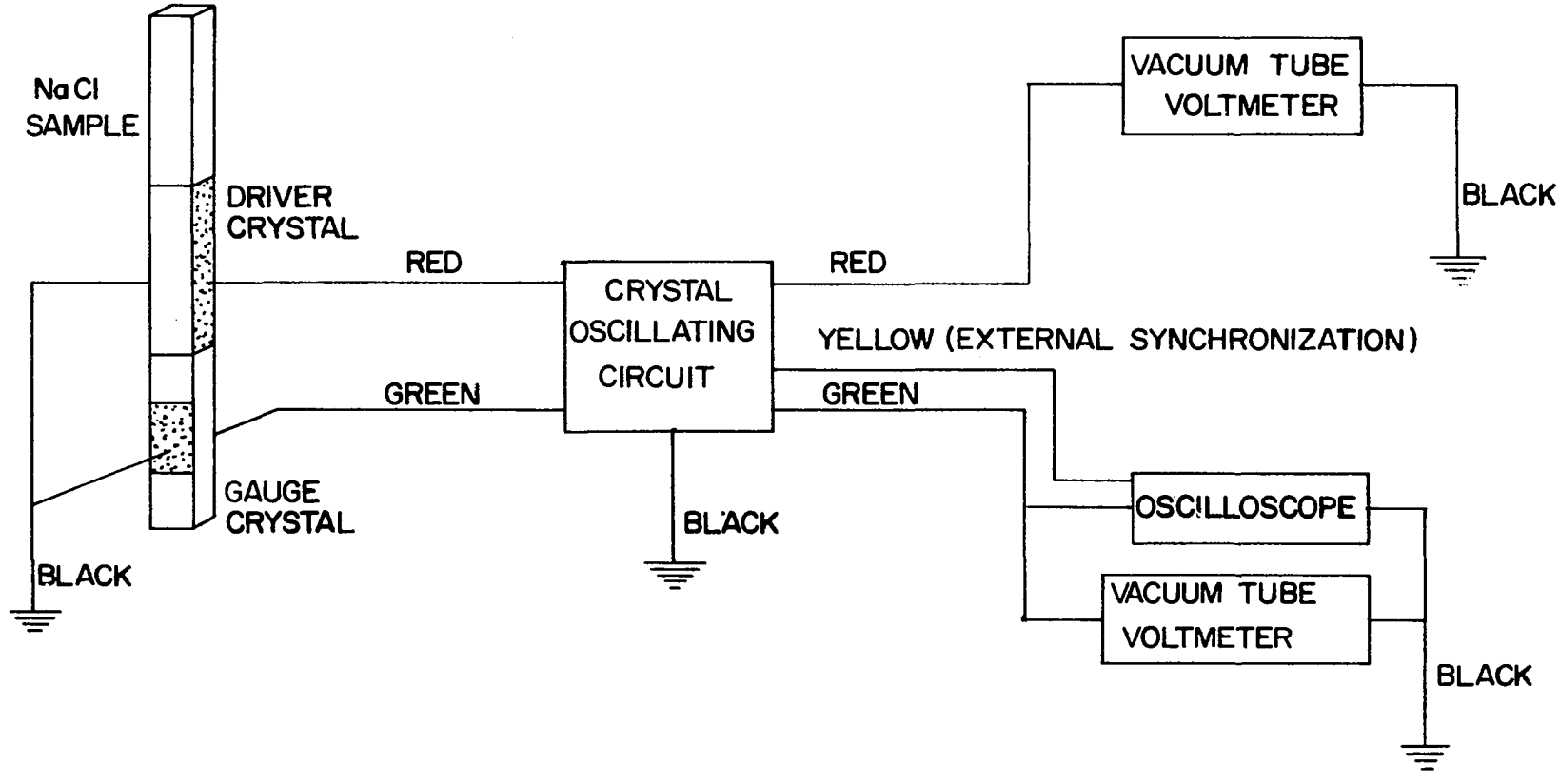
NaCl
SAMPLE
DRIVER
CRYSTAL
GAUGE
CRYSTAL
BLACK
RED
GREEN
CRYSTAL
OSCILLATING
CIRCUIT
BLACK
RED
YELLOW (EXTERNAL SYNCHRONIZATION)
GREEN
VACUUM TUBE
VOLTMETER
BLACK
OSCILLOSCOPE
VACUUM TUBE
VOLTMETER
BLACK

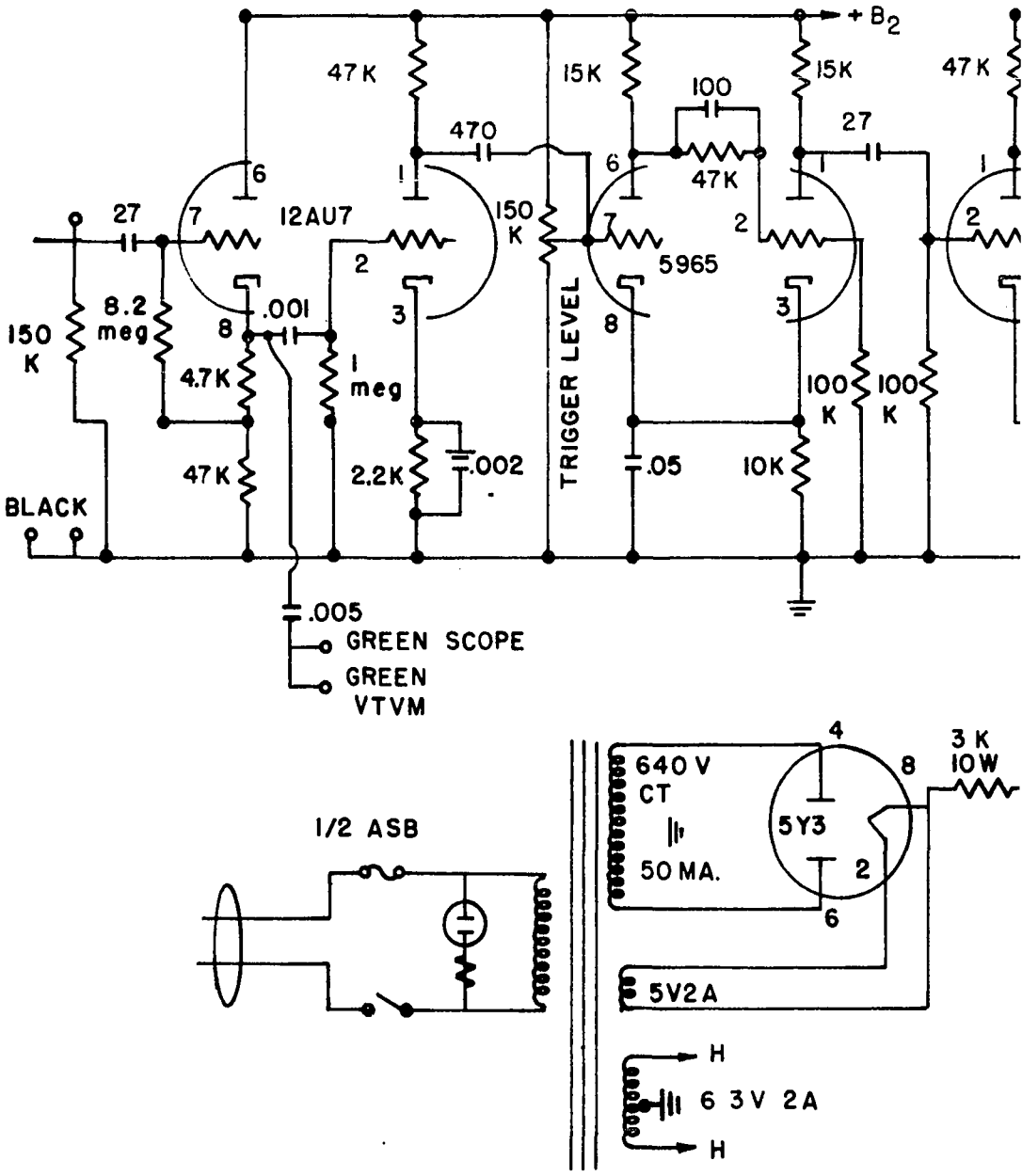

Figure 8. Circuit diagram of crystal oscil

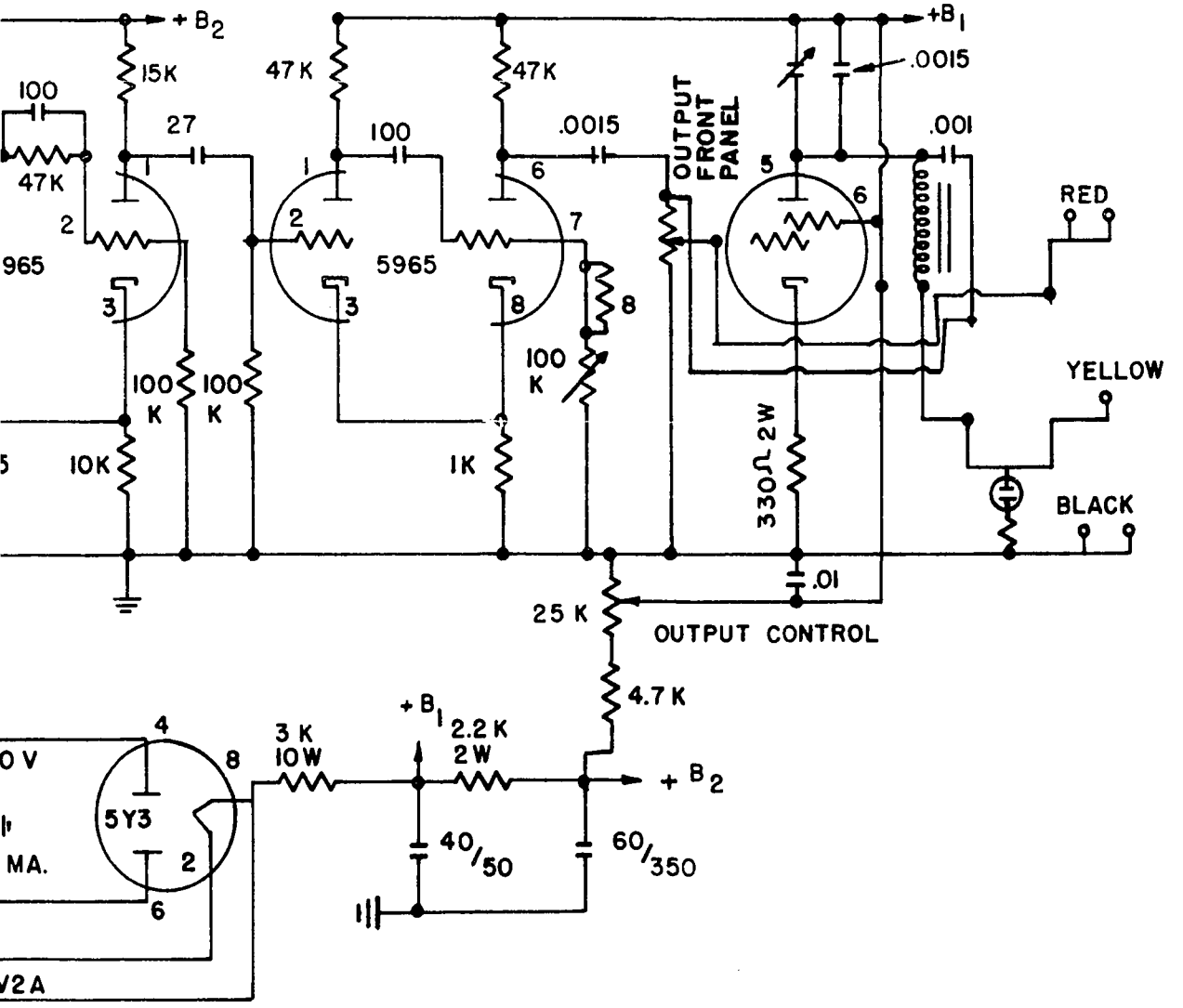

diagram of crystal oscillating circuit –

Figure 9a. Etched NaCl surface (150X)

Figure 9b. Etched NaCl surface (150X)

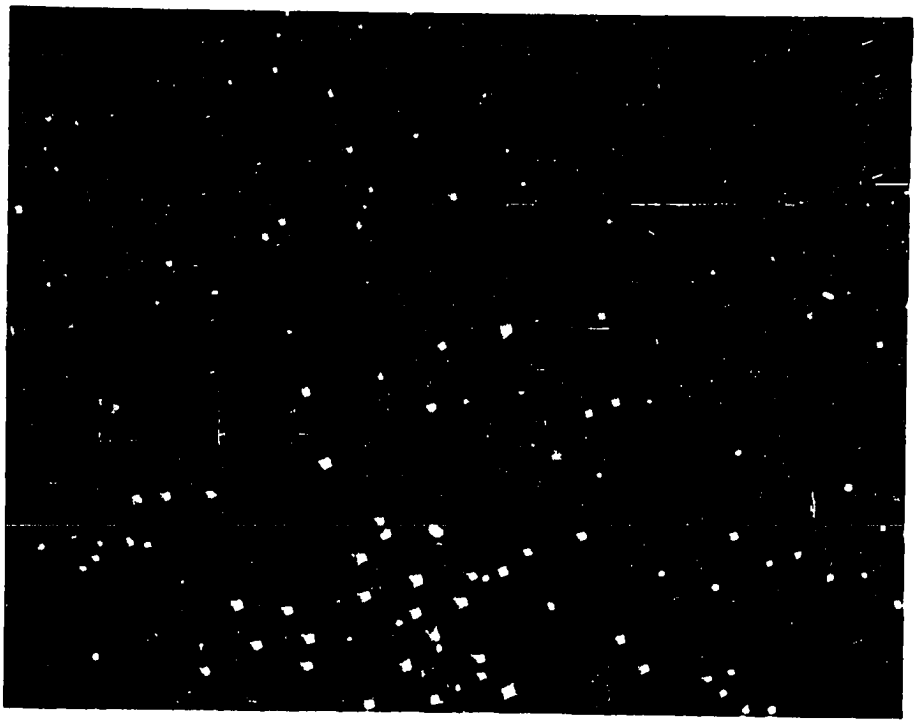

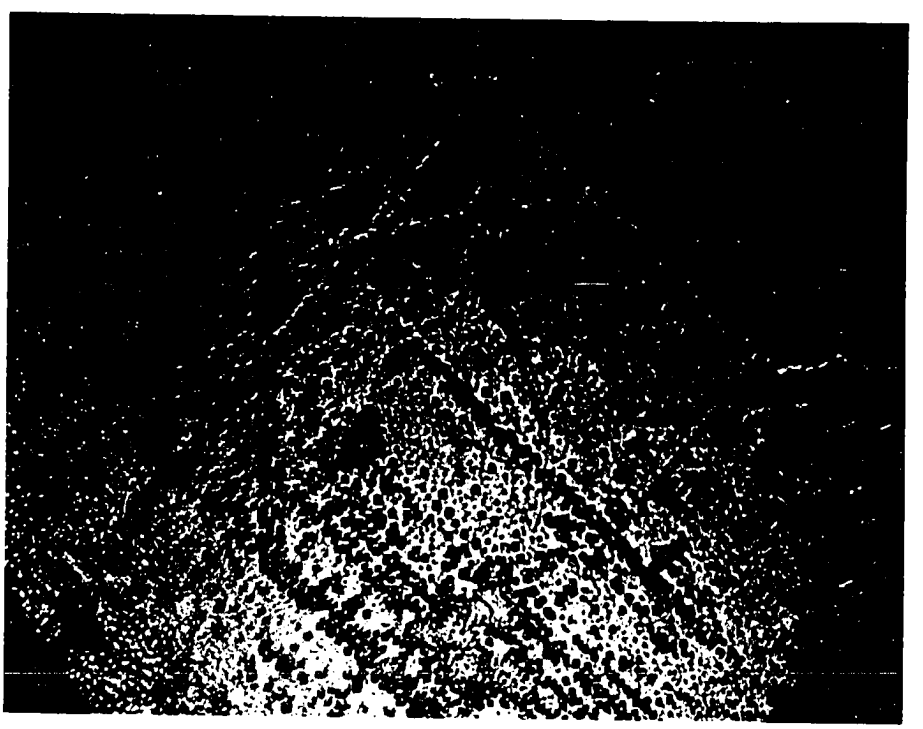

Figure 10. Amplitude decay as shown on oscilloscope

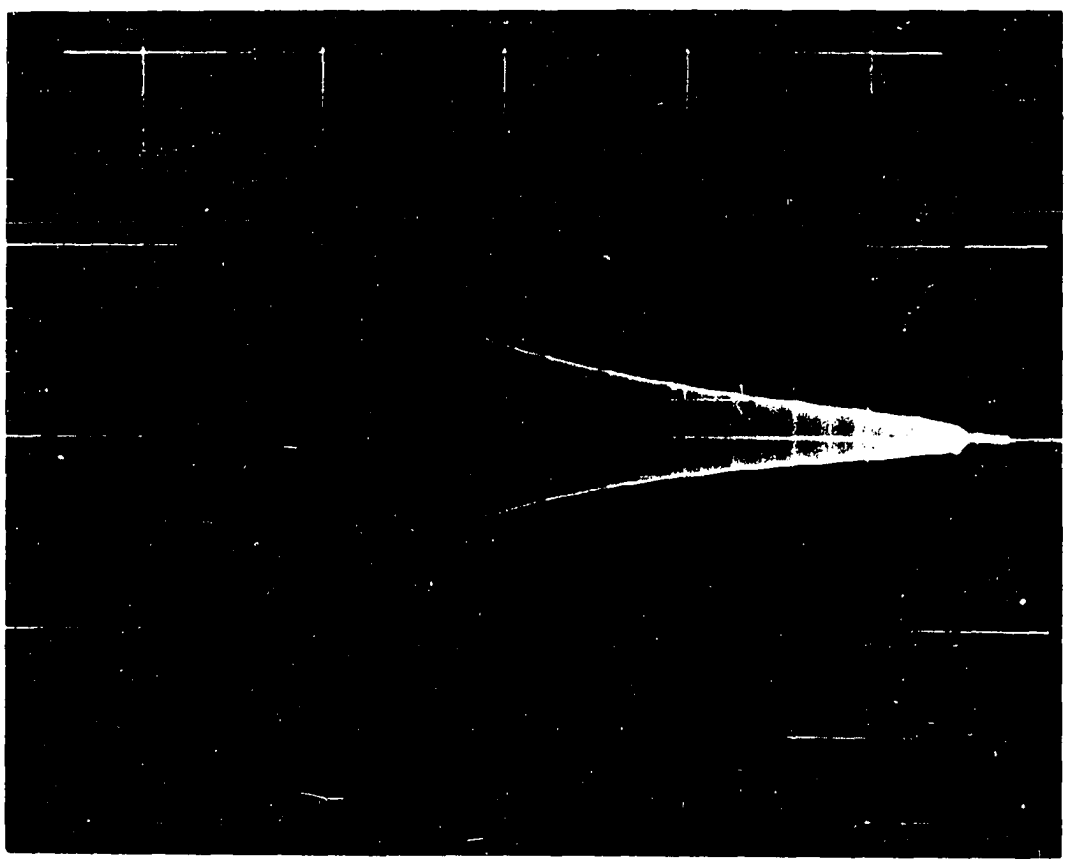

Figure 11. Composite oscillator in support apparatus

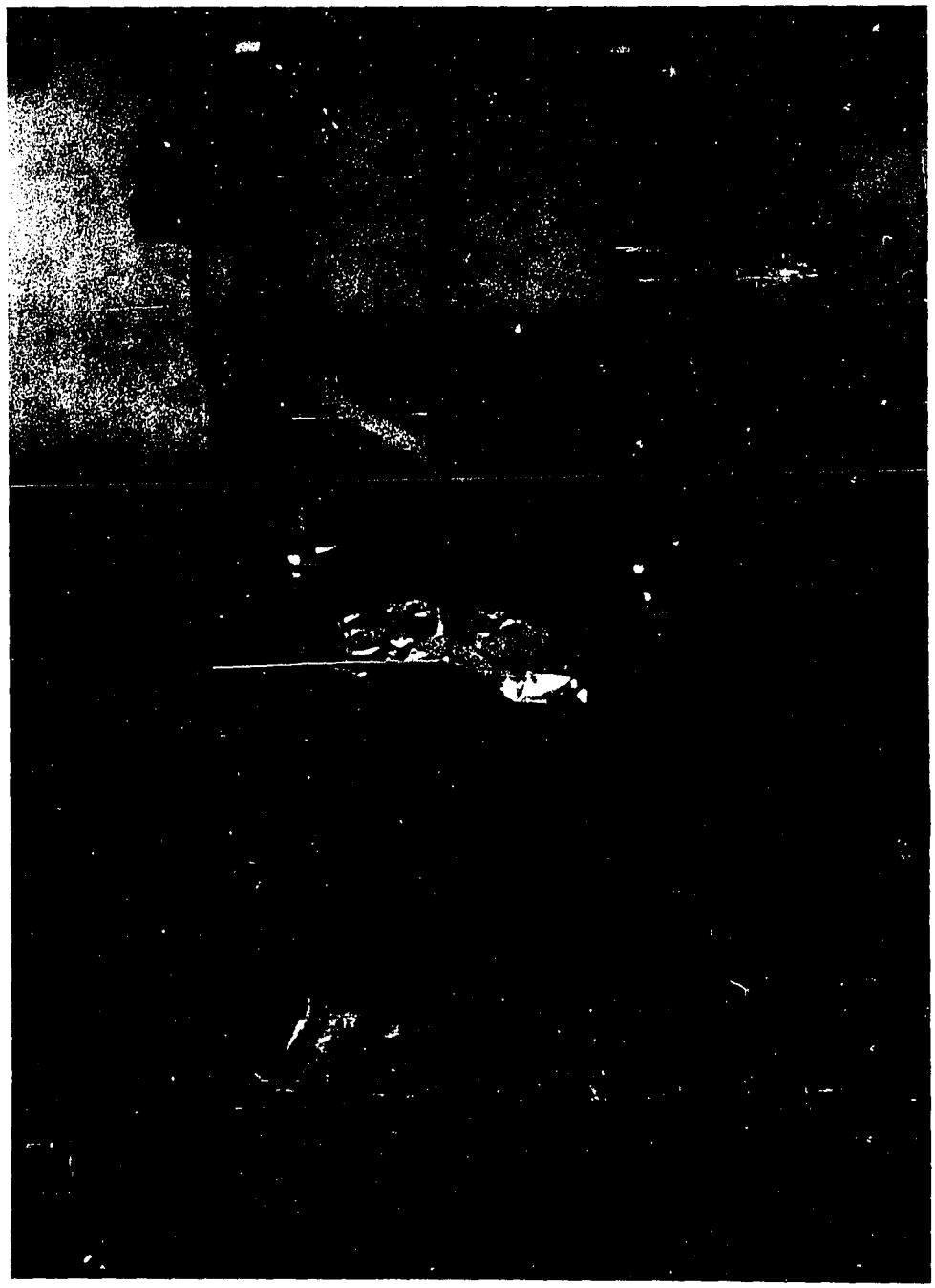

Figure 12. Equipment assembly

To find the log decrement the logarithm of the voltage amplitude was plotted vs. time. The slope of the line at any amplitude divided by the frequency was the logarithmic decrement at that strain amplitude. The following equations were used to calculate the logarithmic decrement of the NaCl.

$$\varepsilon_g = (CF^{-2})V \tag{18}$$

$$\varepsilon_s = (C_g/C_s)\ _g \tag{19}$$

$$\delta_s = (m_t\ \delta_t - m_g\ \delta_g)/m_s \tag{20}$$

where

ε_g = maximum strain amplitude in the gauge crystal

C = factor depending on piezoelectric constants of the quartz and the geometry of the apparatus

F = resonant frequency (100,000 cycles/second)

$(CF^{-2}) = 0.5 \times 10^{-5}$ for apparatus used

V_g = voltage across gauge crystal

ε_s = strain amplitude of salt specimen

C_g = axial velocity of sound in quartz

C_s = axial velocity of sound in NaCl

δ_s = logarithmic decrement of NaCl test specimen

δ_t = logarithmic decrement of total composite oscillator (with NaCl test specimen)

δ_g = that part of logarithmic decrement not due to NaCl (losses due to quartz, glue joints, etc.)

m_t = mass of total assembly

m_g = mass of composite oscilator without NaCl

m_s = mass of NaCl test specimen.

IV. FINDINGS

The experimental data has been divided into two parts. Part A will relate information gained at room temperature. Part B will relate the effect of raised temperatures on the internal friction of the NaCl test specimens. Both parts will include data on single crystal and polycrystalline sodium chloride. Only graphs of the experimental data will be shown in this section. The tables of raw data can be found in the Appendix.

A. Room Temperature Findings

In order to measure the internal friction of the NaCl, it was necessary to find the internal friction of the quartz portion of the composite oscillator (Table 6). The internal friction of the quartz does not change appreciably with strain amplitude. Regular checks were made to insure that the internal friction of the quartz had not changed with usage.

Single crystals were compressed and reheated to form polygonized sodium chloride so the effects of grain boundaries could be studied. Two series of NaCl crystals were compressed varying amounts (Table 2), annealed at 600°C for 24 hours, polished to size and reannealed at 600°C for 24 hours. Each series, G through L and M through V, was taken from a different bulk ingot. The grain size was reported as the average area of the grain. Compression greater than 2% caused polygonization which decreased grain size as compression increased (Figure 13). Effective polygonization was not apparent below 2% compression.

Figure 13. Recrystallized grain boundaries after 0, 1/2, 1, 2, 4, and 8 per cent compression (75X)

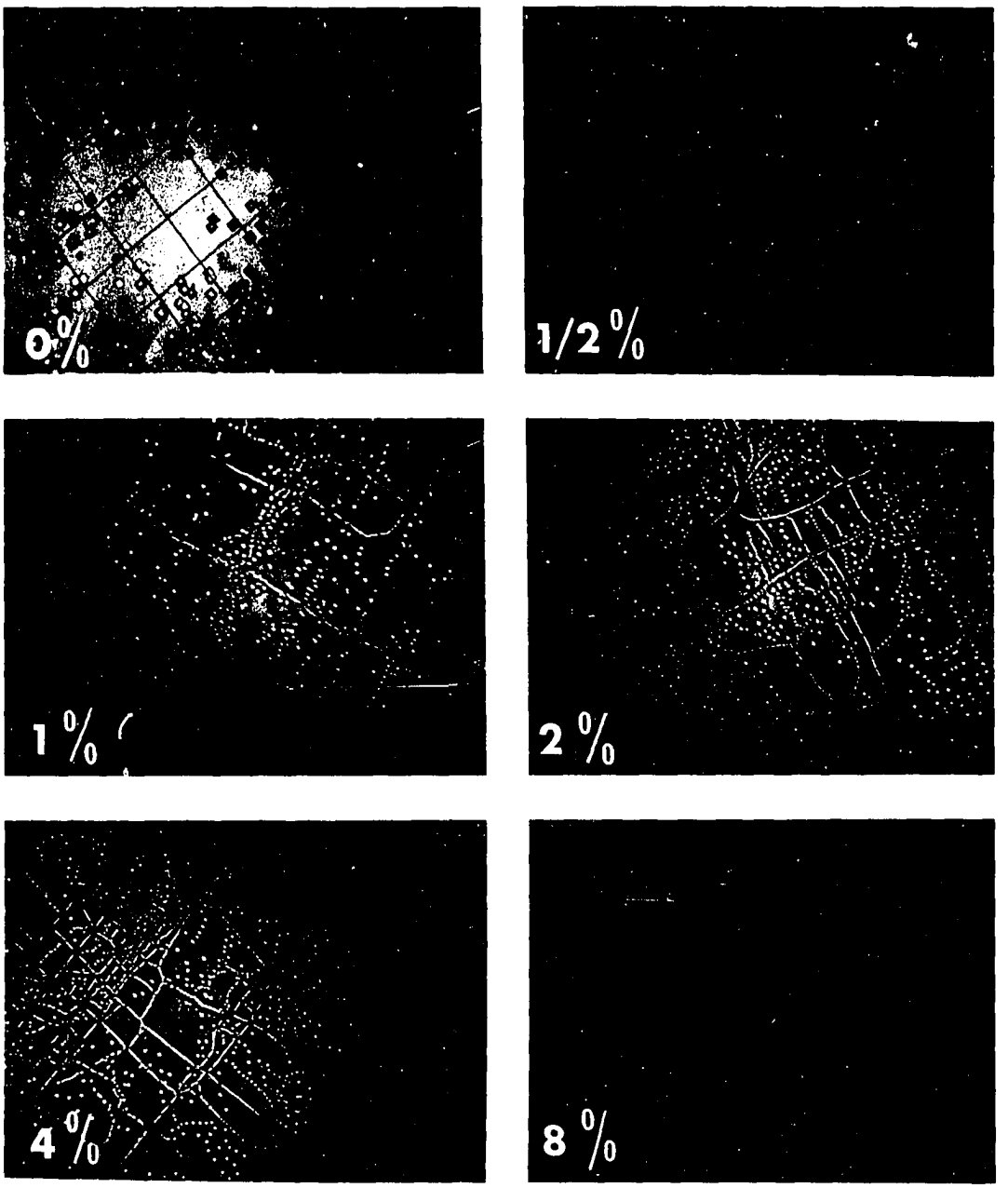
0%
1/2%
1%
2%
4%
8%

Table 2. Compression and resulting grain size (Stockbarger NaCl)

Specimen	Per cent compression	Grain size (cm^2)
G	0	single crystal
H	0.5	very few grain boundaries
I	1.0	very few grain boundaries (slip planes developed)
J	2.0	2×10^{-4} (some areas still single crystal)
K	4.0	3.2×10^{-5}
L	8.0	1×10^{-6}
M	0	single crystal
N	0.2	very few grain boundaries
0	0.8	very few grain boundaries (slip planes developed)
P	1.5	1×10^{-3} (long slender grains)
Q	1.72	2×10^{-4} (long slender grains)
S	2.65	5×10^{-5}
V	5.50	8×10^{-6}

The internal friction increased as the dislocation density increased until they collected to form grain boundaries (Figure 14). The internal friction decreased as the grain size decreased. Even though polygonized, the internal friction of crystals G through L did conform to the Granato-Lücke theory (Figure 15).

The dislocation density is shown as a function of strain amplitude in a standard plot (Figure 16) and in a logarithmic plot (Figure 17). The dislocation density increased logarithmically with strain amplitude over the range tested. Crystal L which was compressed 8 per cent had such a high dislocation density that density measurements could not be made. The 20 X 10^6 dislocation/cm^2 is an approximation made before attaching the crystal to the oscillator.

Figure 18 shows the relationship between the number of free dislocations formed (those not associated with a grain boundary) and the compression strain. The number of free dislocations present agrees well with the internal friction data shown in Figure 14. The maximum internal friction occurs with the maximum number of free dislocations.

Crystals M through V were cut from a second Stockbarger bulk single crystal and then processed as shown in Table 2. Even though this salt appeared to be harder throughout all tests the same trends appeared as were present in crystals G through L. Figure 19 is the internal friction vs. strain amplitude plot and Figure 20 is the Granato-Lücke plot for crystals M through V. Note that in Figure 20 the slopes are all very similar suggesting similar values for L_c.

To separate the effects of free dislocations and dislocations pinned

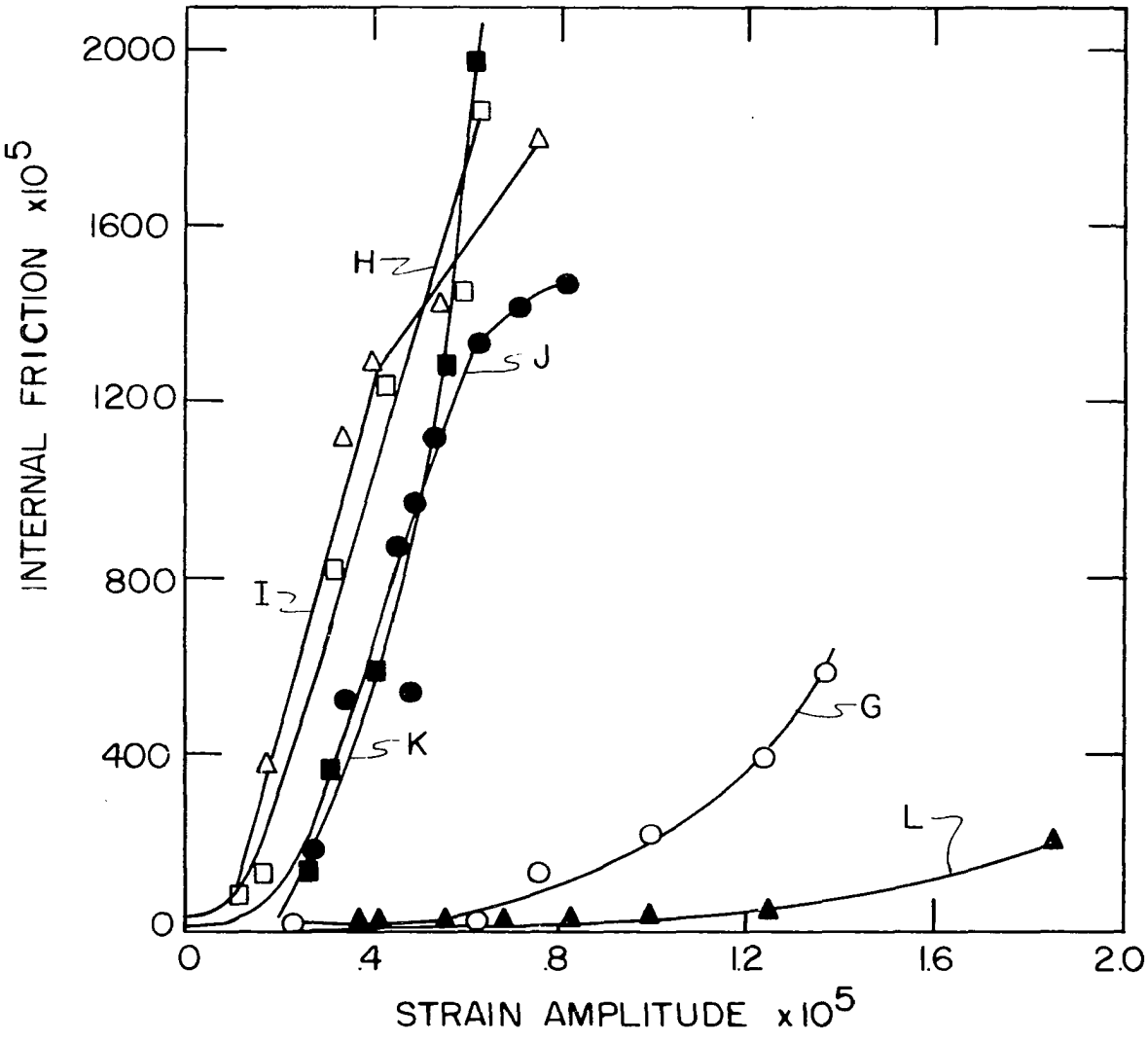

Figure 14. Internal friction versus strain amplitude showing the effect of grain boundaries

10,000
1,000
$(\dot{\epsilon}_s \delta_5 \times 10^{10})$

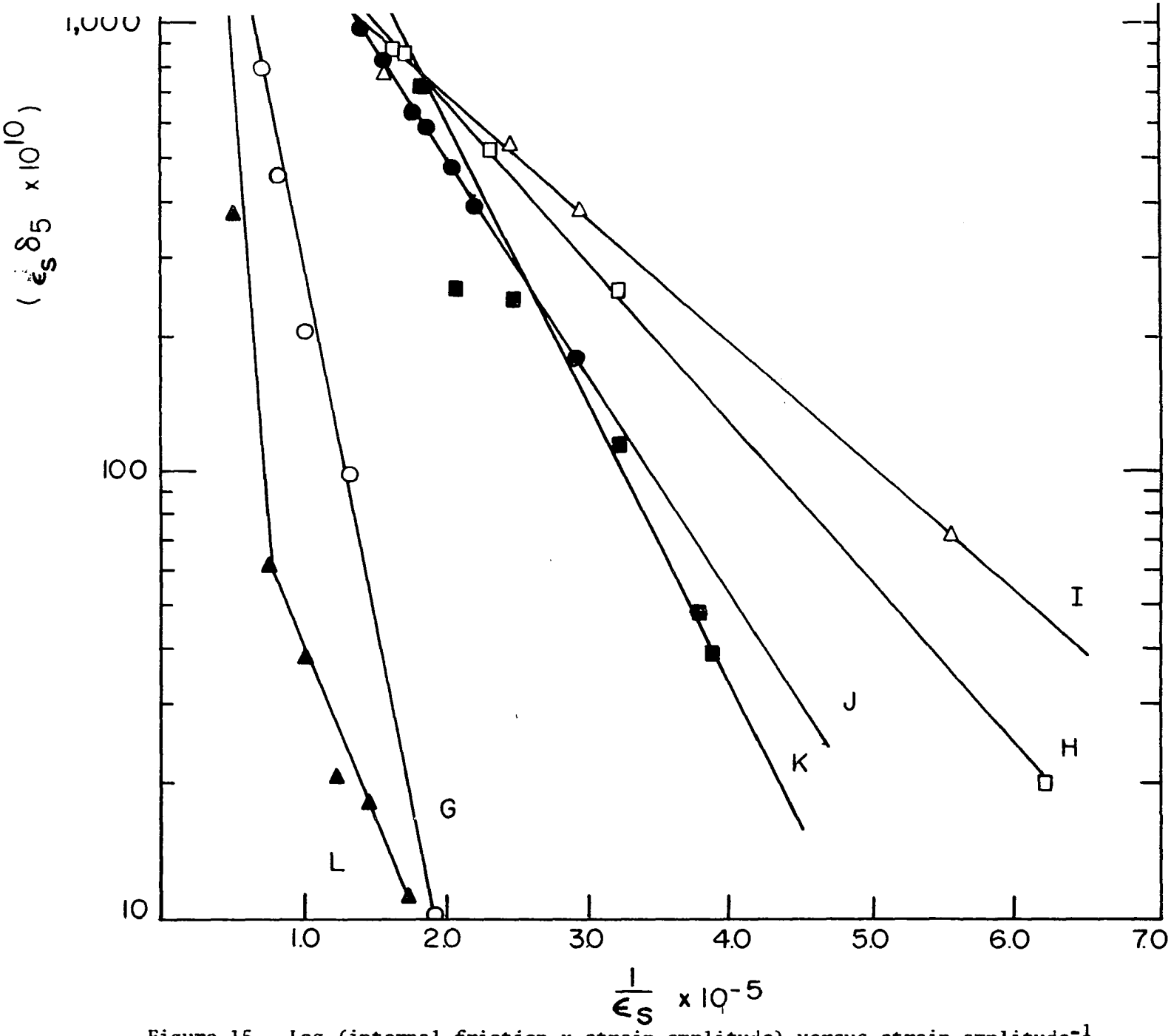

Figure 15. Log (internal friction x strain amplitude) versus strain amplitude^{-1} showing the effect of grain boundaries

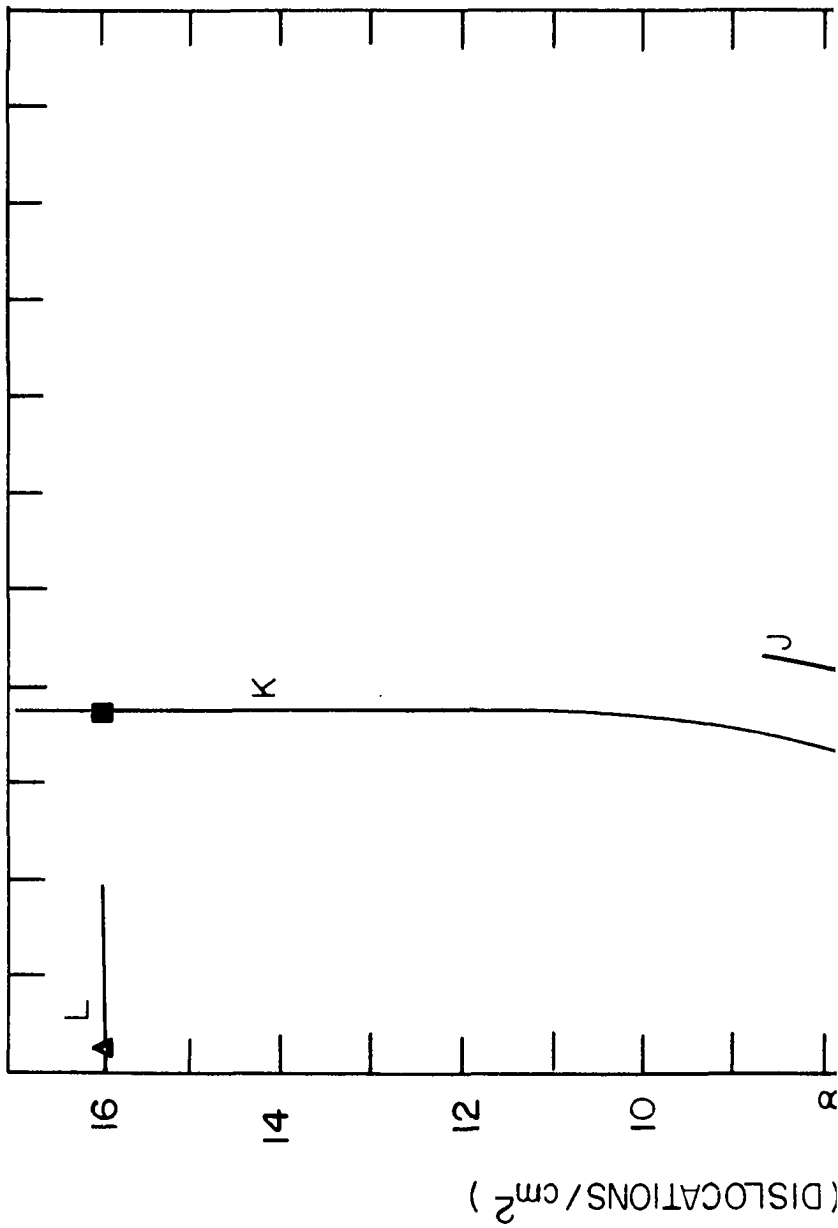
J
K
L
16
14
12
10
α
(DISLOCATIONS / cm²)

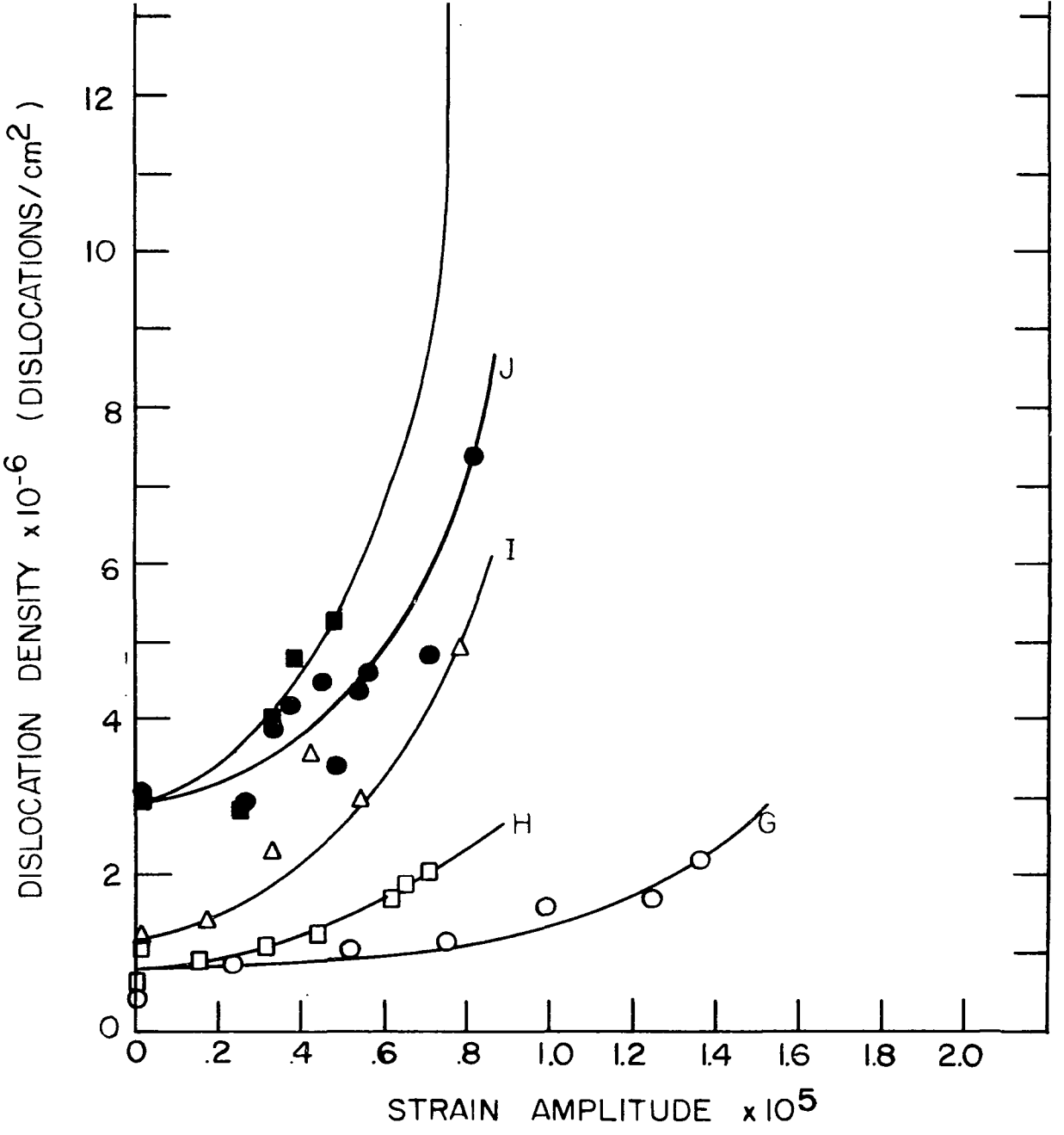

Figure 16. Dislocation density versus strain amplitude showing the effect of grain boundaries

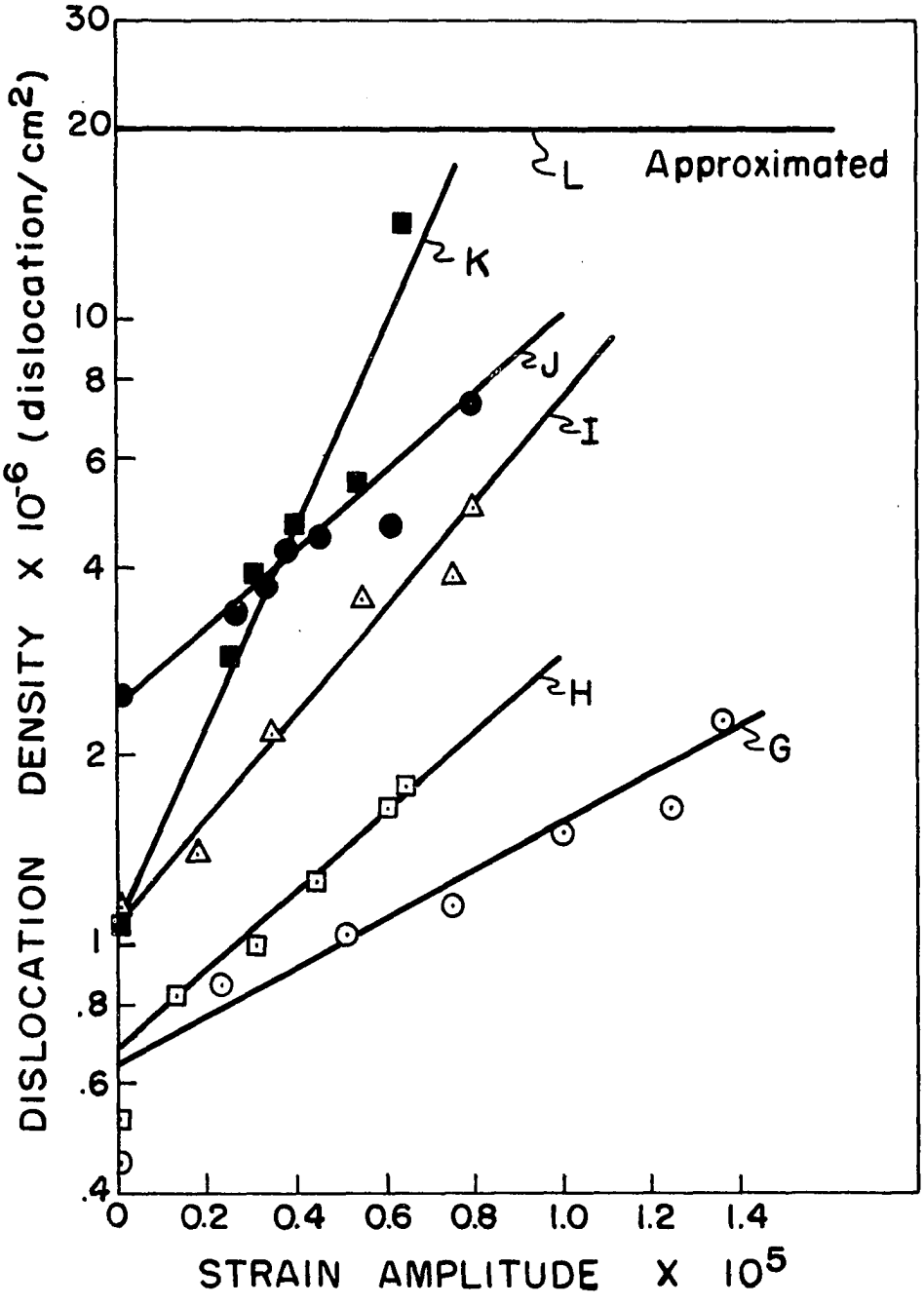

Figure 17. Dislocation density versus strain amplitude showing the effect of grain boundaries

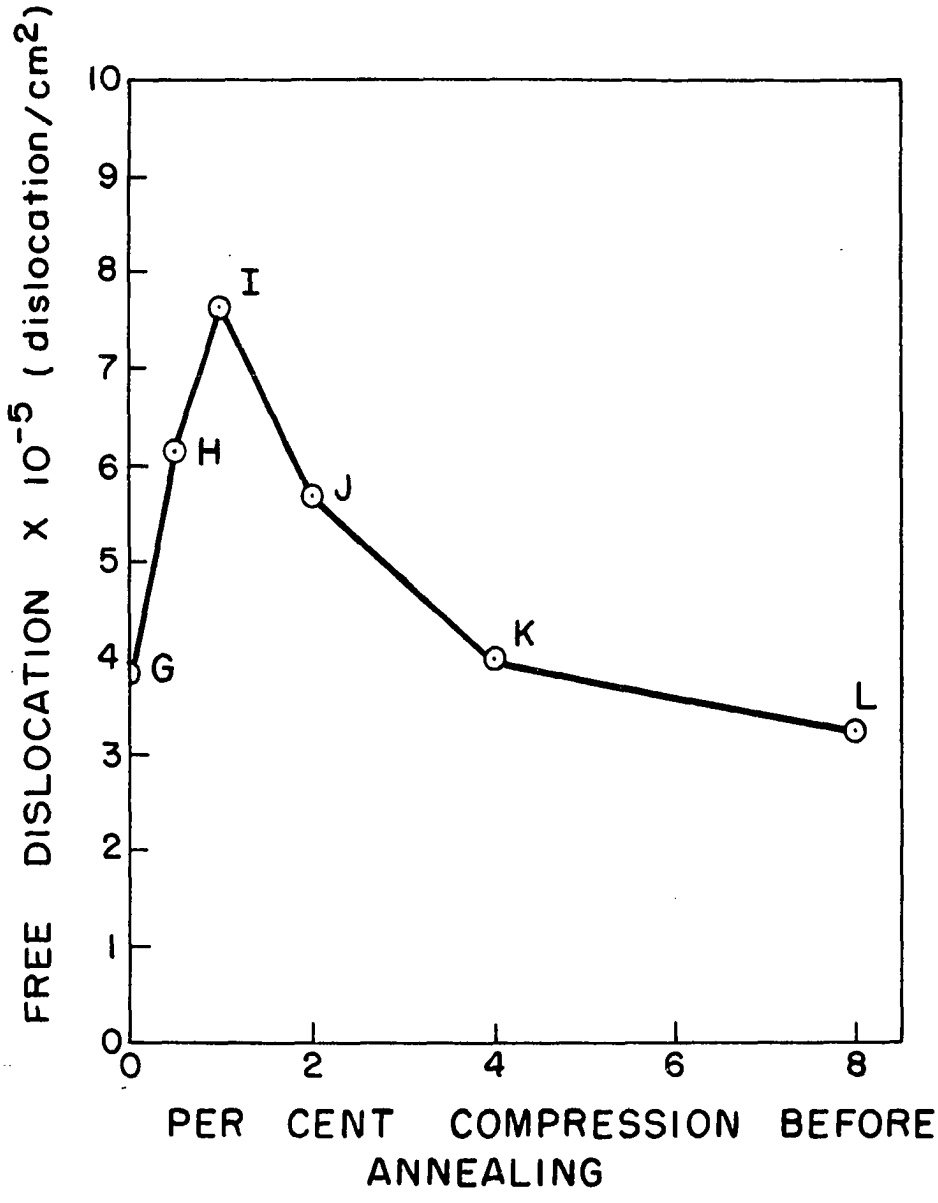

Figure 18. Free dislocations versus preannealing compression

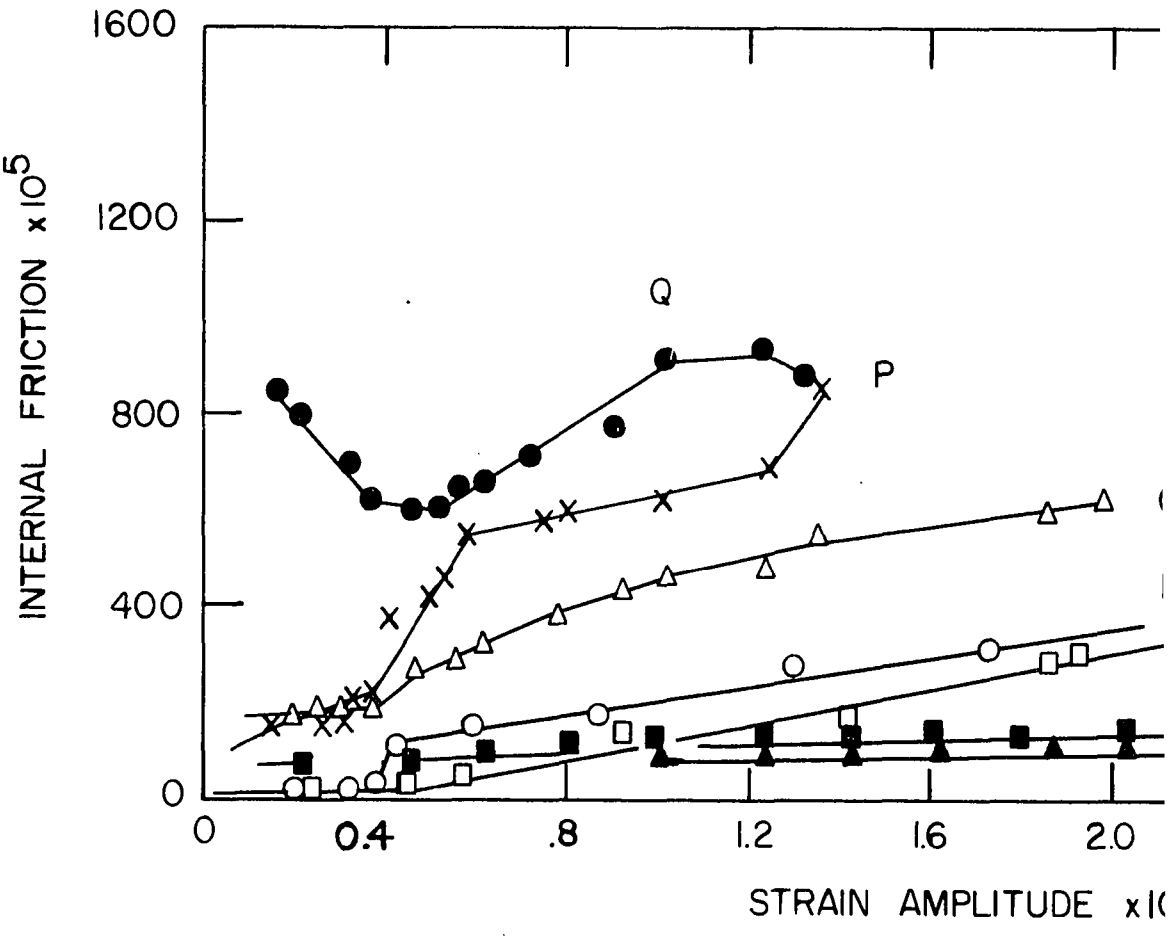

Figure 19. Internal friction versus strain amplitude showing the

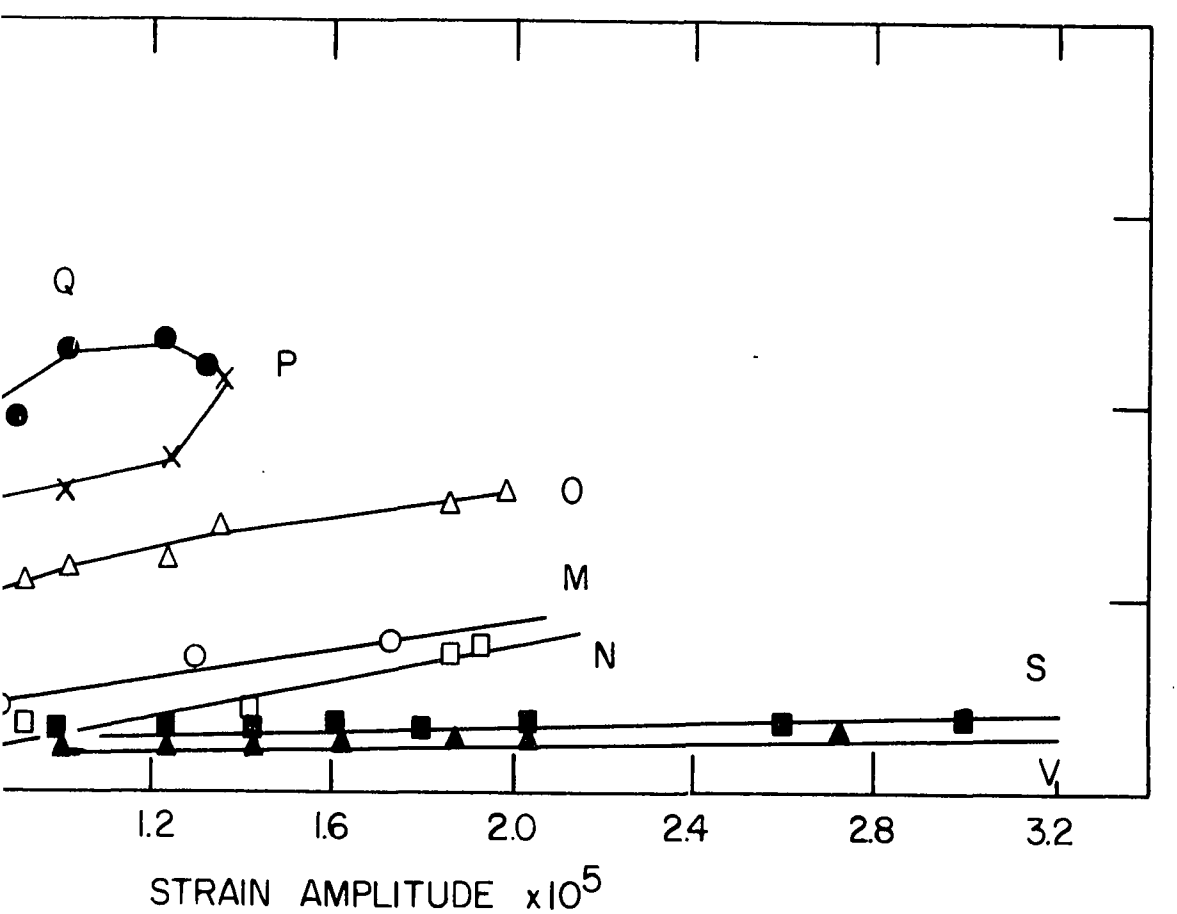

ɔn versus strain amplitude showing the effect of grain boundaries

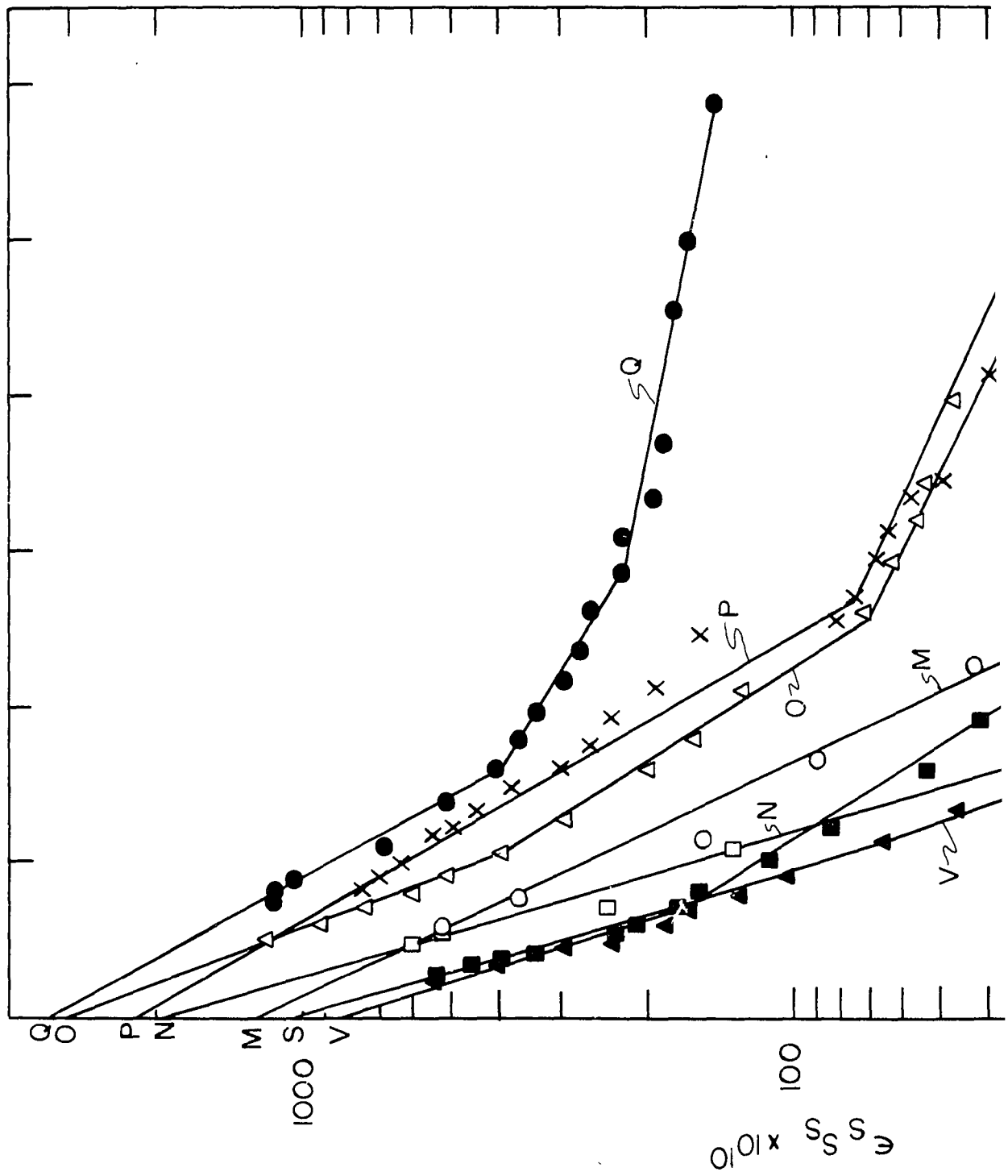
Q
P
N
M
S
V
1000
100
$\epsilon_S S_S \times 10^{10}$

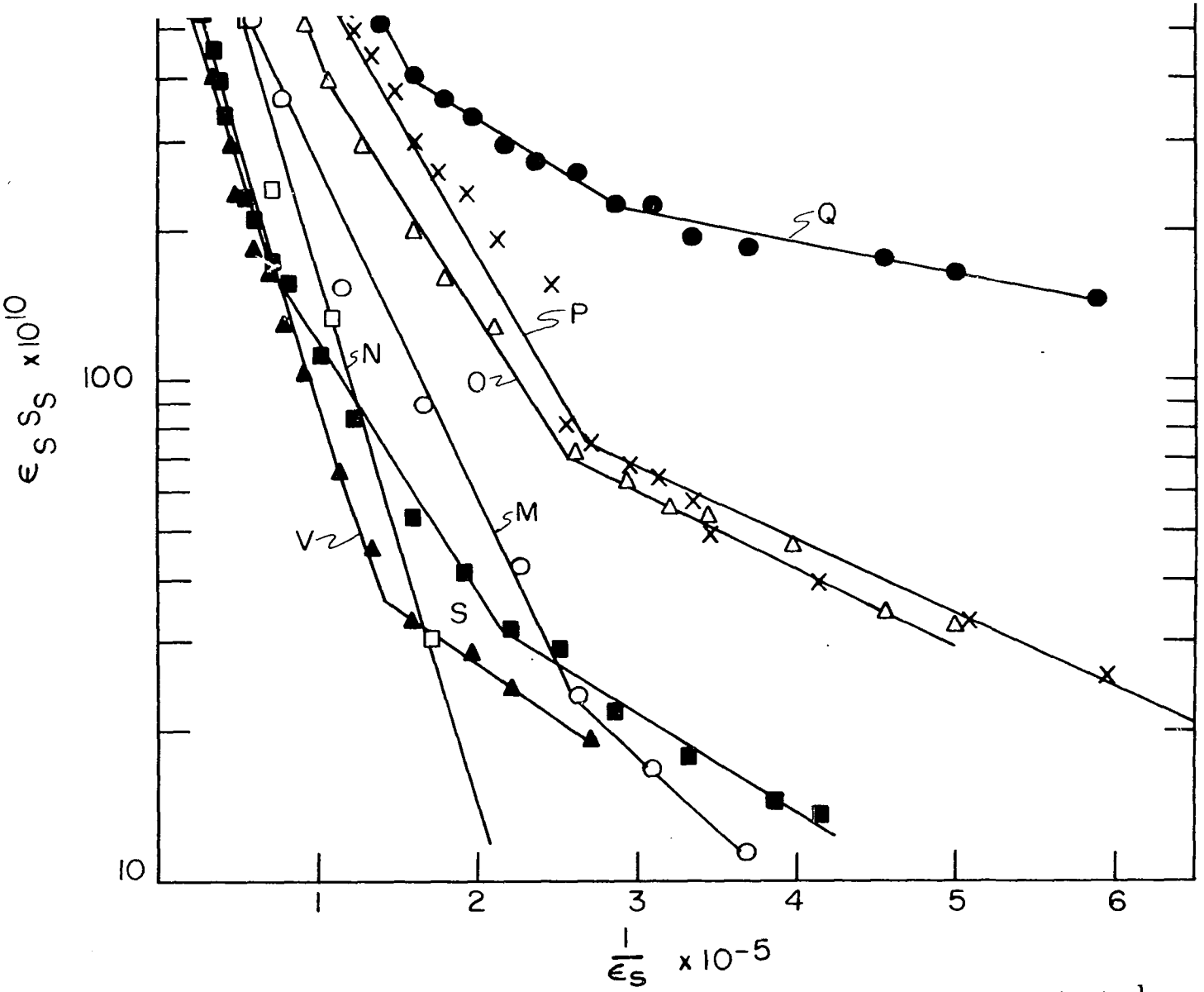

Figure 20. Log (internal friction x strain amplitude) versus strain amplitude^{-1} showing the effect of grain boundaries

as part of a grain boundary, a bulk crystal was annealed at 600°C for 48 hours, compressed 6.85 per cent, polished to test size and tested as crystal X. The crystal was then reannealed at 600°C for 40 hours and retested as crystal Y. Upon reannealing the crystal formed many small-angle grain boundaries. The data for crystals X and Y are given in Tables 20 and 21 and Figures 21 and 22. The dislocation density was not measured. When tested as crystal X the internal friction was very high and there appeared to be very little amplitude dependence. Note, however, that the maximum strain amplitude reached was only 0.5×10^{-5}. After reannealing (crystal Y) the internal friction was much lower (Figure 21). Both tests resulted in typical Granato-Lücke plots (Figure 22).

To study the effect of grain boundaries with free dislocations present, a series of crystals were compressed various amounts, annealed to form grain boundaries, and then recompressed 0.5 per cent to form free dislocations (Table 3). The results are listed in Tables 22 through 27 and Figures 23 and 24. Note that the internal friction found was again quite high. Again, however, the same trend as found in the previously compressed crystals was evident. Any compression less than approximately 2 per cent does not result in grain boundary formation upon reheating. The grain boundaries did pin the dislocation or at least impede their motion.

The effect of impurities was noted by comparing the internal friction of the Kyropoulos, Stockbarger, and Isomet single crystals (Tables 28 and 29, Figure 25). The Kyropoulos NaCl has the highest losses, showing evidence of the pinning effect of impurities. Note that even though the

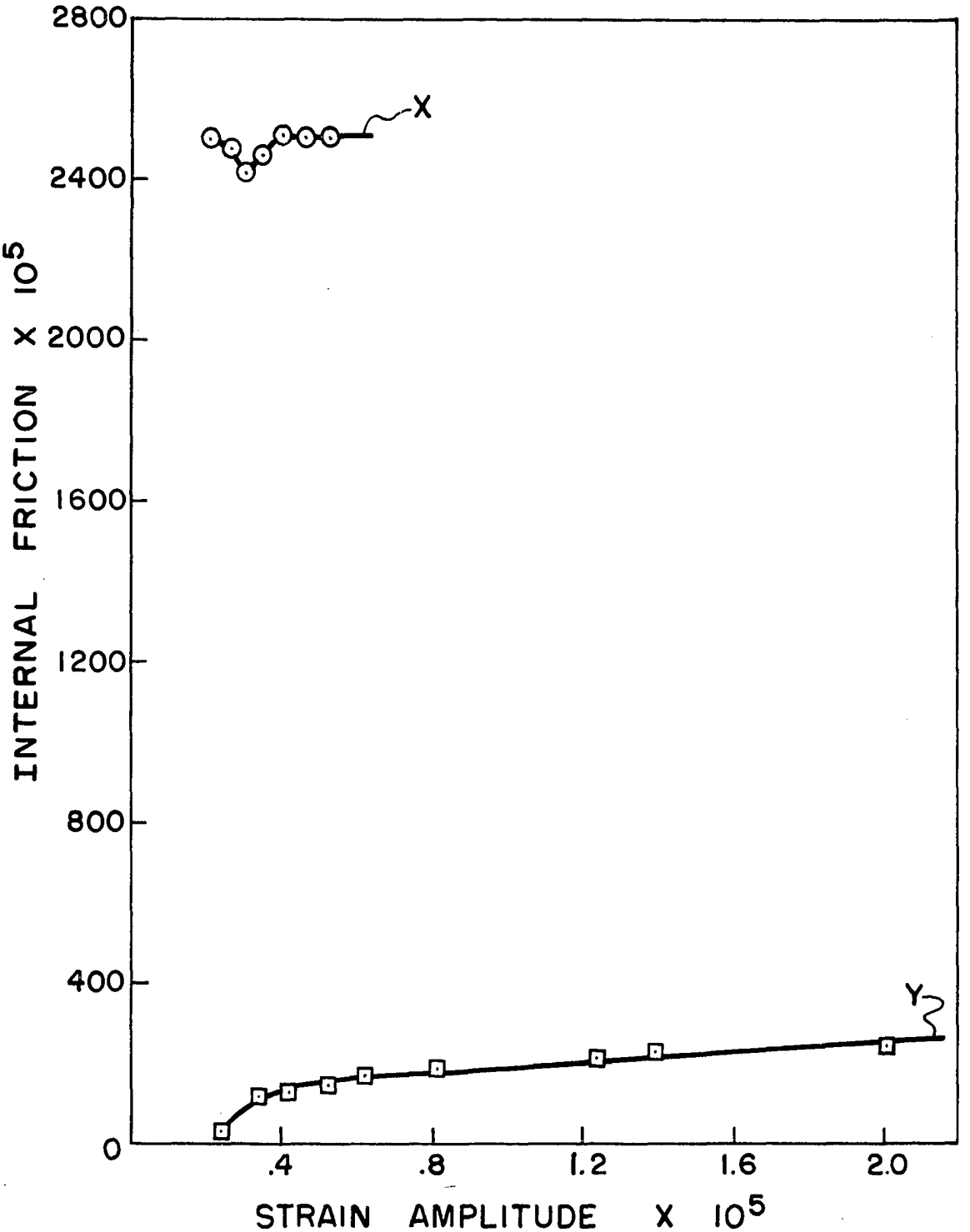

Figure 21. Internal friction versus strain amplitude showing the effect of pinning free dislocations

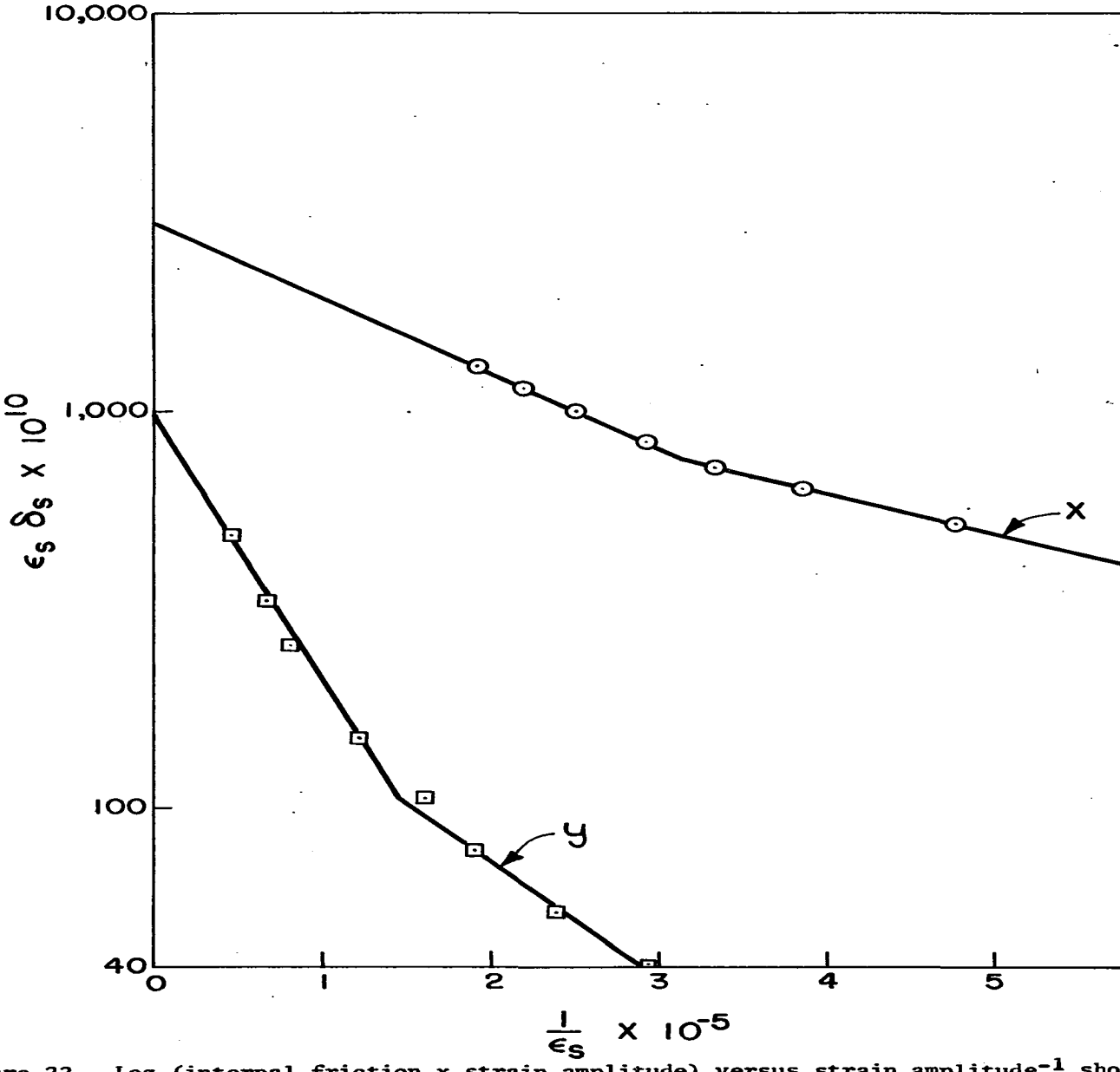

Figure 22. Log (internal friction x strain amplitude) versus strain amplitude^{-1} showing the effect of pinning free dislocations

Table 3. Strained Stockbarger NaCl crystals with various grain sizes

Crystal	Compression before annealing (%)	Compression after annealing (%)	Dislocation density before test (10^6 dislocations/cm^2
α	0	0.5	8.3
β	0.5	0.5	10.0
γ	1.0	0.5	13.8
δ	1.5	0.5	7.2
ε	3.0	0.5	4.7
ζ	6.5	0.5	9.6

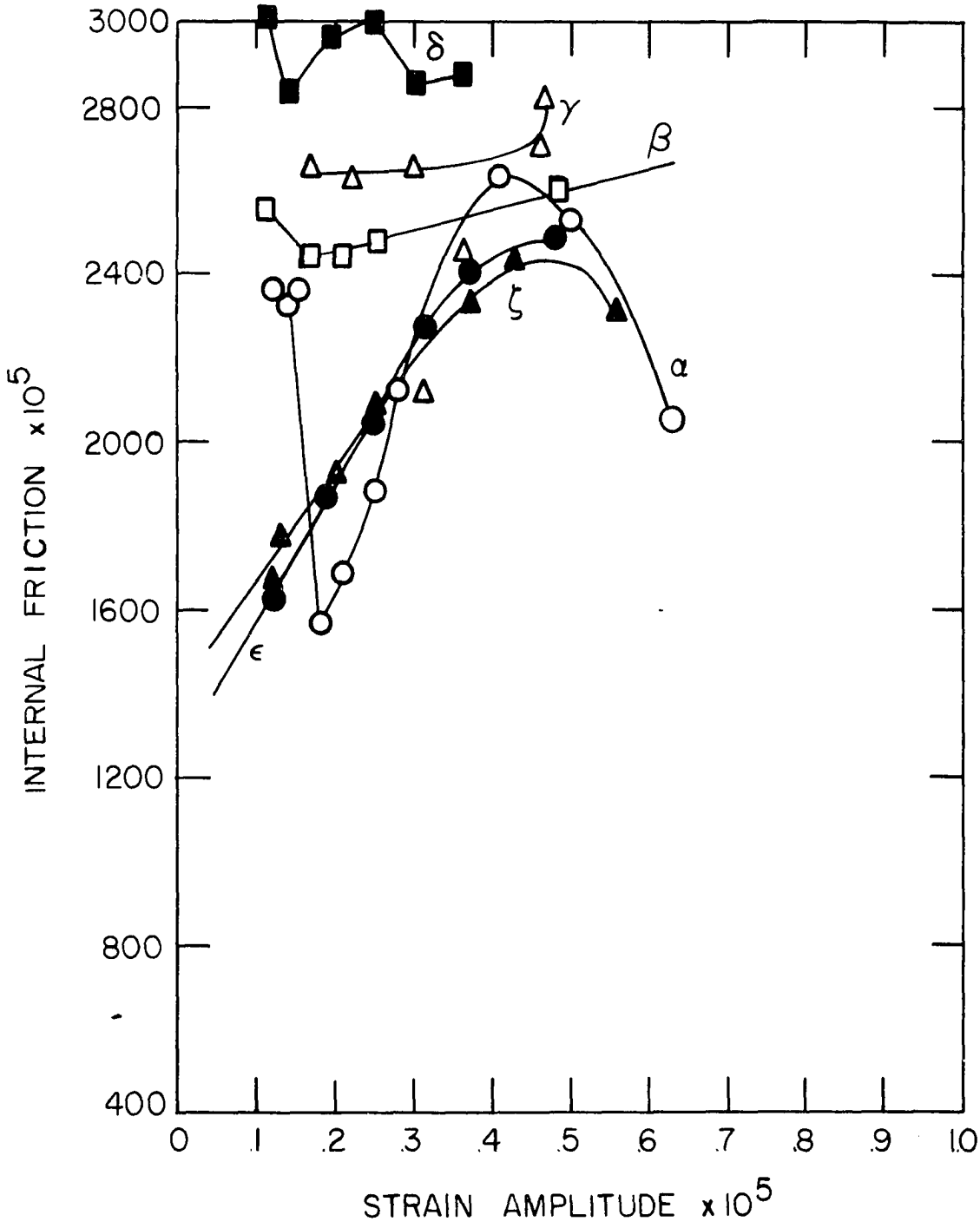

Figure 23. Internal friction versus strain amplitude showing the effect of grain boundaries with a high free-dislocation density

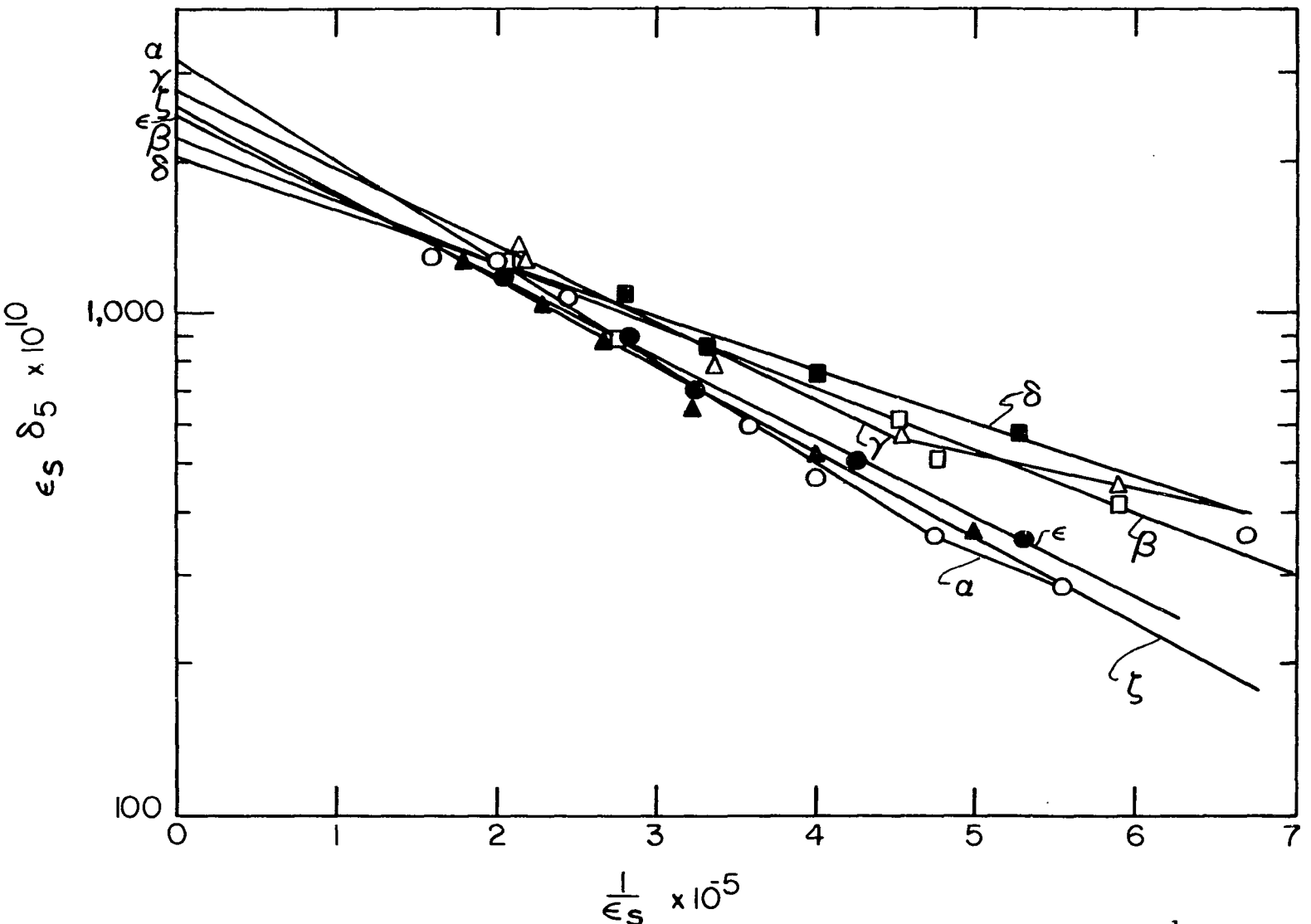

Figure 24. Log (internal friction x strain amplitude) versus strain amplitude^{-1} showing the effect of grain boundaries with a high free-dislocation density

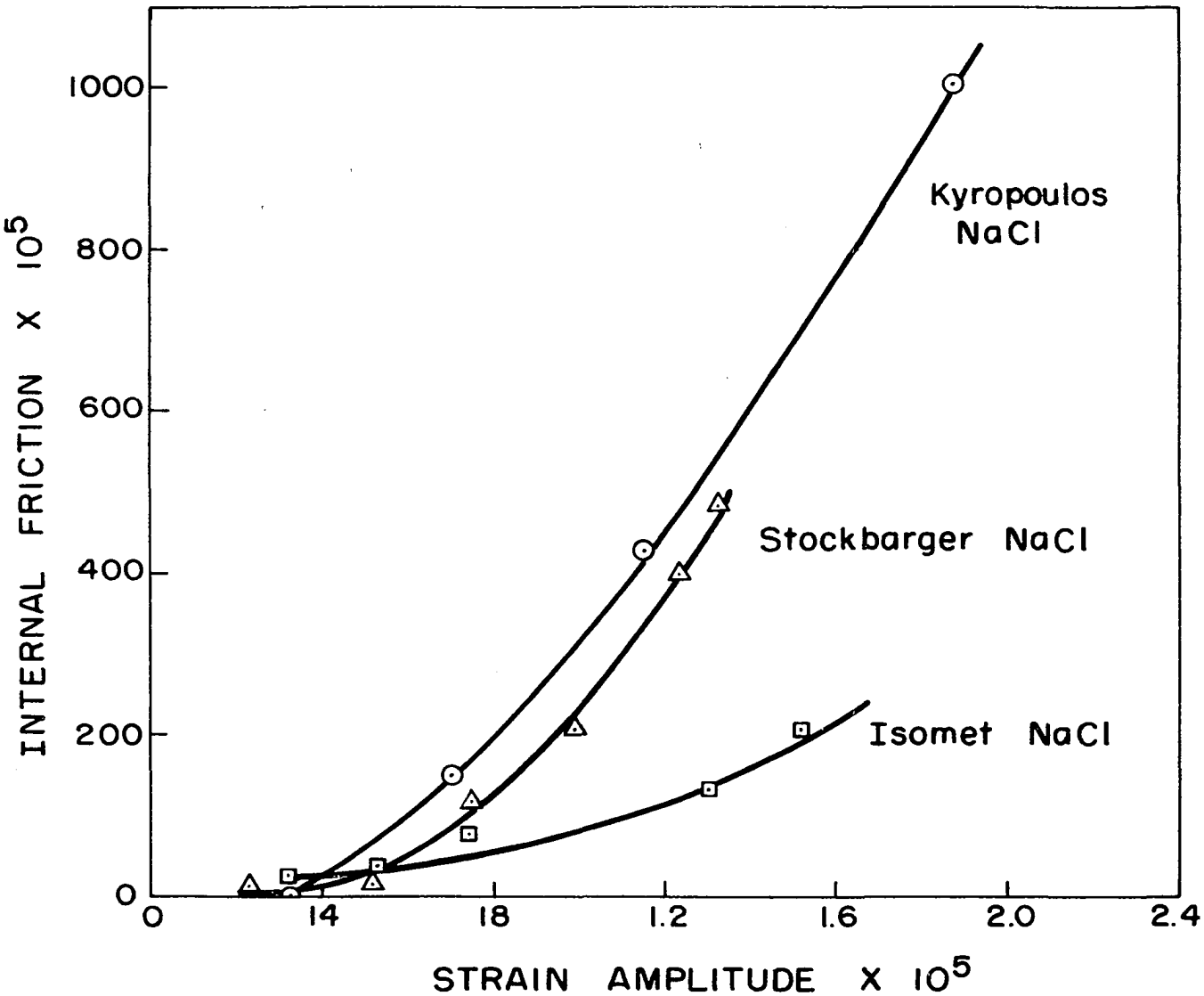

Figure 25. Internal friction versus strain amplitude showing the effect of impurities in single crystals

Stockbarger NaCl has more total impurities than the Isomet salt the Isomet NaCl has the smallest losses. The dominant impurity in the Isomet NaCl is Ca^{++}. Ca^{++} would be expected to replace Na^{+} with the formation of a vacancy.

B. Raised Temperature Findings

The effects of temperature on the internal friction of single crystal and polycrystalline Kyropoulos NaCl was studied. Comparison to Isomet and Stockbarger salts are also included. Amplitude dependence studies were conducted on single crystals at 23°C, 50°C, 75°C, 100°C, 125°C, 200°C, and 300°C. The internal friction as a function of temperature at a strain amplitude of 0.20×10^{-5} is also reported. The low strain amplitude was chosen for the internal friction vs. temperature tests so that breakaway would not have occurred at room temperature. All crystals were annealed at 600°C for 24 hours before testing. The tests completed on the single crystals are given in Table 4.

Figure 26 shows the effect of temperature on the internal friction vs. strain amplitude plots for single crystal Kyropoulos NaCl. The internal friction is much higher at or above 75°C. Those tests completed above 100°C had a maximum in the internal friction strain amplitude plot. This maximum correlates with the widening of the slip bands at the lower temperatures as reported by Shvidkovsky et al. (73), and with grain boundary formation during testing at 300°C. This would explain why the internal friction at 300°C was lower than the internal friction at 200°C. Note that the minimum internal friction at 300°C was higher than the maximum at 23°C or 50°C.

Table 4. Raised temperature Kyropoulos single crystal tests

Single crystals	Tests performed
HT-A	δ_s versus ε_s at 23°C
HT-A'	δ_s versus ε_s at 23°C
HT-B	δ_s versus ε_s at 100°C
HT-C	δ_s versus ε_s at 50°C
HT-D	δ_s versus ε_s at 75°C
HT-E	δ_s versus T up to 300°C at $\varepsilon_s = 0.2 \times 10^{-5}$
HT-E	δ_s versus ε_s at 300°C
HT-F	δ_s versus T up to 200°C at $\varepsilon_s = 20.2 \times 10^{-5}$
HT-F	δ_s versus ε_s at 200°C
HT-Stockbarger	δ_s versus T up to 125°C at $\varepsilon_s = 0.2 \times 10^{-5}$
HT-Stockbarger	δ_s versus ε_s at 125°C
HT-Stockbarger	δ_s versus T up to 300°C at $\varepsilon_s = 20.2 \times 10^{-5}$
HT-Stockbarger	δ_s versus ε_s at 300°C
HT-Isomet	δ_s versus T up to 300°C at $\varepsilon_s = 0.2 \times 10^{-5}$
HT-Isomet	δ_s versus ε_s at 300°C

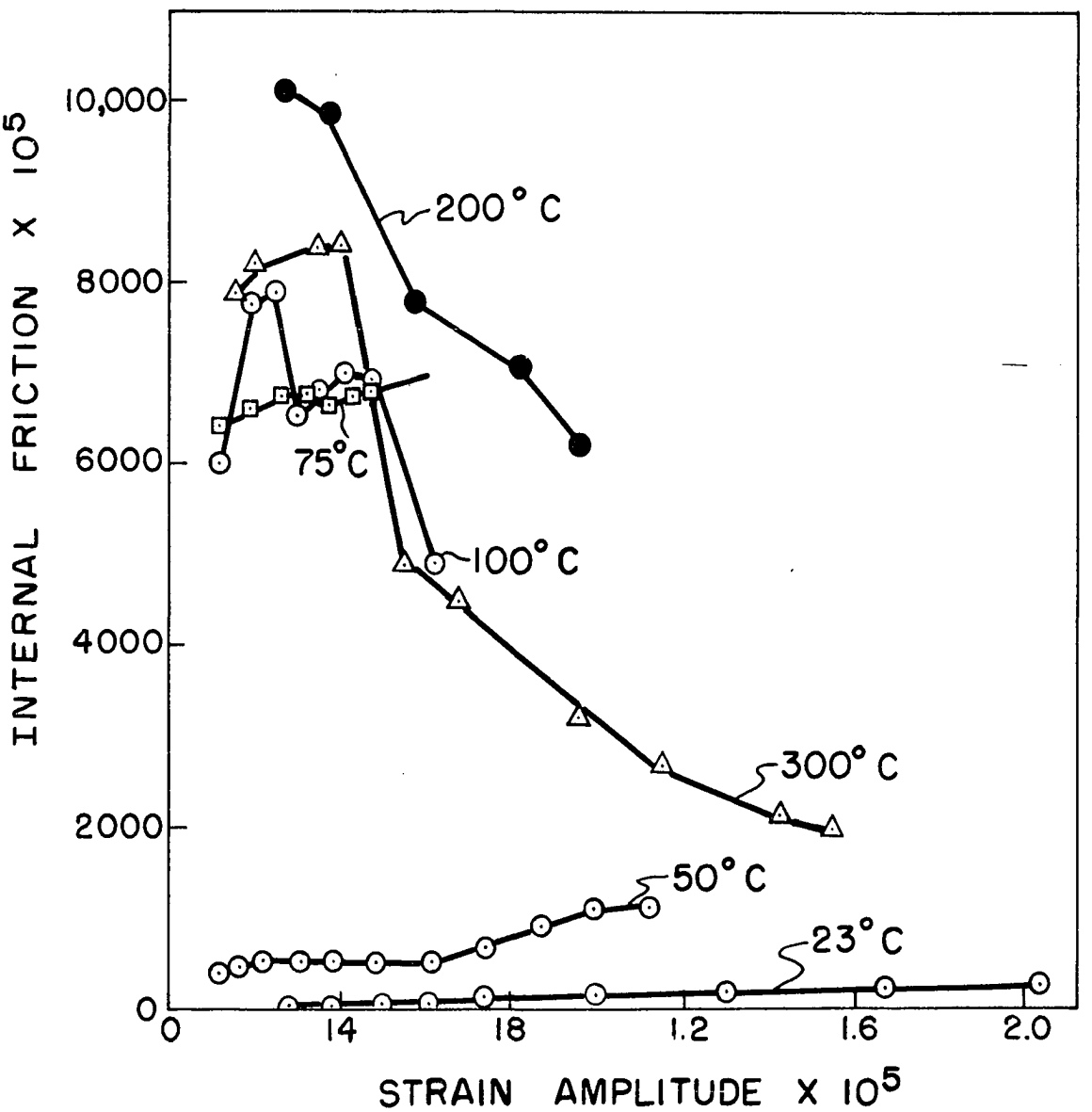

Figure 26. Internal friction versus strain amplitude showing the effect of temperature on single crystals

The Granato-Lücke plots (Figure 27) of the higher temperature single crystal tests were closely aligned within themselves but widely spaced from the lower temperature (23° and 50°C) tests, suggesting a change in L_c. The plot for the 300°C test deviated from the normal plot at high strain amplitudes. This correlates with grain boundary formation which is not included in the Granato-Lücke theory.

The internal friction as a function of strain amplitude was found at 23°C and 300°C for single crystals of the three salts (Figure 28). The kyropoulos salt had a much sharper maximum in internal friction at 300°C than either Stockbarger or Isomet NaCl. The Isomet NaCl did not form grain boundaries during testing. The Stockbarger NaCl formed very few grain boundaries but did have wide diffuse slip bands. Only the Kyropoulos salt had the deviation at high strain amplitudes in the Granato-Lücke plots (Figure 29).

Figure 30 shows the effect of temperature while testing at a low strain amplitude (0.2×10^{-5}). The internal friction took a very sharp jump at 60 - 65°C for the Kyropoulos salt and at 90 110°C for the less pure salts. These temperatures agree well with the brittle-ductile transformation points reported by Stokes (79).

Polycrystalline salt was tested to see whether the sharp increase in internal friction with temperature would be affected by grain boundaries. Both extruded crystals and compressed crystals were tested. (Table 5). After compression the crystals were annealed at 600°C for 24 hours, polished to size and reannealed at 600°C for 24 hours.

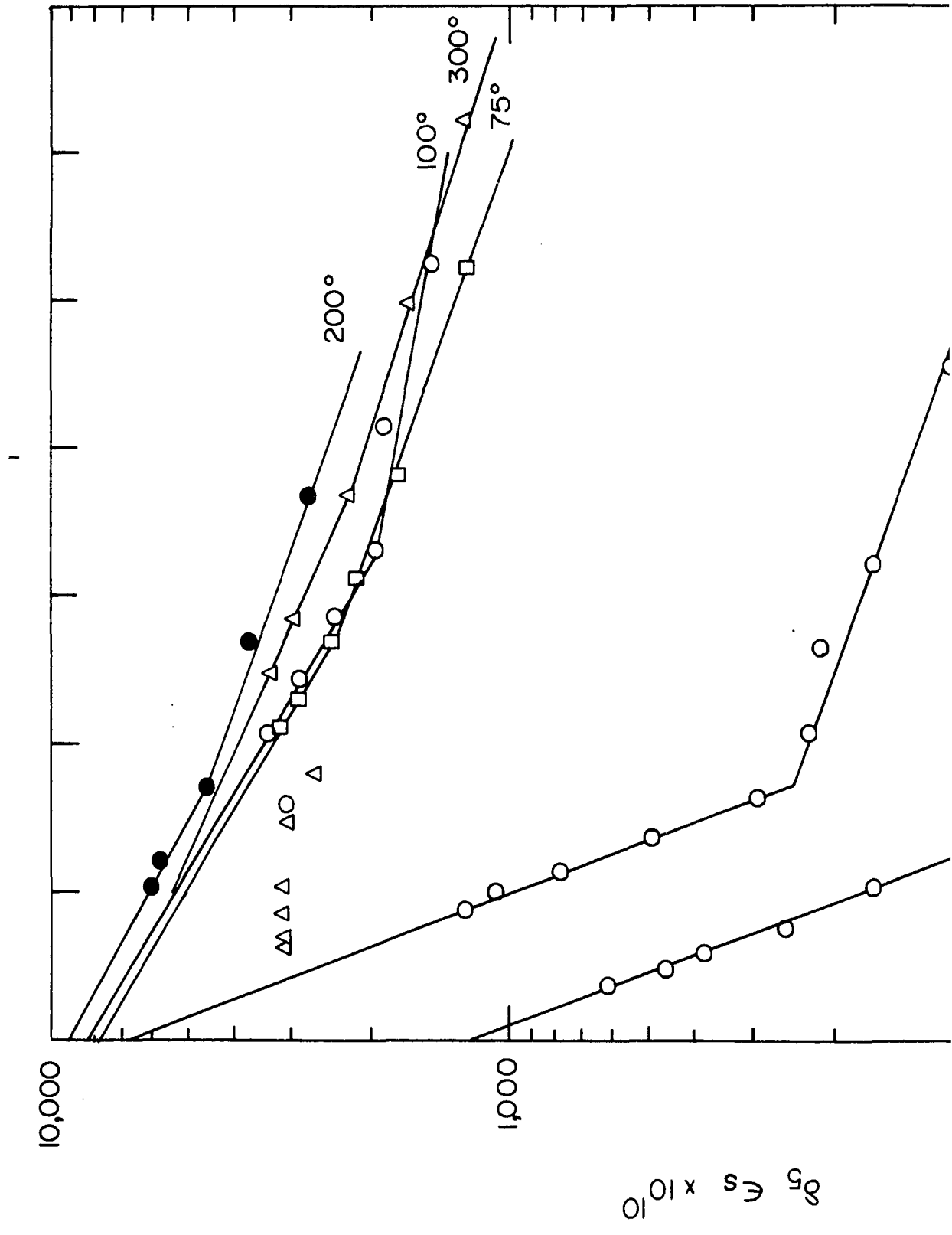
$\delta_5\ \epsilon_s \times 10^{10}$
10,000
1000
300°
100°
75°
200°

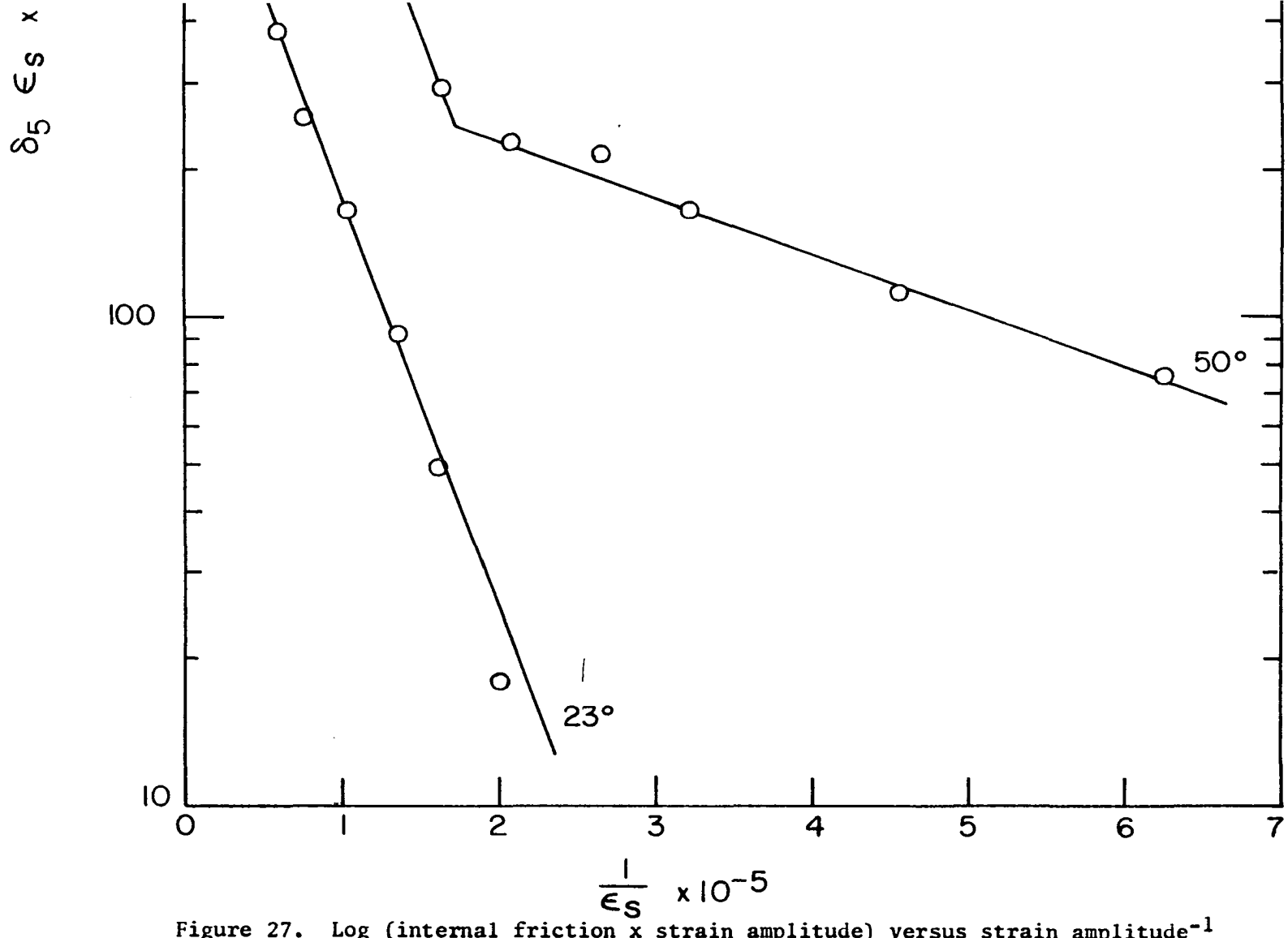

Figure 27. Log (internal friction x strain amplitude) versus strain amplitude^{-1} showing the effect of temperature on single crystals

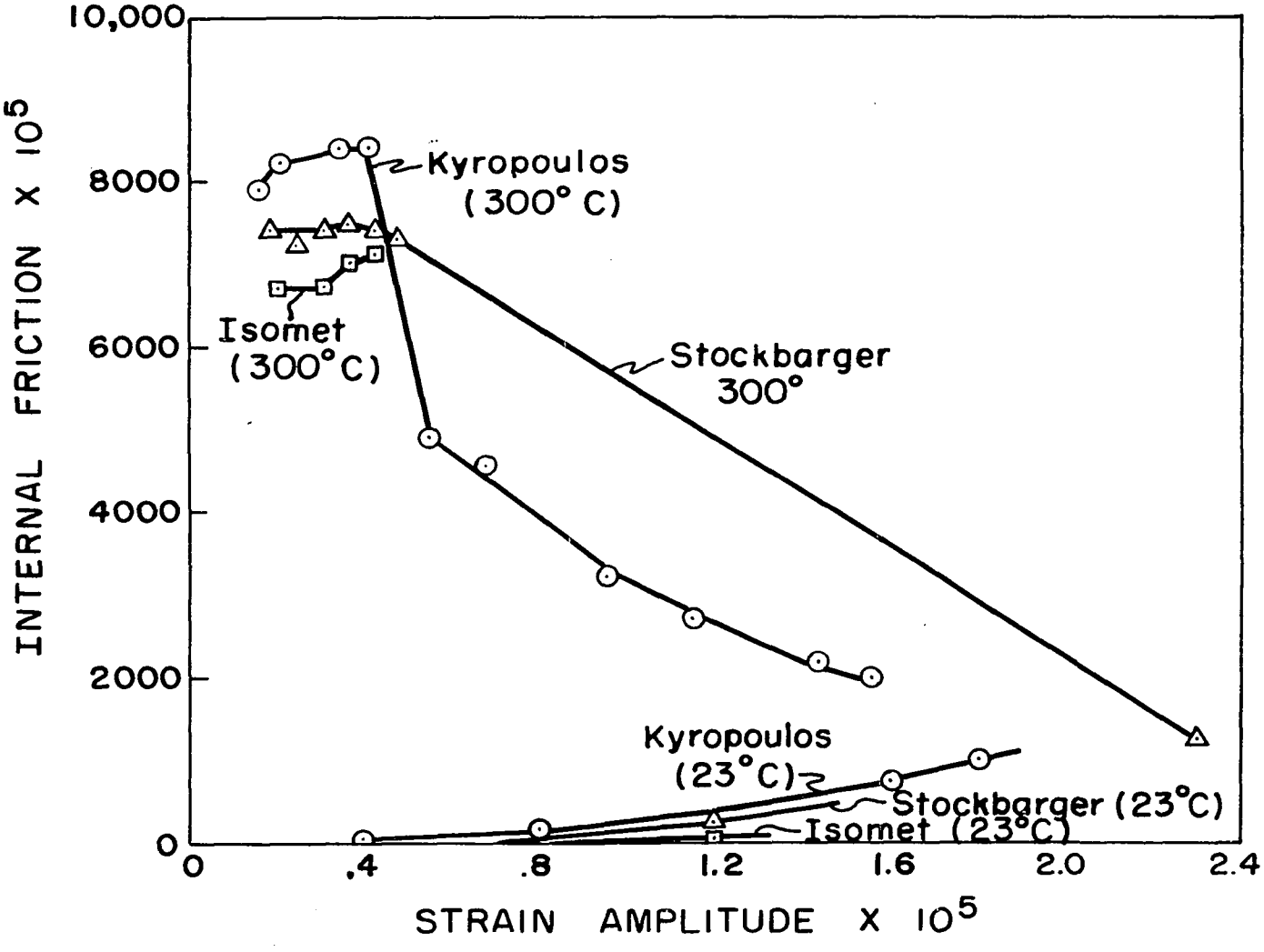

Figure 28. Internal friction versus strain amplitude showing the effect of grain boundary formation at 300°C

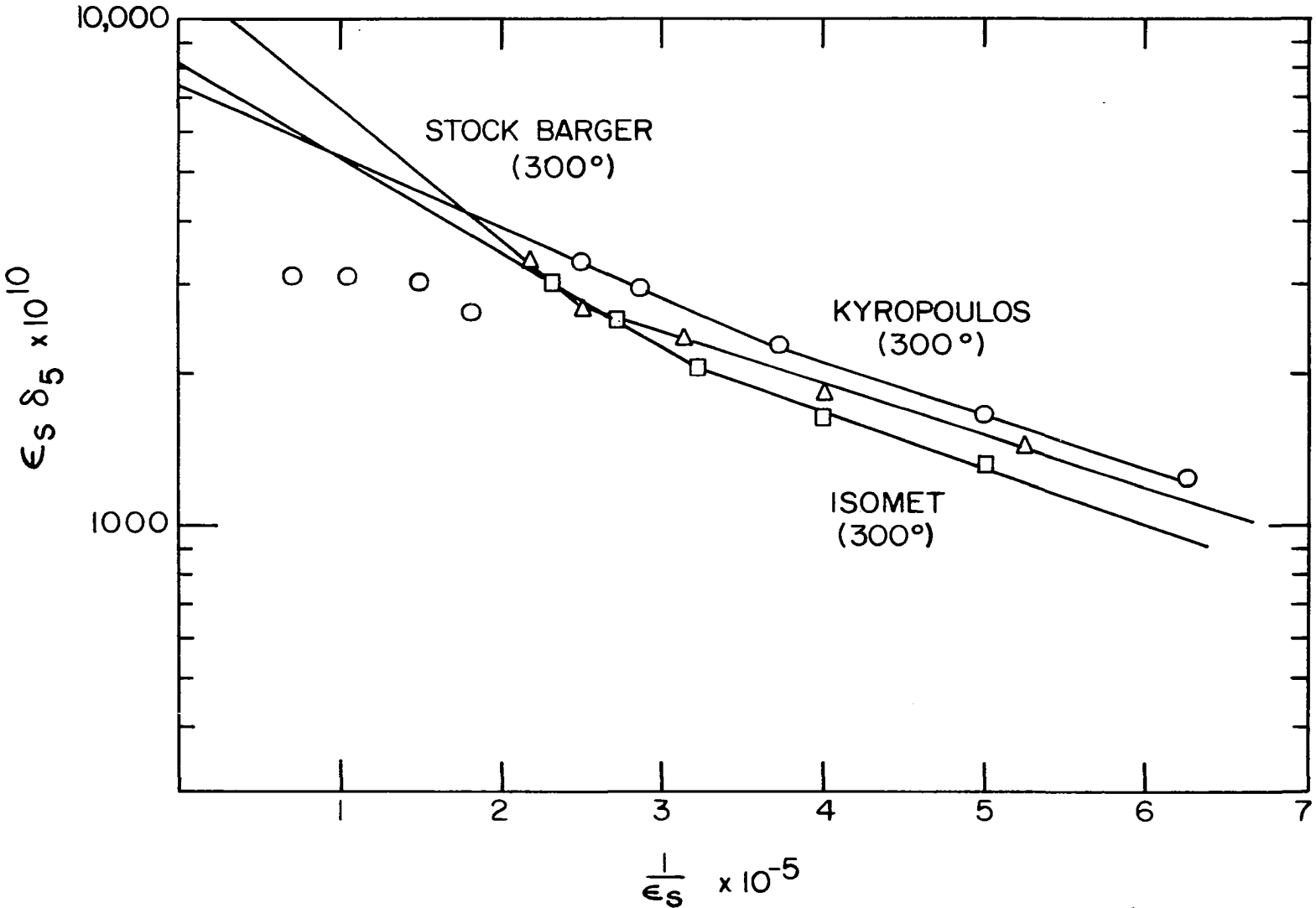

Figure 29. Log (internal friction x strain amplitude) versus strain amplitude^{-1} showing the effect of grain boundary formation at 300°C

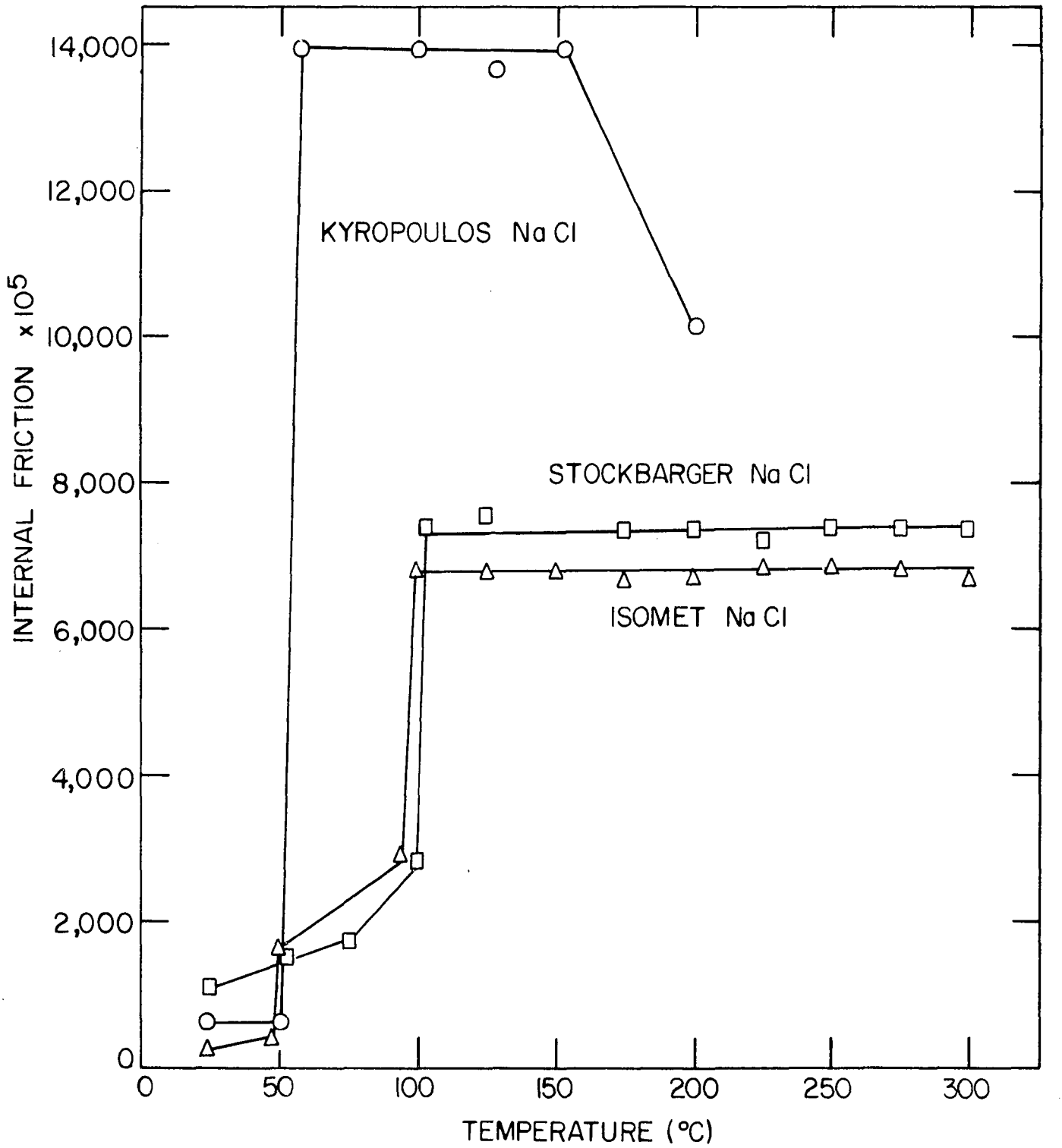

Figure 30. Internal friction versus temperature showing the effect of impurities on the brittle-ductile transformation temperature

Table 5. Kyropolous crystals and processing before testing at raised temperatures

Crystal	Compression	Grain size
HT-G	1%	few grains
HT-H	2%	2×10^{-4} cm^2
HT-I	4%	3.2×10^{-5} cm^2
HT-J	8%	1×10^{-6} cm^2
HT-K	extruded at 500°C	[a] 4.0×10^{-3} cm^2

[a]Extruded crystals developed fairly large grain sizes. The grain boundary angles were much larger than for the compressed crystals.

The results of testing at various temperatures at a low strain amplitude (0.2×10^{-5}) are shown in Figure 31. The 1% compressed crystal had not formed grain boundaries upon annealing so the starting internal friction was expected to be high. The rapid lowering could have been due to the formation of grain boundaries. The 2% compressed crystal had very little internal friction rise with temperature. However, the 4% and 8% compressed crystals and the extruded crystal did have a sharp increase in internal friction.

After reaching 300°C all the crystals were tested at that temperature as a function of strain amplitude (Figure 32). The 1% crystal had already developed grain boundaries before reaching 300°C. It appears that at 300°C the greater the density of grain boundaries the greater the internal friction. This could be attributed to grain boundary sliding. It was noted after the test that some of the grain

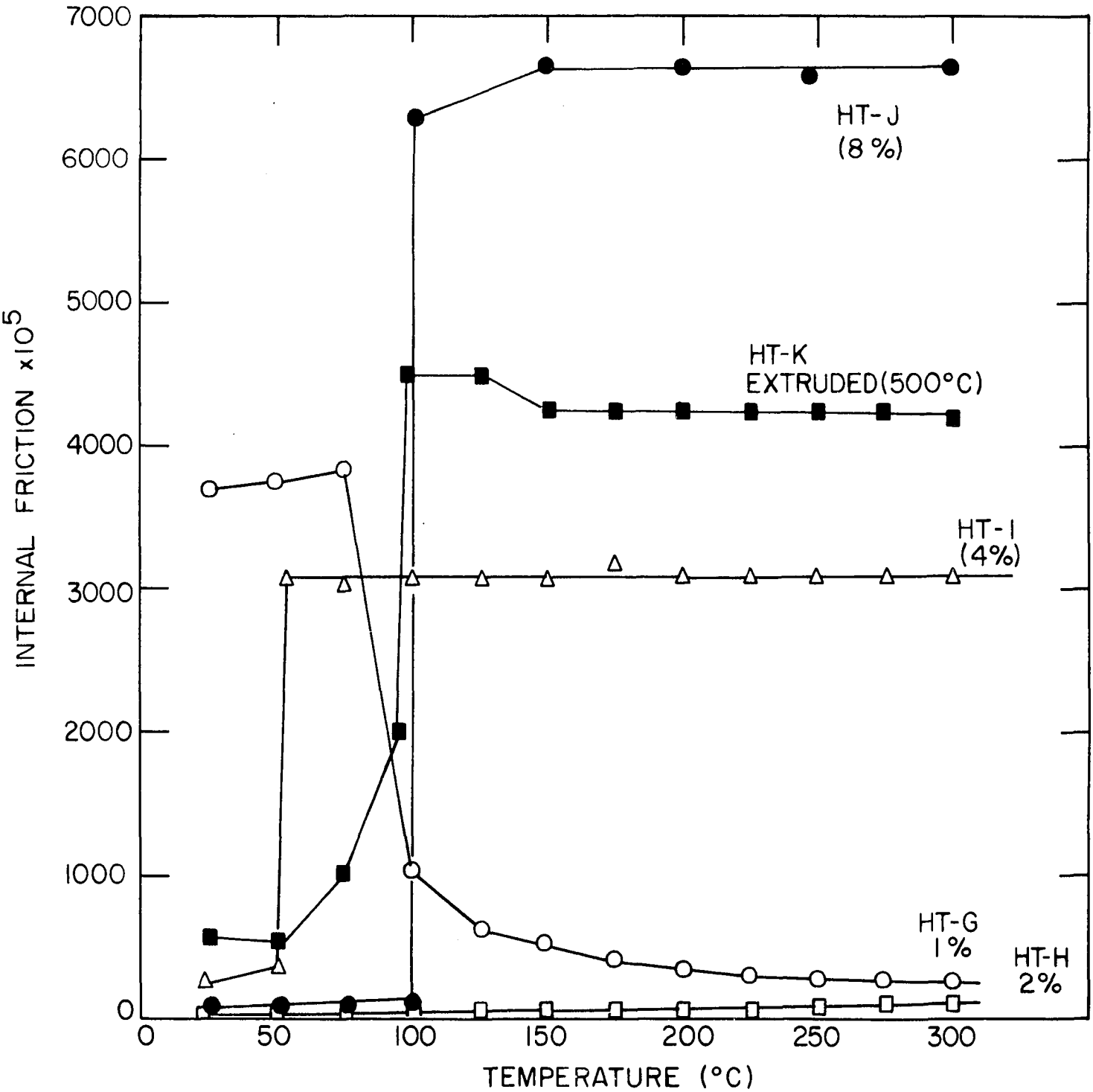

Figure 31. Internal friction versus temperature showing the effect of grain boundaries

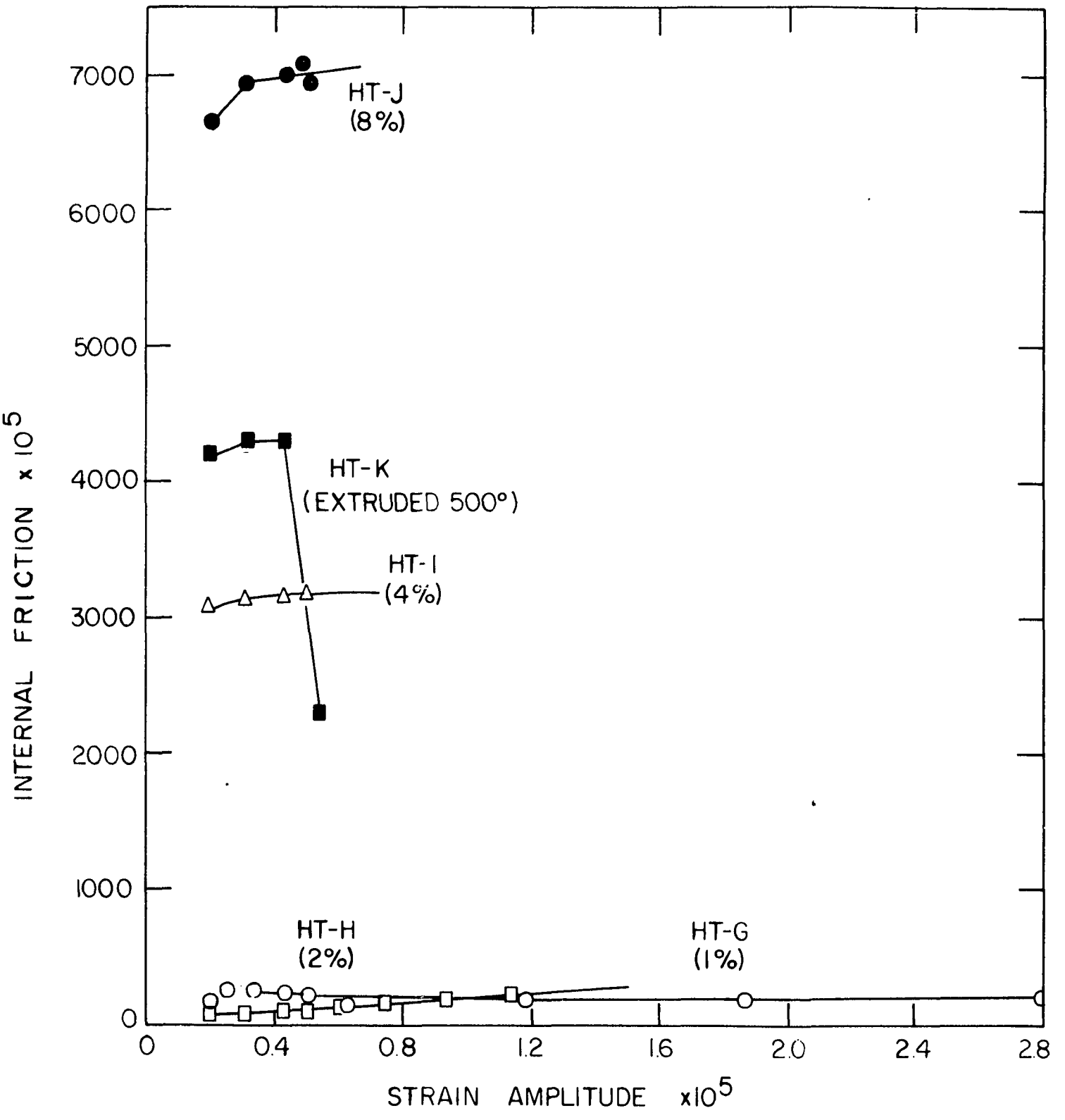

Figure 32. Internal friction versus strain amplitude showing the effect of grain boundaries at 300°C

boundaries in the 4% crystal were partially dissolved. The Granato-Lucke plots (Figure 33) for the 1% and 2% crystals are definitely curves while the higher compressed crystals plots could be either two straight lines or gentle curves.

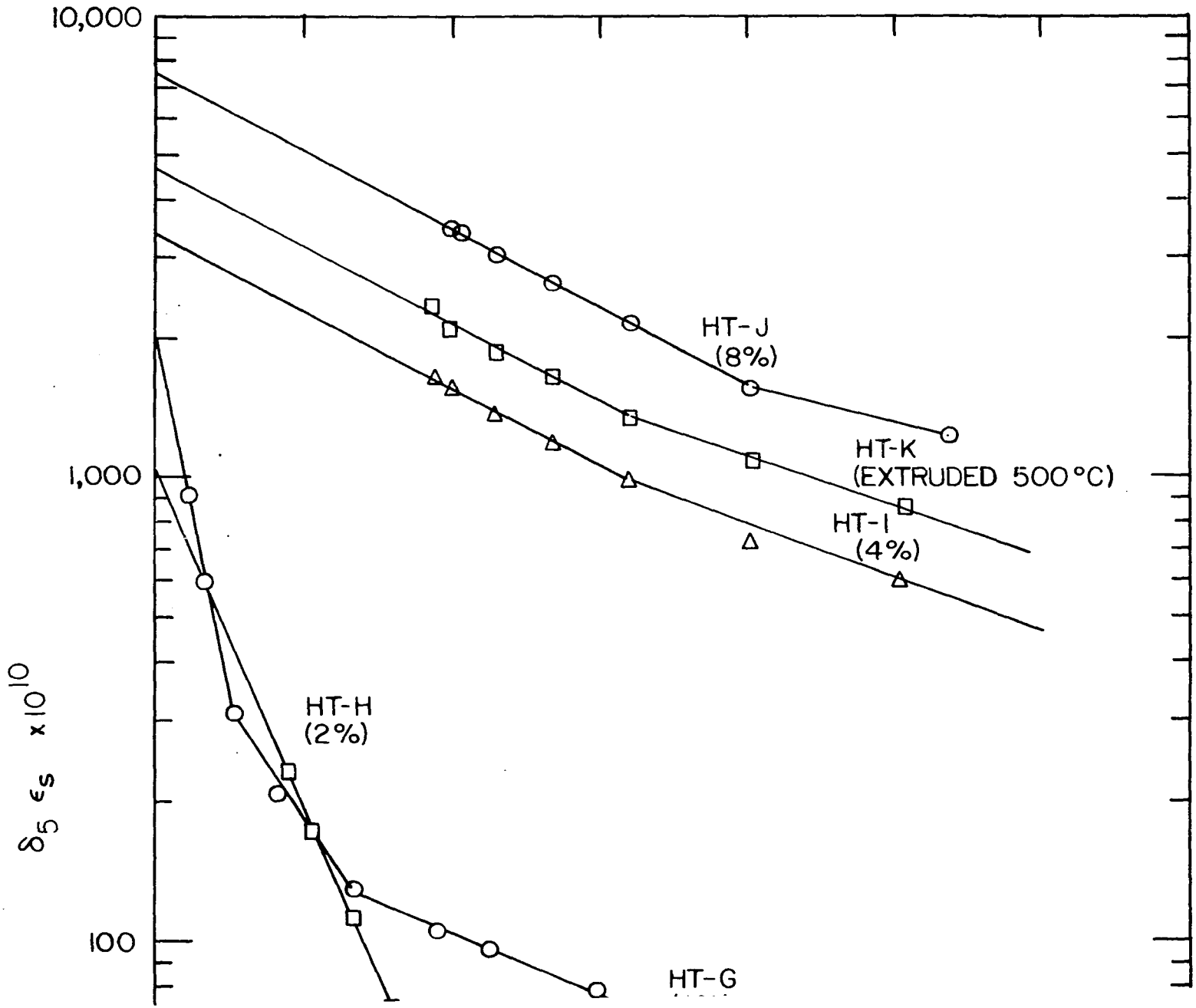
10,000
1,000
100
$\delta_5\ \epsilon_s\ \times 10^{10}$
HT-J
(8%)
HT-K
(EXTRUDED 500°C)
HT-I
(4%)
HT-H
(2%)
HT-G

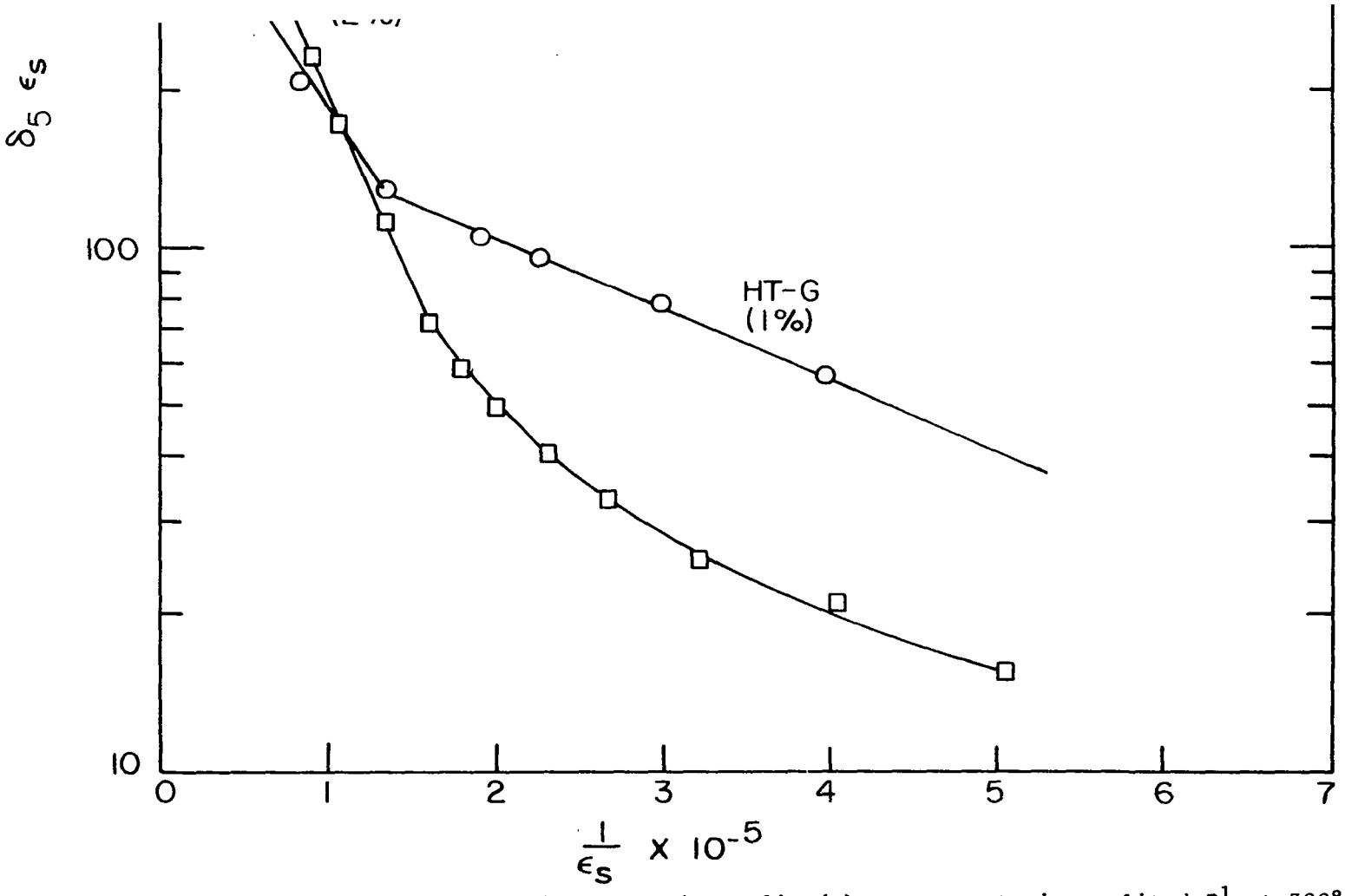

Figure 33. Log (internal friction x strain amplitude) verrsus strain amplitude^{-1} at 300°C showing the effect of grain boundaries at 300°C

V. DISCUSSION

As noted in the Review of Literature the most successful theory in explaining dislocation damping was proposed by Granato and Lücke. In this discussion we will first consider the theory and suggested improvements. The room temperature and raised temperature data will then be compared to the theoretical predictions. Experimental data will be placed into the equation and related factors such as L_n will be calculated and checked for reasonableness.

A. General Theory

The two largest energy losses causing the internal friction were the vibrating string type of loss as considered in the Granato-Lücke theory and the formation of dislocations which was not included in the theory. This suggests that a correct theory can be derived by including additional factors such as dislocation multiplication. The Granato-Lücke equation can be placed into the form

$$\delta_H = \frac{C_1}{\varepsilon} \exp\left(-\frac{C_2}{\varepsilon}\right) \tag{21}$$

where C_1 and C_2 are constants. In the Granato-Lücke plot C_1 is the intercept and C_2 the slope.

$$C_1 = \Omega\Delta_o \frac{\Lambda}{\pi} \frac{L_n^3}{L_c} \frac{K\varepsilon' a}{L_c} \tag{22}$$

and

$$C_2 = \frac{K\varepsilon' a}{L_c} \tag{23}$$

the same notation was used as in Equation 6. If the dislocation density, the network pinning length L_n and the impurity length L_c are left as variables Equation 21 becomes

$$\delta_H = \frac{C_1^1 \Lambda L_n^3}{\varepsilon L_c} \exp(-\frac{C_2^1}{L_c \varepsilon}). \qquad (24)$$

Equation 24 is much like Fiore and Bauer's (43) result reported earlier as Equation 17.

If E is the energy to form a dislocation, then $E(\Lambda - \Lambda_o)$ should be the total energy used in dislocation multiplication. Finding the quantitative effect of time and temperature on dislocation multiplication would facilitate calculating an energy loss per cycle. By consideration of this energy loss, especially above the brittle-ductile transformation temperature, the theoretical equation would more accurately predict the experimental results. Other factors such as grain boundary formation, might also be added to the equation.

B. Room Temperature

By finding a value of L_c from Equation 23 and experimentally measuring the dislocation density and logarithmic decrement, Equation 24 can be solved to find the relationship between the network length and the strain amplitude. The impurity pinning distance L_c probably will not change an order of magnitude while testing. Figures 15 and 20 are not extremely different, hence at room temperature L_c does remain fairly constant even though various grain sizes were tested. The calculated value of L_c and L_n (Table 43) agree with those predicted by Granato and Lucke (27). It was possible to find only one value for L_c for each

crystal. L_n was larger than L_c by at least an order of magnitude in every case.

Figure 34 shows L_n in centimeters, as a function of strain amplitude. The L_n values of crystals G and L rapidly decreased and then gradually lengthened as the strain amplitude increased. The shortest network lengths for those two crystals occurred at the breakaway strain amplitude. Before breakaway, L_c controls the vibration length and L_n appears very large. After breakaway, L_n increases with increasing stress. In the other crystals tested (H through K) the lowest strain amplitude was close enough to breakaway that L_n was found always to increase with increasing strain until a maximum L_n was reached. After the maximum, any additional strain increased the number of dislocations causing further network pinning. L_n reaches a maximum value as the dislocation density increases (Figure 35). Since the dislocation density of crystal L was too high to count, it was not included.

Crystal I which has the greatest number of free dislocations (Figure 18) also has the maximum L_c. The free dislocation density was measured immediately before testing. Since L_c was found from the slope of the Granato-Lücke plot it was impossible to get L_c as a value of strain amplitude, unless one agrees to the idea that where the Granato Lücke plot bends there is a corresponding change in L_c. If there is a bend in the Granato-Lücke plot the slope generally decreases at the lower strain amplitudes which would mean an increase in L_c.

It would be expected that the impurity pinning length L_c should decrease with increasing dislocations, since jogs, vacancies, and other defects which act as impurities are being produced as dislocations are

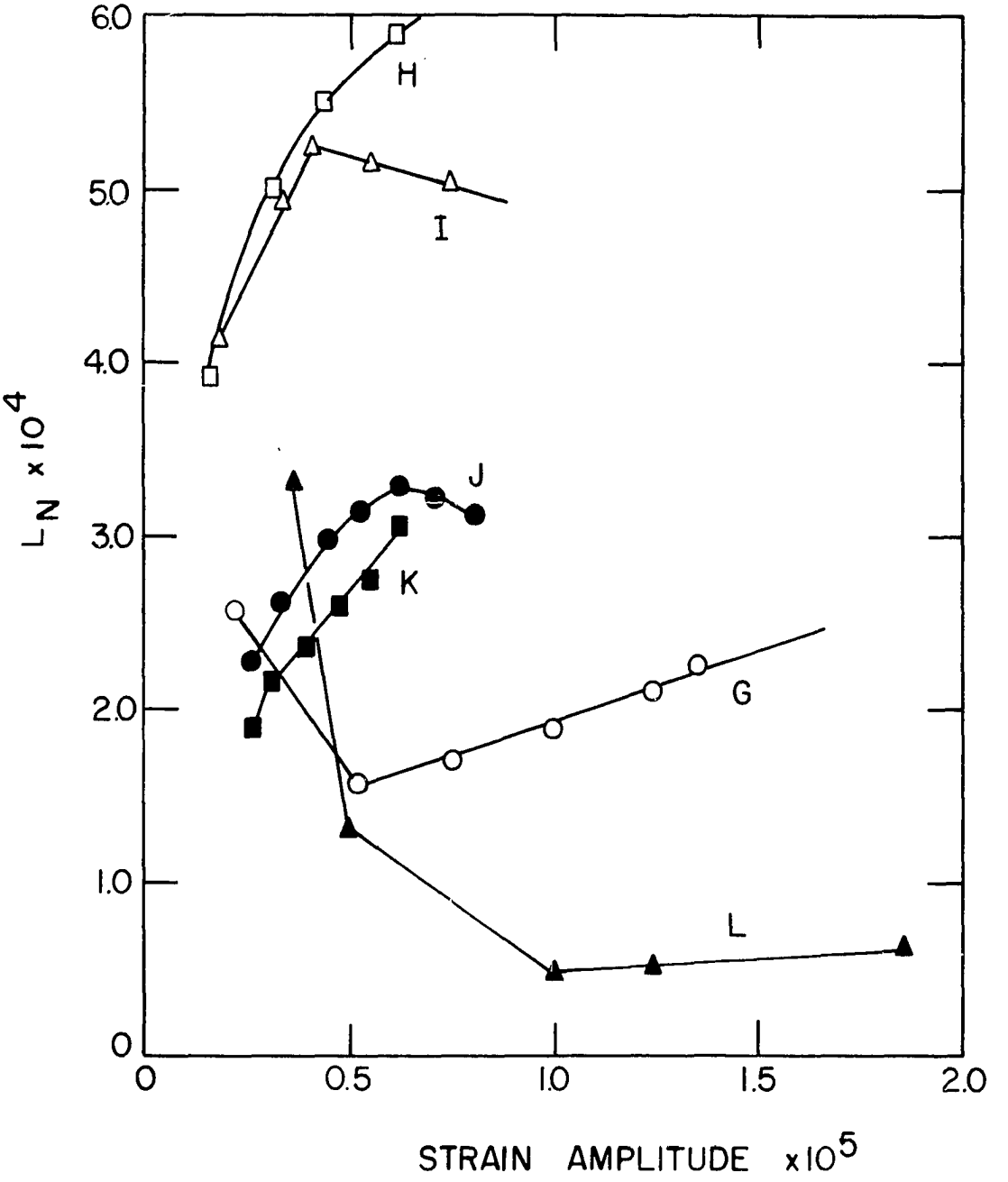

Figure 34. Network pinning length versus strain amplitude showing the effect of grain boundaries

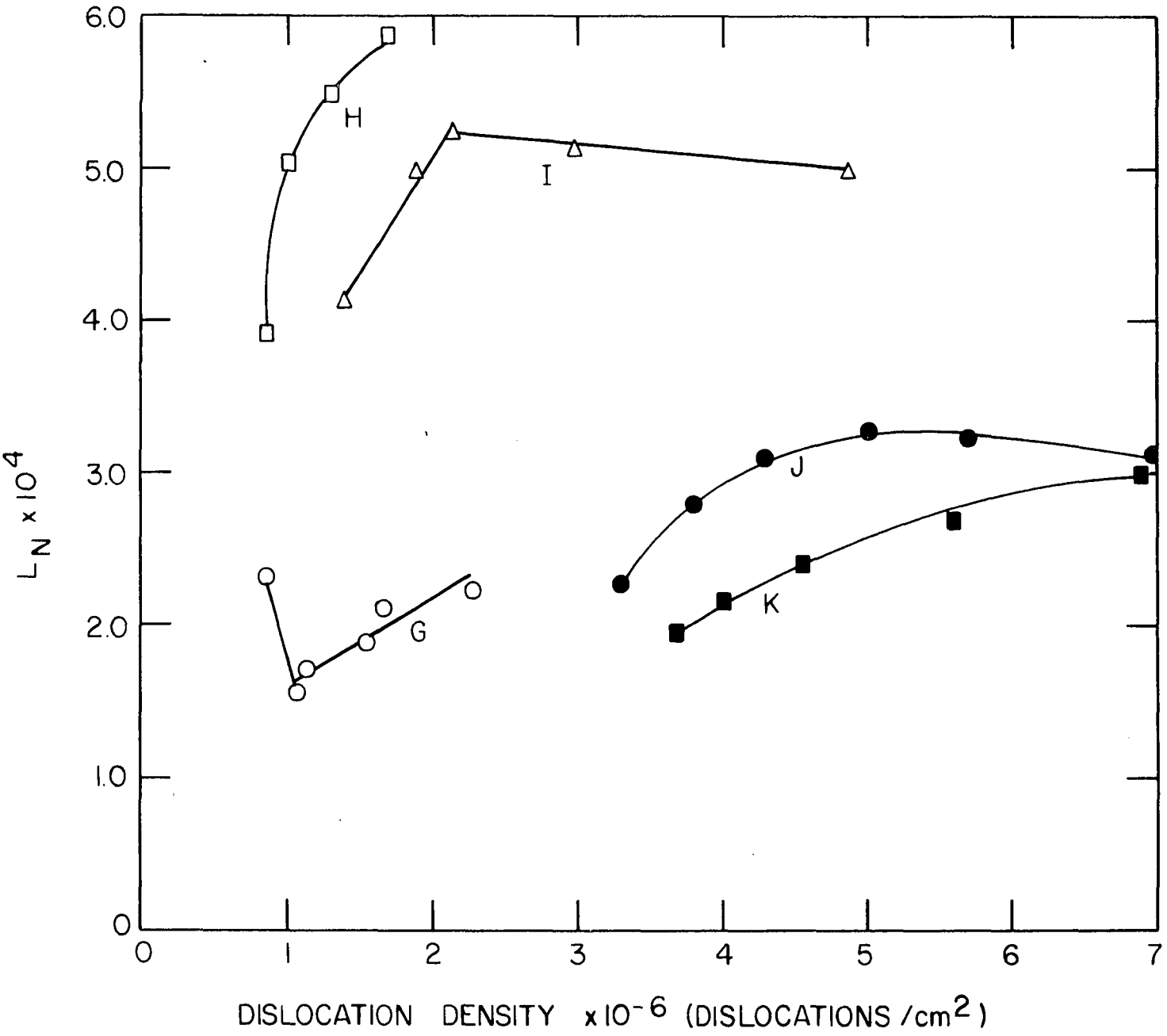

Figure 35. Network pinning length versus dislocation density showing the effect of grain boundaries

moved. Figure 36 suggests that L_c is not adequately considered. The direct relationship between L_c and the free dislocation density would place a dislocation density effect in the exponential term of Equation 22 and remove it from the first term. The correct trends between dislocation density and internal friction would be maintained.

The dislocation density at room temperature was a function of strain amplitude as shown in Equation 25.

$$\Lambda = \Lambda_0 \exp(A\varepsilon_s) \tag{25}$$

where

Λ_0 = ingrown dislocation density (approximately 1.0 X 10^6 dislocations/cm^2 for the NaCl single crystals tested)

Λ = final dislocation density

ε_s = strain amplitude

A = experimentally found constant.

The quantitative effect of time and temperature was not determined.

C. Raised Temperature

Fiore and Bauer (43) suggest that temperature can be added to the Granato-Lücke equation through the use of Equation 26.

$$L_c = \frac{2r_0}{c_0} \exp(-\frac{U_B}{kT}) \tag{26}$$

where

r_0 = radius of solvent atom

c_0 = fraction of impurities or pinning defects

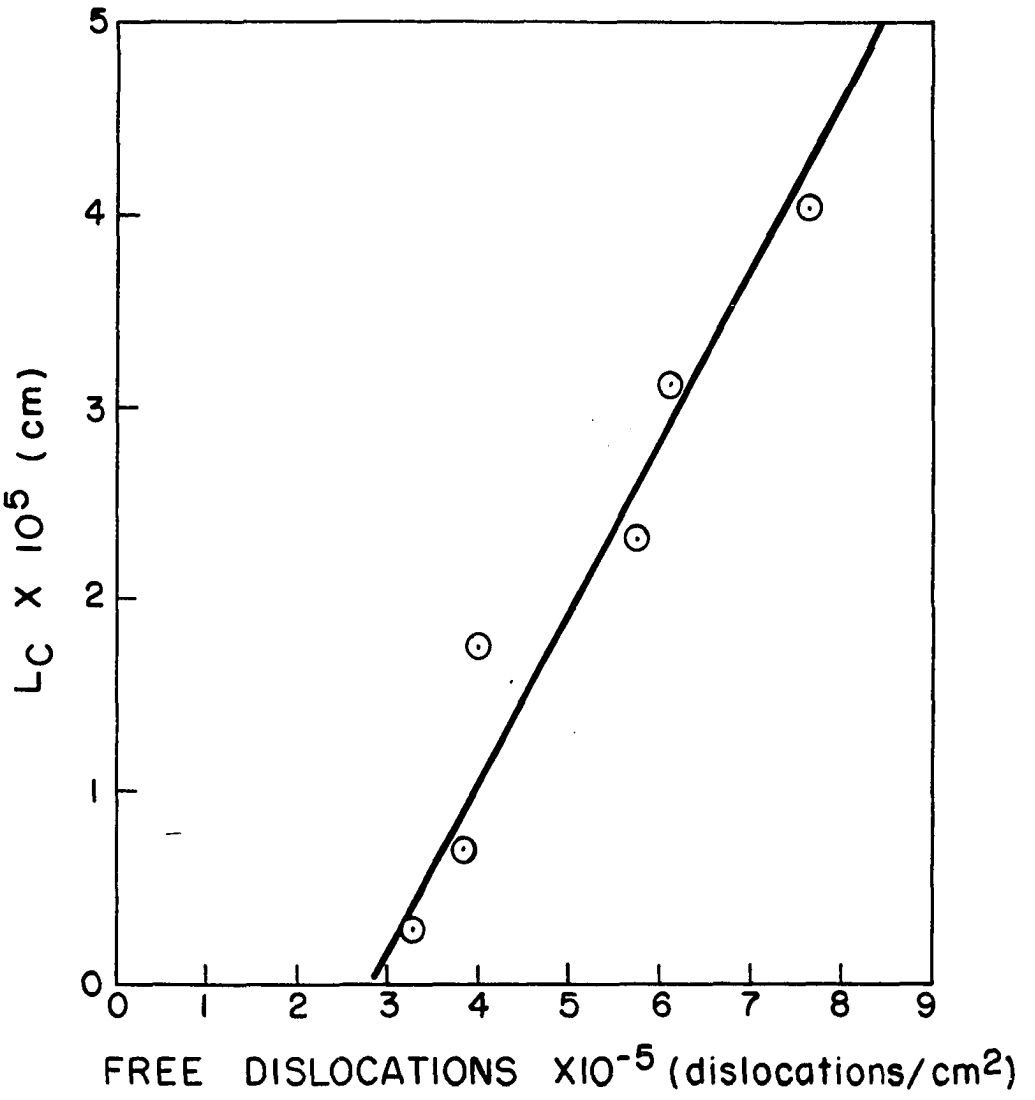

Figure 36. Impurity pinning length versus dislocation density

U_B = binding energy between the dislocation and impurity or defect

k = Boltzman's constant

T = absolute temperature.

By use of Equation 23 and the data from crystals HT-A through HT-F it is possible to check Equation 26. The slope of the Granato-Lücke plot can be related to temperature by Equations 27 and 28.

$$\frac{A}{C_2} = L_c = \frac{2r_o}{c_o} \exp(-\frac{U_B}{kT}) \tag{27}$$

where $A = K\varepsilon'a$ and C_2 is the slope of the Granato-Lücke plot.

$$C_2 = A \frac{c_o}{2r_o} \exp(\frac{U_B}{kT}) \tag{28}$$

In a plot of the log C_2 vs. 1/T (Figure 37) the slope would equal U_B/k and the intercept $Ac_o/2r_o$. It is obvious from Figure 37 that Equation 24 is incapable of explaining the sharp jump in internal friction at transformation temperatures, again suggesting that L_c is not adequately considered. The slope determined does not represent any real activation energy.

The internal friction of NaCl at 200°C is in general higher than at 300°C (Figure 26). This was due to the formation of grain boundaries while testing the crystal at 300°C. It was amazing to find that above 100°C, grain boundaries were rather easily formed in the purest salt while the crystal underwent oscillating stresses. Once testing temperature was reached, the temperature was held constant until the test was completed. This made it impossible to obtain the dislocation density as a function of strain amplitude at the raised temperatures. However, even at low strain amplitudes there was a large dislocation density increase at

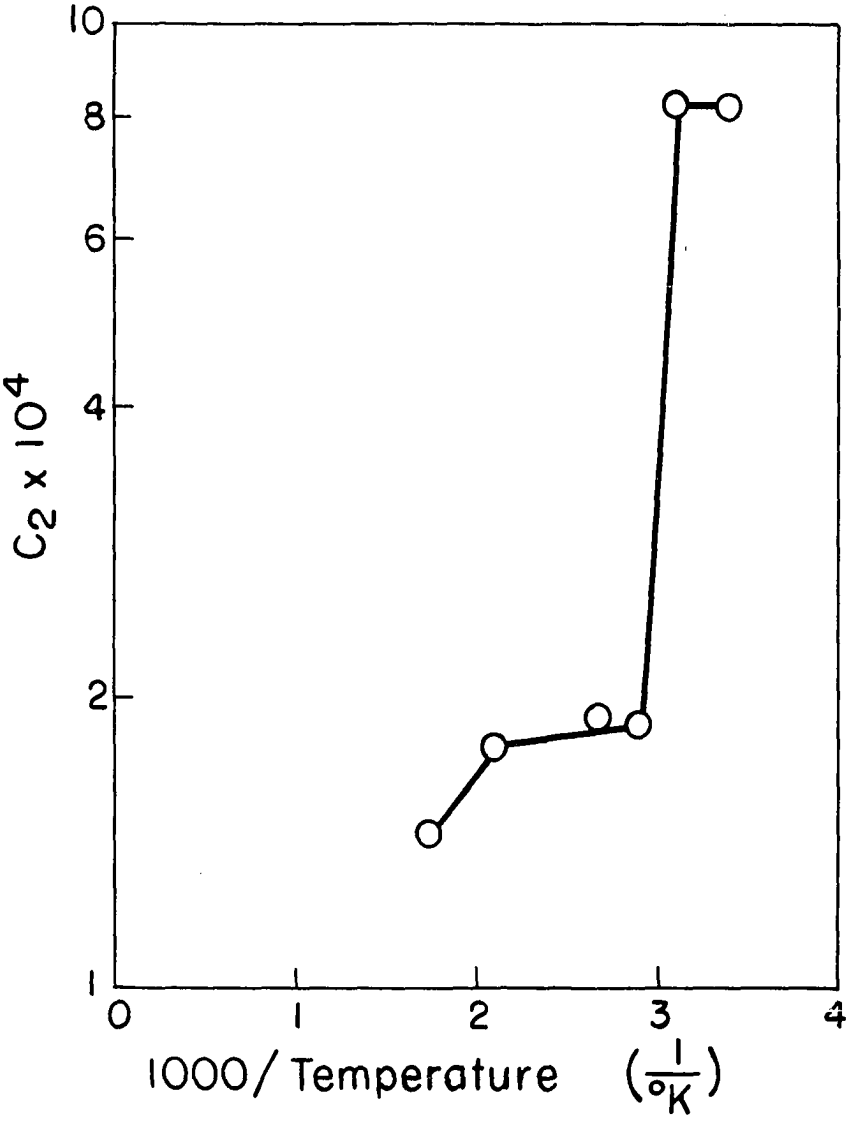

Figure 37. Slope of Granato-Lücke plot versus temperature^{-1}

the brittle-ductile transformation temperature. Examination of the crystal, after testing, revealed that the free dislocations were in the form of wide diffuse slip bands with a high dislocation density.

The Ca^{++} was shown to be the most effective impurity pinning point (Figure 30). Not only was the Isomet NaCl internal friction lower than the other salts for the higher temperatures but the brittle-ductile transformation occurred at a higher temperature than for the Kyropoulos. The transformation occurred much more sharply for the Kyropoulos NaCl than for less pure salts. Even though the impurity ions effect the brittle-ductile transformation temperature they are not the cause of the transformation. Since the purer salts have the sharpest transformation, it would be expected that a direct dislocation-lattice interaction would be the controlling mechanism for the brittle-ductile transformation. Even with a theoretically pure material the transformation would exist. Large increases in the dislocation density, which were found to occur at the brittle-ductile transformation temperature, can account for the sharp increase in the internal friction.

The mechanism which accounts for the transformation is not completely understood. The dislocation density increased with increasing strain amplitude, temperature and time. Since the internal friction found in this research was not time dependent, except when grain boundaries were formed during the test, it would be expected that the dislocation density would reach a maximum at each temperature and strain amplitude. The dislocation density increase would continue until all of the vibrating energy added to the system was used in oscillating the dislocations. The internal friction would remain constant. Belozerova et al. (75) suggest

that at room temperature, the time required to complete the multiplication process in NaCl would be several hours. As the temperature increased the required time to complete the dislocation multiplication, at a particular strain amplitude, would decrease.

Quantitative results are not possible since the quantitative effect of time and temperature on the dislocation multiplication process is not known. The research required to find the needed quantitative relationship would make an excellent thesis project. With this information and the correct useage of the dislocation density an equation could be produced that would predict the experimental results.

VI. CONCLUSIONS

1. The internal friction of NaCl single crystals increases as the strain amplitude increases. The strain amplitude dependent decrement for unstrained single crystals is nearly zero at low strain amplitudes, but can increase abruptly at strain amplitudes approximating the yield point.
2. At room temperature the dislocation density of a NaCl crystal increases logarithmically with increasing strain amplitude. The temperature dependence was not found.
3. The internal friction is a function of both the number of dislocations present and the manner in which they are pinned.
4. Approximately 2% compression is required at room temperature to form enough dislocations for recrystallization to take place at 600°C in 24 hours. Only small angle grain boundaries were formed. Extrusion produced larger grains separated by relatively large angle grain boundaries.
5. The divalent impurity ion such as Ca^{++} is an excellent minor pinning point.
6. The internal friction of NaCl increases with increasing temperature.
7. NaCl crystals form small angle grain boundaries when under the influence of oscillating stresses and raised temperatures (200°C).

8. The brittle-ductile transformation temperature for single crystal Kyropoulos NaCl is approximately 65°C. The transition occurred at approximately 100 - 110°C for the less pure salts.
9. The Granato-Lücke theory works fairly well when used at each of the temperatures tested except when grain boundaries were formed during testing. It is not capable of explaining the brittle-ductile transformation.
10. In general the network length L_n was found to be approximately 10 times as large as the impurity pinning length L_c. L_c was a direct function of the free dislocations present.
11. The largest losses found were from the formation and movement of dislocations. The Granato-Lücke theory does not consider the formation of dislocations though it can be modified to incorporate the added vibration losses after the dislocation multiplication.
12. The total amplitude dependent on internal friction consists of two parts, the vibrating string energy loss and the dislocation multiplication energy loss.

VII. LITERATURE CITED

1. Fehr, Gerald K. Internal friction of sodium chloride. Unpublished M.S. thesis. Ames, Iowa, Library, Iowa State University of Science and Technology. 1964.

2. Dieter, G. E. Metallurgy and metallurgical engineering series. New York, N.Y., McGraw-Hill Book Co., Inc. 1961.

3. Kingery, W. D. Property measurements at high temperature. New York, N.Y., John Wiley and Sons, Inc. 1959.

4. Forster, F. Ein neues messverfahren zur bestimmung des elastizitäts-moduls und der dämping. Zeitschrift für Metallkunde 29: 109-115. 1937.

5. Mason, W. P. Piezoelectric crystals and their application to ultrasonics. New York, N.Y., D. Van Nostrand Co., Inc. 1950.

6. Butterworth, S. On electrically-maintained vibrations. Physical Society of London Proceedings 27: 410-424. 1915.

7. Cady, W. G. The piezo-electric resonator. Institute of Radio Engineers Proceedings 10: 83-114. 1922.

8. Van Dyke, K. S. The piezo-electric resonator and its equivalent network. Institute of Radio Engineers Proceedings 16: 742-764. 1928.

9. Quimby, S. L. On the experimental determinations of the viscosity of vibrating solids. Physical Review 25: 558-573. 1925.

10. Balamuth, L. A new method for measuring elastic moduli and the variations with temperature of the principal Young's modulus of rocksalt between 78° and 273°K. Physical Review 45: 715-720. 1934.

11. Rose, C. F. The variation of the adiabatic elastic moduli of rocksalt with temperature between 80° and 270°K. Physical Review 49: 50-54. 1936.

12. Rinehart, J. S. Temperature dependence of Young's modulus and internal friction of Lucite and Kanolith. Journal of Applied Physics 12: 811-816. 1941.

13. Cooke, W. T. The variation of the internal friction and elastic constants with magnetization in iron. Physical Review 50: 1158-1164. 1936.

14. Read, T. A. The internal friction of single metal crystals. Physical Review 58: 371-380. 1940.

15. Marx, J. Use of the piezoelectric gauge for internal friction measurements. Review of Scientific Instruments, Series 7, 22: 503-509. 1951.

16. Zener, C. Elasticity and anelasticity of metals. Chicago, Illinois, The University of Chicago Press. 1948.

17. Van Bueren, H. G. Imperfections in crystals. New York, N.Y., Interscience Publishers, Inc. 1961.

18. Ke, T. S. Experimental evidence of the viscous behavior of grain boundaries in metals. Physical Review 71: 533-546. 1947.

19. Pearson, W. and R. T. Rotherham. Internal friction and grain boundary viscosity of silver and heavy silver solid solution. Journal of Metals 8: 894-901. 1956.

20. Hasiguti, R. R. Internal friction of metals due to crystal imperfections. In Proceedings of the International Conference of Theoretical Physics, Kyoto and Tokyo. pp. 573-585. Tokyo, Japan, The Organizing Committee International Conference of Theoretical Physics Science Council of Japan. 1953.

21. Snoek, J. L. Effect of small quantities of carbon and nitrogen on the elastic and plastic properties of iron. Physica 8: 711-733. 1941.

22. Seeger, A., P. Scheller and H. Kronmüller. Observations of interstitial atoms in face centered cubic metals. Philosophical Magazine, Series 56, 5: 853-857. 1960.

23. Bordoni, P. G. Elastic and inelastic behavior of some metals at very low temperatures. Acoustical Society of America Journal 26: 495-502. 1954.

24. Mason, W. P. Dislocation relaxation at low temperatures and determination of the limiting shearing stress of a metal. Physical Review, Series 4, 98: 1136-1138. 1955.

25. Seeger, A. On the theory of low-temperature internal friction peak observed in metals. Philosophical Magazine, Series 7, 1: 651-662. 1956.

26. Gordon, R. B. and A. S. Nowick. The pinning of dislocation by X-irradiation of alkali halide crystals. Acta Metallurgica 5: 514-527. 1956.

27. Granato, A. and K. Lücke. Theory of mechanical damping due to dislocations. [I.] Journal of Applied Physics, Series 6, 27: 583-592. 1956.

28. Granato, A. and K. Lücke. Application of dislocation theory to internal friction phenomena at high frequencies. [II.] Journal of Applied Physics, Series 7, 27: 587-595. 1956.

29. Cottrell, A. H. Dislocation and plastic flow in crystals. New York, N.Y., The Clarendon Press. 1958.

30. Swartz, J. C. and J. Weertman. Modification of the Koehler-Granato-Lücke dislocation damping theory. Journal of Applied Physics 32: 1860-1865. 1961.

31. Rogers, D. H. An extension of a theory of mechanical damping due to dislocation. Journal of Applied Physics 33: 781-792. 1962.

32. Teutonico, L. J., A. V. Granato and K. Lücke. Theory of the thermal breakaway of a pinned dislocation line with application to damping phenomena. Journal of Applied Physics 35: 220-234. 1964.

33. Mott, N. F. Mechanical strength and creep in metals. In Shockley, W., editor. Imperfections in nearly perfect crystals. pp. 173-196. New York, N.Y., John Wiley and Sons, Inc. 1952.

34. Granato, A. V., K. Lücke, J. Schlipt and L. J. Teutonico. Entropy factors for thermally activated unpinning of dislocation. Journal of Applied Physics 33: 2732-2745. 1964.

35. Southgate, P. D. and K. S. Mendelson. Dislocation mobility and pinning in hard materials through internal friction studies. Wright-Patterson Air Force Base Technical Documentary Report NR ASP-TDR-62-431. 1963.

36. Chick, B., A. Hikata, G. Anderson, C. Elbaum, and R. Truell. Ultrasonic methods in the study of deformation in single crystals. Wright-Patterson Air Force Base Air Force Materials Laboratory Technical Documentary Report No. ML-TDR-64-34. 1964.

37. Huber, R. J., G. S. Baker and P. Gibbs. Internal friction in aluminum oxide single crystals. University of Utah Department of Physics Technical Report 14. 1960.

38. Rostaker, W. and W. Brentnall. Yielding in polycrystalline metals. Wright-Patterson Air Force Base Aerospace Research Laboratories Technical Documentary Report ARL 63-245. 1964.

39. Butera, R. A. and P. Kafstad. Internal friction in the vanadium-hydrogen system. Journal of Applied Physics 34: 2172-2174. 1963.

40. Hutchison, T. S., D. H. Rogers, and R. R. Turkington. Thermally activated internal friction in aluminum. Journal of Applied Physics 36: 2213-2219. 1965.

41. Hutchison, T. S. and D. H. Rogers. Ultrasonic damping at kilocycle frequencies in aluminum at low temperatures. Journal of Applied Physics 33: 792-799. 1962.

42. Thompson, D. O. and D. K. Holmes. Dislocation contribution contribution to the temperature dependence of the internal friction and Young's modulus of copper. Journal of Applied Physics 30: 525-541. 1959.

43. Fiore, N. F. and C. L. Bauer. Solute atom--dislocation binding energy in dilute Cu-Ge alloys. Acta Metallurgica 12: 1329-1336. 1964.

44. Southgate, P. D. Internal friction in germanium and silicon. Physical Society London Proceedings 76: 385-408. 1960.

45. Berry, B. S. Review of internal friction due to point defects. Acta Metallurgica 10: 271-279. 1962.

46. Turner, T. J. and G. P. Williams, Jr. Internal friction in silver solid solution. Acta Metallurgica 10: 305-311. 1962.

47. Nowick, A. S. and B. S. Berry. The Zener relaxation as a distribution of relaxation time. Acta Metallurgica 10: 312-318. 1962.

48. Stern, R. M. and A. V. Granato. Overdamped resonance of dislocation in copper. Acta Metallurgica 10: 358-381. 1962.

49. Hutchison, T. S., S. L. McBride and D. H. Rogers. Dislocation pinning in aluminum at low temperatures. Acta Metallurgica 10: 397-400. 1962.

50. Chambers, R. H. and J. Schultz. Dislocation relaxation spectra in plastically deformed refractory b.c.c. metals. Acta Metallurgica 10: 466-483. 1962.

51. Tsang-Chu Tsui, R. Low temperature internal friction in plastically deformed magnesium. U.S. Atomic Energy Commission Publication TID-14140. [Division of Technical Information Extension, AEC.] 1960.

52. Baker, G. S. Internal friction in the presence of a static stress. Journal of Applied Physics 28: 734-737. 1957.

53. Wachtman, J. B., Jr., and D. G. Lam, Jr. Young's modulus of various refractory materials as a function of temperature. American Ceramic Society Journal 42: 254-260. 1959.

54. Schoeck, G., E. Bisogni, and J. Shyne. The activation energy of high temperature internal friction. Acta Metallurgica 12: 1466-1468. 1964.

55. Fitzgerald, J. V. Anelasticity of glass: Internal friction and sodium ion diffusion in tank plate glass, a typical soda-lime-silica glass. American Ceramic Society Journal 34: 339-342. 1951.

56. Astbury, N. F. and W. R. Davis. Internal friction in ceramics. British Ceramic Society Transactions 63: 1-18. 1964.

57. Granato, A., J. De Klerk and R. Truell. Dispersion of elastic waves in NaCl. Physical Review 108: 895-896. 1957.

58. Niblett, D. H. and J. Wilks. Dislocation damping in metals. Advances in Physics 9: 1-88. 1960.

59. Frankl, D. R. The internal friction of rock salt single crystals. Physical Review, Series 3, 29: 573-579. 1953.

60. Johnston, W. G. and J. J. Gilman. Dislocation velocities, dislocation densities, and plastic flow in lithium fluoride crystals. Journal of Applied Physics 30: 129-144. 1959.

61. Whitworth, R. W. Some effects of vibration on the internal friction of sodium chloride. Philosophical Magazine, Series 8, 5: 425-440. 1959.

62. Johnston, W. G. and J. J. Gilman. Dislocation multiplication in lithium fluoride crystals. Journal of Applied Physics 4: 632-643. 1960.

63. Bauer, C. L. and R. B. Gordon. Dislocation damping effects in rock salt. Journal of Applied Physics 31: 945-949. 1960.

64. Davidge, R. W. and R. W. Whitworth. Evidence for the production of debris by moving dislocation in sodium chloride. Philosophical Magazine 6: 217-224. 1960.

65. Whitworth, R. W. Change of elastic modulun associated with internal friction in sodium chloride. Philosophical Magazine 7: 1115-1118. 1961.

66. Taylor, A. Low temperature internal friction peaks in single crystals of NaCl and LiF. Journal of Applied Physics 32: 1799-1800. 1961.

67. Bauer, C. L. and R. B. Gordon. Mechanism for dislocation pinning in the alkali halides. Journal of Applied Physics 33: 672-682. 1962.

68. Huntington, H. B., J. E. Dickey and R. Thomson. Dislocation energies in NaCl. Physical Review, Series 4, 100: 117-1128. 1955.

69. Gibbons, D. F. and V. G. Chirba. The effect of plastic deformation on the attenuation of acoustic waves in lithium fluoride crystals. Acta Metallurgica 10: 484-488. 1962.

70. Taylor, A. Low temperature internal friction in monocrystalline lithium fluoride. Acta Metallurgica 10: 489-495. 1962.

71. Baker, G. S. Dislocation mobility and damping in LiF. Journal of Applied Physics 33: 1730-1732. 1962.

72. Okada, T. and T. Suita. Ultrasonic Attenuation and some related behaviors in irradiated alkali halide crystals. Physical Society of Japan Journal Supplement 1, 18: 135-141. 1963.

73. Shvidkovsky, E. G., E. P. Belozerona and N. A. Tyapunina. Effect of high-frequency vibrations on the dislocation structure and on internal friction of alkali halide crystals. Physical Society of Japan Journal Supplement 1, 18: 161-162. 1963.

74. Stepanova, V. M. Cinemicrography of etching and the behavior of dislocations in NaCl crystals. Soviet Physics--Crystallography 8: 543-545. 1963.

75. Belozerova, E. P., N. A. Tyapunina and E. G. Shvidkovskii. Dislocation multiplication in alkali-halide crystals under the influence of high-frequency vibration. Soviety Physics--Crystallography 8: 172-175. 1963.

76. Nadgornyi, E. M. and A. V. Stepanov. Artificial slip formation and dislocation structure in sodium chloride crystals. Soviet Physics-Crystallography 8: 512-519. 1964.

77. Whitworth, R. W. Atomic mechanisms for the transport of charge by dislocation in NaCl type crystals. Philosophical Magazine 11: 83-90. 1965.

78. Barr, L. W., J. A. Morrison and P. A. Schroeder. Anion diffusion in crystals of NaCl. Journal of Applied Physics 36: 624-631. 1965.

79. Stokes, R. J. Mechanical properties of polycrystalline sodium chloride. U.S. Atomic Energy Commission Report ONR 032-451 [Office of Naval Research, Washington, D. C.] 1965.

80. Dryden, J. S., S. Morimato and J. S. Cook. The hardness of alkali halide crystals containing divalent ion impurities. Philosophical Magazine 12: 379-391. 1965.

81. Long, S. A. and T. D. McGee. The effect of grain boundaries on the plastic deformation of sodium chloride. American Ceramic Society Journal 46: 583-587. 1963.

VIII. ACKNOWLEDGMENTS

The author wishes to express his gratitude to Dr. Thomas D. McGee for his guidance and encouragement throughout the course of this research.

The support of this research by the U.S. Army Research Office (Durham) is gratefully acknowledged.

IX. APPENDIX

Table 6. Internal friction and strain amplitude data for quartz oscillator

Input voltage (volts)	Output voltage (volts)	Strain amplitude (10^{-5})	Internal friction (10^{-5})
0.52	0.32	0.20	17.6
1.55	0.75	0.47	17.0
2.90	1.70	1.05	15.3
7.50	3.50	2.17	17.2
15.00	7.60	4.72	16.4
40.00	18.00	11.15	18.0
		Average	16.92

Table 7. Internal friction and dislocation density as a function of strain amplitude for crystal G

Input voltage (volts)	Output voltage (volts)	Strain amplitude (10^{-5})	Internal friction (10^{-5})	Dislocation density (10^6 dislocations/cm^2)
0	0	0	-	0.45
0.83	0.43	0.23	7	0.86
5.60	0.83	0.52	17	1.07
10.20	1.20	0.75	130	1.12
18.70	1.60	0.99	211	1.53
38.50	2.00	1.24	400	1.65
59.00	2.20	1.36	585	2.28

Table 8. Internal friction and dislocation density as a function of strain amplitude for crystal H

Input voltage (volts)	Output voltage (volts)	Strain amplitude (10^{-5})	Internal friction (10^{-5})	Dislocation density (10^6 dislocations/cm^2)
0	0	-	-	0.53
0.58	0.20	0.12	91	-
0.92	0.26	0.16	130	0.84
12.20	0.50	0.31	820	1.01
24.80	0.70	0.43	1230	1.28
40.00	0.95	0.59	1450	-
41.00	0.98	0.61	1430	1.69
60.00	1.10	0.63	1860	1.83
6.80	0.30	0.19	775	-
13.20	0.46	0.29	980	-
22.00	0.60	0.37	1250	-
36.50	0.80	0.50	1700	-
48.00	0.96	0.60	1710	-
62.00	1.15	0.71	1850	2.00

Table 9. Internal friction and dislocation density as a function of strain amplitude for crystal I

Input voltage (volts)	Output voltage (volts)	Strain amplitude (10^{-5})	Internal friction (10^{-5})	Dislocation density (10^6 dislocations/cm^2)
0	0	-	-	1.19
3.40	0.29	0.18	394	1.39
18.00	0.54	0.34	1135	2.29
25.00	0.66	0.41	1295	3.57
37.00	0.88	0.55	1440	2.99
63.10	1.20	0.75	1800	3.00
63.50	1.27	0.78	1710	4.98
46.00	1.00	0.62	1570	-
20.00	0.60	0.37	1140	-
7.00	0.25	0.16	960	-
	Crystal I reannealed 600°C for 24 hours			
2.80	0.31	0.19	310	-
6.00	0.40	0.25	510	-
10.50	0.50	0.31	720	-
20.00	0.65	0.40	1055	-
29.50	0.80	0.50	1260	-
40.00	0.95	0.59	1450	-
49.10	1.10	0.68	1530	-
59.00	1.25	0.78	1610	6.37

Table 10. Internal friction and dislocation density as a function of strain amplitude for crystal J

Input voltage (volts)	Output voltage (volts)	Strain amplitude (10^{-5})	Internal friction (10^{-5})	Dislocation density (10^6 dislocations/cm^2)
0	0	-	-	3.00
2.3	0.43	0.27	180	3.14
8.4	0.54	0.34	530	3.87
18.4	0.72	0.45	875	4.47
23.0	0.80	0.49	975	4.00
28.0	0.86	0.53	1120	4.40
29.0	0.90	0.56	1110	4.60
3910	1.00	0.62	1330	-
47.0	1.15	0.71	1400	4.76
56.00	1.30	0.81	1470	7.40
42.0	1.00	0.62	1440	-
26.0	0.80	0.45	1110	-
13.6	0.58	0.36	805	-
3.2	0.40	0.25	274	-
7.1	0.50	0.31	485	-
17.2	0.70	0.43	842	-
24.8	0.89	0.55	960	-
42.0	1.10	0.68	1310	-
51.0	1.20	0.75	1450	7.40

Table 11. Internal friction and dislocation density as a function of strain amplitude for crystal K

Input voltage (volts)	Output voltage (volts)	Strain amplitude (10^{-5})	Internal friction (10^{-5})	Dislocation density (10^6 dislocations/cm^2)
0	0	-	-	1.18
1.8	0.42	0.26	147	2.90
5.4	0.50	0.31	370	3.90
11.5	0.64	0.40	615	4.70
12.0	0.76	0.48	540	5.33
28.0	0.86	0.55	1285	16.00
58.0	1.00	0.62	1980	16.00

Table 12. Internal friction and dislocation density as a function of strain amplitude for crystal L

Input voltage (volts)	Output voltage (volts)	Strain amplitude (10^{-5})	Internal friction (10^{-5})	Dislocation density (10^6 dislocations/cm^2)
0	0	-	-	*-
1.8	0.30	0.19	0	-
2.4	0.38	0.24	0	-
3.2	0.46	0.29	0	-

*Dislocation density was so high that no count could be made with aid of optical microscope

Table 12. (Continued)

Input voltage (volts)	Output voltage (volts)	Strain amplitude (10^{-5})	Internal friction (10^{-5})	Dislocation density (10^6 dislocations/cm^2)
3.40	0.54	0.34	0	-
4.0	0.61	0.37	26	-
4.6	0.67	0.41	30	-
5.8	0.80	0.50	16	-
6.7	0.90	0.56	20	-
8.9	1.10	0.68	26	-
11.2	1.30	0.81	25	-
18.0	1.60	0.99	39	-
26.8	2.00	1.24	49	-
62.0	3.00	1.86	206	-
2.5	0.36	0.22	26	-
9.1	0.90	0.56	37	-
38.0	2.1	1.30	158	-
6.6	0.81	0.50	22	-
13.0	1.30	0.71	37	-
38.0	2.20	1.36	120	-
62.0	3.00	1.86	215	-

Table 13. Internal friction and dislocation density as a function of strain amplitude for crystal M

Input voltage (volts)	Output voltage (volts)	Strain amplitude (10^{-5})	Internal friction (10^{-5})	Dislocation density (10^6 dislocations/cm^2)
0	0	-	-	0.60
2.6	0.34	0.21	19	0.90
3.6	0.43	0.27	27	1.10
3.1	0.52	0.32	9	-
4.8	0.62	0.38	27	0.60
7.9	0.80	0.43	102	0.85
11.5	0.96	0.60	149	1.10
20.0	1.40	0.87	174	1.30
39.0	2.10	1.30	283	1.30
60.0	2.78	1.73	303	1.50
59.0	2.74	1.70	303	-
34.0	1.85	1.15	258	-
13.3	0.98	0.62	191	-
2.4	0.34	0.21	15	-
14.4	1.00	0.62	144	-
29.0	1.6	0.99	200	-
39.5	2.0	1.24	274	-
59.5	2.8	1.75	297	1.80

Table 14. Internal friction and dislocation density as a function of strain amplitude for crystal N

Input voltage (volts)	Output voltage (volts)	Strain amplitude (10^{-5})	Internal friction (10^{-5})	Dislocation density (10^6 dislocations/cm^2)
0	0	-	-	1.75
3.0	0.38	0.24	12	1.76
4.6	0.52	0.32	29	1.90
4.8	0.72	0.45	1	1.70
8.0	0.94	0.58	52	1.70
19.2	1.50	0.93	145	2.30
26.7	2.30	1.43	169	2.60
50.0	3.00	1.86	285	2.80
59.0	3.42	2.12	285	3.90
54.0	3.10	1.92	300	-
27.0	2.00	1.24	169	-
9.1	1.0	0.62	50	-
4.9	0.69	0.42	0	-
1.3	0.30	0.19	0	-
3.3	0.61	0.38	9	-
5.4	0.80	0.50	16	-
18.0	1.55	0.96	92	-
30.0	2.15	1.33	130	-
42.5	2.70	1.67	154	-
56.5	3.10	1.92	255	4.9

Table 15. Internal friction and dislocation density as a function of strain amplitude for crystal 0

Input voltage (volts)	Output voltage (volts)	Strain amplitude (10^{-5})	Internal friction (10^{-5})	Dislocation density (10^6 dislocations/cm^2)
0	0	-	-	1.0
1.7	0.32	0.20	170	1.3
1.9	0.36	0.22	180	-
2.2	0.40	0.25	186	-
2.5	0.46	0.29	185	1.6
2.7	0.50	0.30	185	-
2.9	0.55	0.34	186	-
3.3	0.61	0.38	186	1.8
6.0	0.76	0.47	270	-
7.5	0.90	0.56	286	-
9.4	1.00	0.62	322	1.93
14.2	1.25	0.78	380	-
18.8	1.50	0.93	425	-
23.7	1.75	1.09	458	2.1
28.5	2.0	1.24	483	-
37.0	2.2	1.36	556	-
36.2	2.4	1.49	510	-
43.0	2.7	1.68	540	-
50.0	3.0	1.86	564	-
58.0	3.2	1.98	618	2.5

Table 16. Internal friction and dislocation density as a function of strain amplitude for crystal P

Input voltage (volts)	Output voltage (volts)	Strain amplitude (10^{-5})	Internal friction (10^{-5})	Dislocation density (10^6 dislocations/cm^2)
0	0	-	-	1.08
1.2	0.28	0.17	150	-
1.5	0.32	0.20	161	-
1.8	0.38	0.24	165	1.06
2.3	0.44	0.29	174	-
2.7	0.48	0.30	191	-
3.0	0.52	0.32	198	1.21
3.2	0.55	0.34	198	-
3.55	0.6	0.37	200	-
3.9	0.64	0.39	208	1.28
7.5	0.66	0.41	382	-
9.2	0.76	0.47	412	-
11.0	0.84	0.52	450	1.60
12.0	0.90	0.56	455	-
14.0	1.00	0.62	480	1.81
17.8	1.10	0.68	552	-
20.3	1.20	0.75	580	-
22.9	1.3	0.81	600	-
25.3	1.4	0.87	620	2.53
30.0	1.65	1.02	620	-
32.5	1.82	1.13	615	-
40.0	2.00	1.24	685	4.20
55.0	2.20	1.36	855	-

Table 17. Internal friction and dislocation density as a function of strain amplitude for crystal Q

Input voltage (volts)	Output voltage (volts)	Strain amplitude (10^{-5})	Internal friction (10^{-5})	Dislocation density (10^6 dislocations/cm^2)
0	0	-	-	1.12
7.0	0.28	0.17	855	-
7.8	0.32	0.20	825	-
8.6	0.36	0.22	800	-
8.7	0.44	0.27	690	-
9.2	0.48	0.30	650	-
9.8	0.52	0.32	695	-
10.0	0.57	0.35	600	-
10.2	0.61	0.38	600	-
11.2	0.67	0.42	600	-
12.8	0.74	0.46	600	-
14.5	0.82	0.51	610	-
16.6	0.90	0.56	645	-
19.0	1.00	0.62	650	-
24.8	1.20	0.72	710	-
34.0	1.50	0.90	775	-
49.0	1.85	1.15	910	-
54.0	1.99	1.23	930	-
46.0	2.14	1.33	855	4.2

Table 18. Internal friction and dislocation density as a function of strain amplitude for crystal S

Input voltage (volts)	Output voltage (volts)	Strain amplitude (10^{-5})	Internal friction (10^{-5})	Dislocation density (10^6 dislocations/cm^2)
0	0	-	-	0.8
1.5	0.38	0.24	57	-
1.6	0.42	0.26	55	-
1.9	0.48	0.30	59	-
2.3	0.56	0.35	62	-
2.9	0.64	0.40	67	1.0
3.4	0.72	0.45	70	-
4.4	0.84	0.52	78	-
5.8	1.0	0.62	87	-
9.1	1.3	0.81	105	-
12.0	1.6	0.99	112	1.3
16.8	2.0	1.24	126	-
18.7	2.3	1.43	120	-
22.5	2.6	1.61	130	-
26.0	2.9	1.80	135	-
36.0	3.7	2.29	146	-
42.5	4.2	2.60	151	-
49.0	4.8	2.98	153	-
58.0	5.4	3.35	160	1.8

Table 19. Internal friction and dislocation density as a function of strain amplitude for crystal V

Input voltage (volts)	Output voltage (volts)	Strain amplitude (10^{-5})	Internal friction (10^{-5})	Dislocation density (10^6 dislocations/cm^2)
0	0	-	-	1.6
2.4	0.34	0.21	23	-
2.3	0.41	0.25	10	-
2.7	0.51	0.32	8	-
3.1	0.60	0.37	52	-
4.0	0.72	0.45	55	-
4.6	0.82	0.51	56	-
5.6	1.0	0.62	55	-
7.6	1.2	0.74	63	-
8.8	1.4	0.87	77	-
11.8	1.8	1.09	97	-
14.2	2.0	1.24	105	-
18.5	2.3	1.43	120	-
20.0	2.6	1.61	115	-
32.0	3.6	2.23	133	-
43.2	4.4	2.73	147	-
59.0	6.5	4.03	137	2.1

Table 20. Internal friction as a function of strain amplitude for crystal x (stockbarger NaCl)

Input voltage (volts)	Output voltage (volts)	Strain amplitude 10^{-5}	Internal friction 10^{-5}
24.8	0.34	0.21	2500
30.1	0.42	0.26	2480
34.0	0.48	0.30	2420
39.0	0.54	0.34	2460
46.5	0.64	0.40	2500
54.0	0.74	0.46	2500
61.5	0.84	0.52	2500

Table 21. Internal friction as a function of strain amplitude for crystal y

Input vol tage (volts)	Output voltage (volts)	Strain amplitude (10^{-5})	Internal friction (10^{-5})
3.2	0.38	0.24	29
4.35	0.54	0.34	117
6.0	0.68	0.42	131
8.4	0.84	0.52	150
11.5	1.00	0.62	172
16.2	1.30	0.81	185
28.3	2.00	1.24	210
36.0	2.40	1.49	225
53.5	3.30	2.04	243

Table 22. Internal friction as a function of strain amplitude for crystal α

Input voltage (volts)	Output voltage (volts)	Strain amplitude 10^{-5}	Internal friction 10^{-5}
13.8	0.20	0.12	2370
15.0	0.22	0.14	2340
16.6	0.24	0.15	2370
13.8	0.30	0.18	1570
16.8	0.34	0.21	1690
22.0	0.40	0.25	1890
28.0	0.45	0.28	2130
51.0	0.66	0.41	2640
59.0	0.80	0.50	2530
61.0	1.02	0.63	2050

Table 23. Internal friction as a function of strain amplitude for crystal β

Input voltage (volts)	Output voltage (volts)	Strain amplitude 10^{-5}	Internal friction 10^{-5}
13.5	0.18	0.11	2560
20.0	0.28	0.17	2440
24.4	0.34	0.21	2450
29.0	0.40	0.25	2480
58.5	0.77	0.48	2600

Table 24. Internal friction as a function of strain amplitude for crystal γ

Input voltage (volts)	Output voltage (volts)	Strain amplitude 10^{-5}	Internal friction 10^{-5}
21.0	0.27	0.17	2660
27.3	0.36	0.22	2630
37.5	0.48	0.30	2670
46.0	0.58	0.36	2460
58.0	0.73	0.46	2700
62.0	0.75	0.47	2820

Table 25. Internal friction as a function of strain amplitude for crystal δ

Input voltage (volts)	Output voltage (volts)	Strain amplitude 10^{-5}	Internal friction 10^{-5}
14.5	0.17	0.11	3020
17.1	0.23	0.14	2840
27.0	0.31	0.19	2970
36.0	0.41	0.25	3000
41.0	0.49	0.30	2860
50.0	0.58	0.36	2880

Table 26. Internal friction as a function of strain amplitude for crystal ε

Input voltage (volts)	Output voltage (volts)	Strain amplitude 10^{-5}	Internal friction 10^{-5}
9.4	0.20	0.12	1630
16.2	0.30	0.15	1880
26.0	0.40	0.25	2050
33.0	0.50	0.31	2290
41.5	0.60	0.37	2400
55.5	0.78	0.48	2500

Table 27. Internal friction as a function of strain amplitude for crystal

Input voltage (volts)	Output voltage (volts)	Strain amplitude 10^{-5}	Internal friction 10^{-5}
9.8	0.20	0.12	1670
13.0	0.25	0.13	1780
18.0	0.32	0.20	1920
24.4	0.40	0.25	2080
32.0	0.50	0.31	2120
41.0	0.60	0.37	2340
50.0	0.70	0.43	2440
61.0	0.90	0.56	2320

Table 28. Internal friction as a function of strain amplitude for kyropolous grown single crystal A and B

Input voltage (volts)	Output voltage (volts)	Strain amplitude 10^{-5}	Internal friction 10^{-5}
Kyropolous A			
4.0	0.34	0.21	0
5.3	0.42	0.26	0
6.6	0.51	0.32	15
10.5	0.63	0.39	22
12.0	0.64	0.40	652
16.0	0.79	0.49	700
19.0	1.00	0.62	650
29.0	1.60	0.99	620
41.0	2.00	1.24	710
Kyropolous B			
4.0	0.52	0.33	0
6.4	0.89	0.55	16
10.0	1.10	0.68	150
13.5	1.45	0.90	180
28.0	1.85	1.15	430
52.0	2.70	1.67	660
60.0	3.00	1.86	1010

Table 29. Internal friction as a function of strain amplitude for isomet crystals A, B, and C

Input voltage (volts)	Output voltage (volts)	Strain amplitude 10^{-5}	Internal friction 10^{-5}
Isomet A			
2.0	0.38	0.24	23
2.9	0.52	0.32	33
3.8	0.63	0.39	72
6.0	0.82	0.51	87
8.1	1.20	0.74	80
15.0	1.49	0.92	119
23.3	2.10	1.30	734
42.0	2.45	1.52	205
48.0	3.40	2.11	170
49.5	3.70	3.39	161
Isomet B			
3.0	0.2	0.12	180
5.4	0.3	0.19	216
10.8	0.48	0.30	270
15.8	0.60	0.37	308
21.0	0.79	0.49	320
24.0	1.10	0.68	262
29.0	1.85	1.15	189
32.0	2.70	1.67	142
39.0	3.60	2.23	130
45.5	4.40	2.72	122
48.5	3.0	3.10	118

Table 29. (Continued)

Input voltage (volts)	Output voltage (volts)	Strain amplitude 10^{-5}	Internal friction 10^{-5}
Isomet C			
0.6	0.28	0.17	24
1.2	0.66	0.41	22
1.6	0.90	0.56	21
2.7	1.55	0.96	20
4.1	2.50	1.55	20
6.4	4.00	2.48	19
13.5	8.0	4.96	20
31.0	14.5	9.00	26
46.0	19.0	11.8	29

Table 30. Internal friction as a function of strain amplitude at 23°C for crystals HT-A and HT-A'

Input voltage (volts)	Output voltage (volts)	Strain amplitude 10^{-5}	Internal friction 10^{-5}
HT-A			
0.7	0.28	0.17	1
1.0	0.41	0.25	0
1.4	0.58	0.36	9
2.6	0.82	0.51	11
5.4	1.10	0.68	36
9.5	1.50	0.93	56
17.0	2.00	1.24	87
23.5	2.50	1.55	100
30.0	3.00	1.86	110
44.0	4.0	2.48	125
58.0	5.0	3.10	134
HT-A'			
0.9	0.46	0.29	1
1.5	0.62	0.38	10
3.0	0.80	0.50	36
6.0	1.00	0.62	80
10.0	1.20	0.74	125
17.0	1.60	0.99	168
25.0	2.10	1.30	192
37.0	2.70	1.67	227

Table 30. (Continued)

Input voltage (volts)	Output voltage (volts)	Strain amplitude 10^{-5}	Internal friction 10^{-5}
45.5	3.30	2.04	229
59.0	4.30	2.66	227

Table 31. Internal friction as a function of strain amplitude at 100°C for crystal HT-B

Input voltage (volts)	Output voltage (volts)	Strain amplitude 10^{-5}	Internal friction 10^{-5}
12.0	0.20	0.12	6000
23.4	0.30	0.19	7800
30.0	0.38	0.24	7900
31.5	0.48	0.30	6560
38.0	0.56	0.35	6800
46.0	0.66	0.41	7000
50.0	0.72	0.48	6950
49.0	1.00	0.62	4900

Table 32. Internal friction as a function of strain amplitude at 50°C for crystal HT-C

Input voltage (volts)	Output voltage (volts)	Strain amplitude 10^{-5}	Internal friction 10^{-5}
1.7	0.20	0.12	390
2.7	0.26	0.16	480
4.0	0.36	0.22	515
2.6	0.44	0.27	300
5.8	0.50	0.31	536
7.6	0.62	0.38	570
8.0	0.78	0.48	475
9.9	0.98	0.61	480
17.2	1.20	0.74	678
26.5	1.40	0.87	900
36.0	1.60	0.99	1090
51.0	1.80	1.12	1105

Table 33. Internal friction as a function of strain amplitude at 75°C for crystal HT-D

Input voltage (volts)	Output voltage (volts)	Strain amplitude 10^{-5}	Internal friction 10^{-5}
12.8	0.20	0.12	6400
19.8	0.30	0.19	6600
28.4	0.42	0.26	6760
35.0	0.52	0.32	6730
40.0	0.60	0.37	6670
47.5	0.70	0.43	6780
51.0	0.75	0.47	6800

Table 34. Internal friction as a function of strain amplitude and temperature for crystal HT-E

Input voltage (volts)	Output voltage (volts)	Strain amplitude 10^{-5}	Internal friction 10^{-5}	Temperature °C
3.4	0.24	0.15	124	24
19.0	0.25	0.16	7600	28
18.5	0.24	0.15	7710	50
18.5	0.24	0.15	7710	75
19.0	0.24	0.15	7930	100
19.5	0.24	0.15	8140	125
19.5	0.24	0.15	8100	150
19.5	0.24	0.15	8140	175

Table 34. (Continued)

Input voltage (volts)	Output voltage (volts)	Strain amplitude 10^{-5}	Internal friction 10^{-5}	Temperature °C
20.0	0.24	0.15	8300	200
20.0	0.24	0.15	8300	225
19.8	0.24	0.15	8250	250
19.8	0.24	0.15	8250	275
19.8	0.25	0.16	7930	300
27.0	0.33	0.20	8200	300
36.5	0.44	0.27	8300	300
47.0	0.56	0.35	8400	300
54.0	0.64	0.40	8430	300
43.0	0.88	0.55	4890	300
50.0	1.10	0.68	4540	300
50.5[a]	1.55	0.96	3250	300
50.0[a]	1.85	1.15	2700	300
50.0[a]	2.30	1.43	2170	300
50.0[a]	2.50	1.55	2000	300

[a]-10 minutes oscillating time since last measurement.

Table 35. Internal friction as a function of strain amplitude and temperature for crystal HT-F

Input voltage (volts)	Output voltage (volts)	Strain amplitude 10^{-5}	Internal friction 10^{-5}	Temperature °C
2.4	0.30	0.19	600	24
2.4	0.30	0.19	600	50
24.0	0.32	0.20	13,930	65
24.0	0.32	0.20	13,930	100
25.0	0.34	0.21	13,630	132
24.0	0.32	0.20	13,930	154
24.0	0.44	0.27	10,130	200
32.0	0.60	0.37	9870	200
40.0	0.94	0.58	7800	200
50.0	1.30	0.81	7100	200
52.0	1.55	0.96	6200	200

Table 36. Internal friction as a function of strain amplitude and temperature for crystal HT-stockbarger

Input voltage (volts)	Output voltage (volts)	Strain amplitude 10^{-5}	Internal friction 10^{-5}	Temperature °C
4.1	0.30	0.19	1300	24
3.6	0.30	0.19	1120	25
5.0	0.30	0.19	1600	26
4.8	0.26	0.16	1760	50
5.4	0.30	0.19	1710	75
8.9	0.30	0.19	2870	100
22.5	0.30	0.19	7370	105
23.0	0.30	0.19	7550	125
30.0	0.40	0.25	7370	125
35.0	0.52	0.32	7370	125
44.0	0.64	0.40	6750	125
55.0	0.74	0.46	7300	125
Crystal allowed to cool				
4.0	0.30	0.19	1200	23
4.0	0.32	0.20	1160	50
23.5	0.32	0.20	7230	75
24.0	0.32	0.20	7400	100
14.2	0.32	0.20	4330	125
11.1	0.32	0.20	3370	150
22.5	0.30	0.19	7400	175
22.5	0.30	0.19	7400	200

Table 36. (Continued)

Input voltage (volts)	Output voltage (volts)	Strain amplitude 10^{-5}	Internal friction 10^{-5}	Temperature °C
22.0	0.30	0.19	7230	225
22.5	0.30	0.19	7400	250
22.5	0.30	0.19	7400	275
22.5	0.30	0.19	7400	300
29.5	0.40	0.25	7230	300
37.5	0.50	0.31	7400	300
46.5	0.60	0.37	7500	300
52.5	0.70	0.43	7400	300
55.0	0.74	0.46	7300	300
15 minutes of maximum strain oscillating time at 300°C				
51.0	7.40	4.58	600	300

Table 37. Internal friction as a function of strain amplitude and temperature for crystal HT-isomet

Input voltage (volts)	Output voltage (volts)	Strain amplitude 10^{-5}	Internal friction 10^{-5}	Temperature °C
1.0	0.32	0.20	210	25
2.0	0.32	0.20	490	46
5.2	0.30	0.19	1500	50
2.7	0.30	0.19	730	75
10.0	0.30	0.19	2900	90
24.5	0.32	0.20	6800	100
24.5	0.32	0.20	6800	125
24.5	0.32	0.20	6800	150
24.0	0.32	0.20	6700	175
24.0	0.32	0.20	6700	200
24.7	0.32	0.20	6870	225
24.7	0.32	0.20	6870	250
24.7	0.32	0.20	6870	275
24.0	0.32	0.20	6700	300
30.0	0.40	0.25	6700	300
38.0	0.50	0.31	6730	300
47.0	0.60	0.37	7000	300
56.0	0.70	0.43	7100	300

Table 38. Internal friction as a function of strain amplitude and temperature for crystal HT-G

Input voltage (volts)	Output voltage (volts)	Strain amplitude 10^{-5}	Internal friction 10^{-5}	Temperature °C
2.4	0.18	0.11	630	23
6.9	0.26	0.16	1310	23
22.0	0.31	0.19	3630	23
30.0	0.41	0.25	3750	23
38.0	0.51	0.32	3800	23
45.0	0.61	0.39	3770	23
52.0	0.70	0.43	3800	23
56.0	0.79	0.49	3610	23
23.2	0.32	0.20	3700	23
23.5	0.32	0.20	3750	50
24.0	0.32	0.20	3830	75
6.7	0.32	0.20	1010	100
4.8	0.32	0.20	640	125
4.8	0.32	0.20	710	125
3.5	0.32	0.20	515	150
2.9	0.32	0.20	400	175
2.6	0.32	0.20	350	200
2.2	0.32	0.20	290	225
2.0	0.32	0.20	255	250
2.0	0.32	0.20	255	275

Table 38. (Continued)

Input voltage (volts)	Output voltage (volts)	Strain amplitude 10^{-5}	Internal friction 10^{-5}	Temperature °C
1.9	0.32	0.20	240	300
1.4	0.32	0.20	157	300
2.3	0.40	0.25	230	300
3.0	0.53	0.33	245	300
3.9	0.70	0.43	221	300
4.4	0.84	0.52	203	300
5.4	1.00	0.62	130	300
9.0	1.90	1.18	177	300
14.5	3.0	1.86	182	300
25.0	4.8	2.98	201	300
37.2	7.2	4.56	199	300
21.5	3.7	2.39	232	300
19.5	3.0	1.86	270	300
2.8	0.32	0.20	385	300

Table 39. Internal friction as a function of strain amplitude and temperature for crystal HT-H

Input voltage (volts)	Output voltage (volts)	Strain amplitude 10^{-5}	Internal friction 10^{-5}	Temperature °C
0.5	0.24	0.15	0	22
0.7	0.32	0.20	0	22
1.6	0.32	0.20	5	50
2.3	0.32	0.20	10	75
4.2	0.32	0.20	79	100
3.2	0.32	0.20	44	125
3.3	0.32	0.20	51	150
2.8	0.32	0.20	30	175
2.9	0.32	0.20	34	200
3.6	0.32	0.20	58	225
4.3	0.32	0.20	83	250
4.9	0.32	0.20	105	275
4.2	0.32	0.20	79	300
5.4	0.40	0.25	84	300
6.8	0.50	0.31	86	300
8.4	0.60	0.37	90	300
10.1	0.70	0.43	94	300
12.0	0.81	0.50	99	300
13.8	0.90	0.56	105	300
16.0	1.00	0.62	113	300
21.2	1.20	0.74	152	300
34.0	1.50	0.93	190	300
44.0	1.80	1.12	209	300

Table 40. Internal friction as a function of strain amplitude and temperature for crystal HT-I

Input voltage (volts)	Output voltage (volts)	Strain amplitude 10^{-5}	Internal friction 10^{-5}	Temperature °C
0.7	0.21	0.13	86	23
1.10	0.33	0.21	107	23
2.0	0.32	0.20	230	23
4.1	0.52	0.32	309	23
4.8	0.60	0.37	316	23
5.5	0.80	0.50	262	23
8.4	1.50	0.93	200	23
13.0	2.00	1.24	243	23
17.5	2.30	1.43	297	23
20.0	2.55	1.58	308	23
25.0	2.70	1.68	376	23
2.3	0.34	0.21	257	23
2.9	0.32	0.20	365	50
21.0	0.32	0.20	3090	55
20.5	0.32	0.20	3026	75
21.0	0.32	0.20	3090	100
21.0	0.32	0.20	3090	125
21.0	0.32	0.20	3090	150
21.5	0.32	0.20	3170	175
21.0	0.32	0.20	3090	200
21.0	0.32	0.20	3090	225

Table 40. (Continued)

Input voltage (volts)	Output voltage (volts)	Strain amplitude 10^{-5}	Internal friction 10^{-5}	Temperature °C
21.0	0.32	0.20	3090	250
21.0	0.32	0.20	3090	275
21.0	0.32	0.20	3090	300
29.5	0.40	0.25	3120	300
33.5	0.50	0.31	3160	300
40.5	0.60	0.37	3190	300
47.0	0.70	0.43	3170	300
54.0	0.80	0.50	3190	300
56.5	0.84	0.52	3170	300
20.75	0.32	0.20	3060	200
20.50	0.32	0.20	3020	150
4.4	0.32	0.20	593	150
5.0	0.46	0.29	456	150
6.5	0.52	0.32	513	150
7.9	0.62	0.38	533	150
10.5	0.80	0.50	562	150
12.3	0.92	0.57	568	150
13.3	1.00	0.62	568	150
21.5	1.50	0.93	717	150
33.5	2.00	1.24	739	150
44.0	2.50	1.55	776	150
4.5	0.32	0.20	712	150
4.5	0.5	0.20	712	125

Table 40. (Continued)

Input voltage (volts)	Output voltage (volts)	Strain amplitude 10^{-5}	Internal friction 10^{-5}	Temperature °C
17.0	0.80	0.50	952	100
4.5	0.32	0.20	712	80
4.1	0.32	0.20	544	50

Table 41. Internal friction as a function of strain amplitude and temperature for crystal HT-J

Input voltage (volts)	Output voltage (volts)	Strain amplitude 10^{-5}	Internal friction 10^{-5}	Temperature °C
0.5	0.30	0.19	0	25
1.5	0.44	0.19	0	25
1.7	0.30	0.19	0	50
2.0	0.30	0.19	11	75
4.2	0.30	0.19	98	98
20.0	0.30	0.19	6350	100
19.0	0.30	0.19	6010	70
18.5	0.30	0.19	5850	65
17.5	0.30	0.19	5550	55
16.3	0.30	0.19	5150	50
18.0	0.30	0.19	5690	100
21.0	0.30	0.19	6650	100

Table 41. (Continued)

Input voltage (volts)	Output voltage (volts)	Strain amplitude 10^{-5}	Internal friction 10^{-5}	Temperature °C
21.0	0.30	0.19	6650	200
20.8	0.30	0.19	6570	250
21.0	0.30	0.19	6650	300
28.5	0.40	0.25	6270	300
36.5	0.50	0.31	6940	300
44.5	0.60	0.37	7060	300
51.5	0.70	0.43	7000	300
57.5	0.78	0.48	7070	300
58.0	0.80	0.50	6890	300
50.0	0.70	0.43	6790	300
35.5	0.50	0.31	6750	300
20.0	0.30	0.19	6330	300
13.8	0.20	0.12	6550	300
4.7	0.10	0.06	4390	300
2.0	0.05	0.03	3770	300
20.0	0.30	0.19	6330	200
20.0	0.30	0.19	6330	100
20.0	0.30	0.19	6330	25

Table 42. Internal friction as a function of strain amplitude and temperature for crystal HT-K

Input voltage (volts)	Output voltage (volts)	Strain amplitude 10^{-5}	Internal friction 10^{-5}	Temperature °C
3.0	0.32	0.20	570	23
2.7	0.32	0.20	500	50
4.8	0.31	0.20	1000	75
9.0	0.30	0.19	2000	90
20.0	0.30	0.19	4500	100
20.0	0.30	0.19	4500	125
19.5	0.31	0.20	4230	150
19.5	0.31	0.20	4230	175
19.5	0.31	0.20	4230	200
19.5	0.31	0.20	4230	225
19.5	0.31	0.20	4230	250
19.5	0.31	0.20	4230	275
20.0	0.32	0.20	4200	300
25.5	0.40	0.25	4300	300
32.0	0.50	0.31	4300	300
39.0	0.60	0.37	4470	300
45.0	0.70	0.43	4300	300
52.0	0.81	0.50	2160	300
56.0	0.87	0.54	2310	300

Table 43. L_c and L_n for crystals G through L

Crystal	Strain amplitude 10^{-5}	L_n 10^{-4} cm
G ($L_n = 0.7 \times 10^{-5}$ cm)	0.23	2.6
	0.52	1.6
	0.75	1.7
	1.00	1.9
	1.24	2.1
	1.36	2.2
H ($L_c = 3.1 \times 10^{-5}$ cm)	0.16	3.9
	0.31	5.0
	0.43	5.5
	0.61	5.9
I ($L_c = 4.0 \times 10^{-5}$ cm)	0.18	4.1
	0.34	5.0
	0.41	5.3
	0.55	5.2
	0.75	5.0
J ($L_c = 2.3 \times 10^{-5}$ cm)	0.27	2.3
	0.34	2.6
	0.45	3.0
	0.53	3.1
	0.62	3.3
	0.71	3.2
	0.81	3.1

Table 43. (Continued)

Crystal	Strain amplitude 10^{-5}	L_n 10^{-4} cm
K (L_c = 1.8 X 10^{-5} cm)	0.26	1.9
	0.31	2.1
	0.40	2.4
	0.48	2.6
	0.55	2.7
	0.62	3.1
L[a] (L_c = 0.29 X 10^{-5} cm)	0.37	3.3
	0.50	1.3
	0.99	0.5
	1.24	0.5
	1.86	0.7

[a]Dislocation density approximated at 16.0 X 10^6 dislocations/ cm^2.